Universidad de Málaga

Escuela Técnica Superior de Ingeniería de Telecomunicación

Programa de Doctorado en Ingeniería de Telecomunicación

TESIS DOCTORAL

On the Connection between Noncircularly-symmetric and Noncentral Fading Models: Univariate and Multivariate Analysis.

Autor:

LAUREANO MORENO POZAS

Doctorado en Ingeniería de Telecomunicación

Ph.D. in Electronics and Telecommunications

Directores:

EDUARDO MARTOS NAYA

FRANCISCO JAVIER LÓPEZ MARTÍNEZ

AÑO 2017

AUTORIZACIÓN PARA LA LECTURA DE LA TESIS

D. Eduardo Martos Naya y D. Francisco Javier López Martínez, profesores doctores del Departamento de Ingeniería de Comunicaciones de la Universidad de Málaga

CERTIFICAN

Que D. Laureano Moreno Pozas, Ingeniero de Telecomunicación, ha realizado en el Departamento de Ingeniería de Comunicaciones de la Universidad de Málaga, bajo su dirección el trabajo de investigación correspondiente a su TESIS DOCTORAL titulada:

"**On the Connection between Noncircularly-symmetric and Noncentral Fading Models: Univariate and Multivariate Analysis.** "

En dicho trabajo, se han propuesto aportaciones originales en el problema de análisis de modelos de desvanecimiento no-circularmente simétricos. Esto ha dado lugar a varias publicaciones científicas, superando el requisito de 1 punto ANECA del programa de doctorado regulado por el Real Decreto 99/2011.

Por todo ello, los directores de la tesis consideran que esta tesis es apta para su presentación al Tribunal que ha de juzgarla y AUTORIZAN la presentación de la tesis en la Universidad de Málaga.

Málaga, 29 de mayo de 2017

Los directores:

Fdo.: Eduardo Martos Naya

Fdo.: F. Javier López Martínez

UNIVERSIDAD DE MÁLAGA

ESCUELA TÉCNICA SUPERIOR DE INGENIERÍA DE TELECOMUNICACIÓN

Reunido el tribunal examinador en el día de la fecha, constituido por:

Presidente: Dr. D. _____

Secretario: Dr. D. _____

Vocal: Dr. D. _____

para juzgar la Tesis Doctoral titulada "*On the Connection between Noncircularly-symmetric and Noncentral Fading Models: Univariate and Multivariate Analysis.* ", realizada por D. Laureano Moreno Pozas y dirigida por los Dres. D. Eduardo Martos Naya y D. Francisco Javier López Martínez,

acordó por _____ otorgar la calificación de

_____

y, para que conste, se extiende firmada por los componentes del tribunal la presente diligencia.

Málaga, a ____ de _____ del ____

El presidente: El secretario: El vocal:

Fdo.: _____ Fdo.: _____ Fdo.: _____

"There is something more important than logic: imagination."

Alfred Hitchcock

Acknowledgements

This work was supported by the Consejería de Economía, Innovación, Ciencia y Empleo of the Junta de Andalucía, by the Spanish Government, and by the European Regional Development Fund under Project P2011-TIC-7109, Project P2011-TIC-8238, Project TEC2011-25473, Project COFUND2013-40259, and Project TEC2014-57901-R.

First of all, I would like to acknowledge Unai Fernandez-Plazaola to introduce me to the research group where I have developed this thesis. Although I came from microwave circuit design area, Unai proposed me the challenge of working towards obtaining the Ph.D. degree in communication theory. Without his proposition, this thesis would not have been possible.

I also want to express a sincere thank you to my supervisors, Eduardo Martos-Naya and F. Javier Lopez-Martinez, for their invaluable support and guidance. They always gave very generously of their time. Javier was almost 24-hours connected to Google Hangout and available to answer any question that I posed. I also appreciated when Eduardo and I were discussing with passion some technical points of this work without caring about time. I am truly privileged to have had them as mentors.

I would also like to thank the various other people with whom I have had the amazing experience of working with over the past three years.

Firstly, I want to thank the various collaborators who have contributed to the material presented in this thesis, providing additional support and supervision. These include Prof. Jose F. Paris from the University of Málaga, Prof. Matthew R. McKay and Dr. David Morales-Jimenez from the Hong

Kong University of Science and Technology (HKUST). It was an absolute pleasure and privilege to have received additional support from these great minds of communication and random matrix theory. I would also like to thank Maite, David's wife, as well as David and Matthew for their kind support when I was settling into the HKUST Residence. The 6-months internship at the HKUST was very comfortable. I have good memories of those random matrix theory discussions at the University Bar while drinking some beers at the end of my internship.

Thanks must also go to Prof. Iain Johnstone from Stanford University for his nice feedback referring to a new random matrix theoretical framework that I have started to develop during my internship in HKUST. This has stimulated many interesting ideas for future work.

I must also give a big thank to my good friends Miguel, Alberto, Leticia, Mabel, Emilio, Carlos and Elena. Also, I would like to thank my colleagues Adrián and Julio for making my Ph. D. a fun experience. Of special mention is Nicolas Auguin who was my strongest support during my visit to HKUST. I appreciate he introduced me to his friends there.

Finally, I can never forget the overwhelming love and support of my parents and my brother. They have always been there for me, and this work would simply not have been possible without them.

Abstract

This thesis provides new statistical connections between noncircularly-symmetric central and circularly-symmetric noncentral underlying complex Gaussian models. This is particularly interesting since it facilitates the analysis of noncircularly-symmetric models, which are often underused despite their practical interest, since their analysis is more challenging.

Although these statistical connections have a wide range of applications in different areas of univariate and multivariate analysis, this thesis is framed in the context of wireless communications, to jointly analyze noncentral and noncircularly-symmetric fading models. We provide an unified framework for the five classical univariate fading models, i.e. the one-sided Gaussian, Rayleigh, Nakagami-m, Nakagami-q and Rician, and their most popular generalizations, i.e the Rician shadowed, η-μ, κ-μ and κ-μ shadowed. Moreover, we present new simple results regarding the ergodic capacity of single-input single-output systems subject to κ-μ shadowed, κ-μ and η-μ fadings.

With applications to multiple-input multiple-output communications, we are interested in matrices of the form $\mathbf{W} = \mathbf{X}\mathbf{X}^\dagger$ (or $\mathbf{W} = \mathbf{X}^\dagger\mathbf{X}$), where $\mathbf{X}$ is a complex Gaussian matrix with unequal variance in the real and imaginary parts of its entries, i.e., $\mathbf{X}$ belongs to the noncircularly-symmetric Gaussian subclass. By establishing a novel connection with the well-known complex Wishart ensemble, we facilitate the statistical analysis of $\mathbf{W}$ and give new insights on the effects of such asymmetric variance profile.

Resumen

Esta tesis proporciona nuevas conexiones estadísticas entre los modelos Gaussianos complejos no-circularmente simétricos centrales y circularmente simétricos no centrales. Esto es particularmente interesante, ya que facilita el análisis de modelos no-circularmente simétricos, que a menudo son infrautilizados a pesar de su interés práctico, ya que su análisis es más difícil.

Aunque estas conexiones estadísticas tienen una amplia gama de aplicaciones en diferentes áreas del análisis de variable aleatoria y de múltiples variables aleatorias, esta tesis se enmarca en el contexto de las comunicaciones inalámbricas, para analizar conjuntamente los modelos de desvanecimiento no centrales y no-circularmente simétricos. Proporcionamos un marco unificado para los cinco modelos clásicos de desvanecimiento, es decir, los modelos Gaussiano unilateral, Rayleigh, Nakagami-m, Nakagami-q y Rician, así como sus generalizaciones más populares, es decir los modelos Rician con ensombrecimiento, η-μ, κ-μ y κ-μ con ensombrecimiento.

Para comunicaciones con múltiples antenas, esta tesis se interesa por matrices de la forma $\mathbf{W} = \mathbf{X}\mathbf{X}^\dagger$ (o $\mathbf{W} = \mathbf{X}^\dagger\mathbf{X}$), donde $\mathbf{X}$ es una matriz Gaussiana compleja con varianzas desiguales en las partes real e imaginaria de sus entradas, es decir, $\mathbf{X}$ pertenece a la subclase Gaussiana no-circularmente simétrica. Estableciendo una nueva conexión con el conocido conjunto complejo de Wishart, se facilita el analísis estadístico de $\mathbf{W}$, a la vez que damos una mayor comprensión de los efectos de este perfil de varianza asimétrico.

Contents

List of Figures

List of Tables

List of Acronyms

AWGN	**A**dditive **W**hite **G**aussian **N**oise
BF	**B**eam**F**orming
CDF	**C**umulative **D**istribution **F**unction
IID	**I**ndependent and **I**dentically **D**istributed
JPDF	**J**oint **P**robability **D**ensity **F**unction
LOS	**L**ine-**O**f-**S**ight
MIMO	**M**ultiple-**I**nput **M**ultiple-**O**utput
MGF	**M**oment **G**enerating **F**unction
MRC	**M**aximal **R**atio **C**ombining
NLOS	**N**on **L**ine-**O**f-**S**ight
PDF	**P**robability **D**ensity **F**unction
RV	**R**andom **V**ariable
SISO	**S**ingle-**I**nput **S**ingle-**O**utput
SNR	**S**ignal-to-**N**oise **R**atio

To my parents and my brother. Special dedication to my mother, for her unconditional support.

Chapter 1

Introduction

Complex Gaussian random variables (RVs) are widely used to model random fluctuations in many different areas, such as optics [1], nuclear physics [2], signal processing [3], principal component analysis [4], and wireless communications [5], to name a few. In all of these areas, it is often assumed (usually implicitly) that these RVs are circularly-symmetric, i.e. with equal variance in their real and imaginary parts. This assumption actually simplifies the analysis of a multitude of problems.

However, there are many other cases where the circularity assumption is even inappropriate. In optics, the roughness of transmitting or reflecting surfaces affects unequally the variances of the real and imaginary parts of the scattering far-field, which can no longer be modeled with circularly-symmetric Gaussian RVs [6], [7]. In nuclear physics, the study of nuclear energy-level spacings requires the analysis of noncircularly-symmetric (or improper) Gaussian random matrices [8]. In signal processing, the imbalance between the in-phase and quadrature (I/Q) branches due to I/Q mismatches makes the received signal improper [9]. In wireless communications, noncircularly-symmetric underlying Gaussian models are convenient when a heavy shadowing or a strong ionosphere scintillation are present in mobile-satellite and inter-satellite communications [5], [10], [11].

Despite the vast number of applications, the analysis of noncircularly-symmetric models is far more scarce than that of circularly-symmetric ones.

Considering an imbalance between the real and imaginary parts presents a significant challenge as classical RV properties are often not applicable.

In this context, the main focus of this thesis is to simplify the analysis of models arising from noncircularly-symmetric Gaussian RVs in a wireless communication context. Specifically, we are interested in establishing new statistical connections between noncircularly-symmetric fading models and the more tractable circularly-symmetric ones. These will be employed to study the performance of single-input single-output (SISO) and multiple-input multiple-output (MIMO) systems subject to fadings that consider a power imbalance between the in-phase and quadrature channel components.

In SISO scenarios, a particular noncircularly-symmetric fading model has found its niche among classical fading models: the Nakagami-q (Hoyt) model. This model arises when studying the envelope of a complex baseband received signal $Z = X + jY$, where X and Y are zero-mean real Gaussian RVs with different variances σ_X^2 and σ_Y^2, respectively. When $\sigma_X^2 = \sigma_Y^2$, $|Z|^2$ follows an exponential distribution (central chi-squared distribution with 2 degrees of freedom), or equivalently, $|Z|$ is Rayleigh-distributed. When $\sigma_X^2 = 0$ or $\sigma_Y^2 = 0$, $|Z|^2$ follows a central chi-squared distribution, or equivalently, $|Z|$ is one-sided Gaussian-distributed [12]. The distribution of $|Z|$ is well-known [13], [14] and is commonly given in terms of the parameter q which gives the ratio between the typical deviation of the real and imaginary parts such that $q \in [0, 1]$. Then, $q = 0$ corresponds to $\sigma_X^2 = 0$ or $\sigma_Y^2 = 0$ (one-sided Gaussian) and $q = 1$ corresponds to $\sigma_X^2 = \sigma_Y^2$ (Rayleigh).

This intermediate model finds applications in very different wireless communication scenarios to model the diffuse component or scattering, oftenly referred to as small-scale propagation effects [15]. In mobile communication systems, the Nakagami-q model is considered for error-rate performance analysis [16], outage analysis [17], statistics of noise spikes occurring in

limiter-discriminator FM receivers [18], and mobile satellite channel modeling when there is a heavy shadowing [11]. In inter-satellite communication systems, the Nakagami-q is employed when a strong ionosphere scintillation is present [5]. In general, the Nakagami-q model is suitable for those scenarios where the propagation conditions are more severe than Rayleigh, since the Nakagami-q distribution includes all the intermediate cases between the Rayleigh ($q = 1$) and the one-sided Gaussian ($q = 0$) models.

The statistical characterization of such model has been extended over more than sixty years [5], [10], [11], [13], [14], [16]–[19]. Actually, we still find recent contributions [19]–[23], even for its fundamental statistics; e.g., the cumulative distribution function (cdf) was given in closed-form for the first time in 2009 [19]. This justifies that a very recent work was interested on simplifying the analysis of such noncircularly-symmetric model. In [23], a novel connection is established between this model and the well-known Rayleigh model. Key of this approach is to adopt a "condition and average" method which allows to connect the statistical properties of the Nakagami-q model with those of the Rayleigh model, and to leverage existing results for such model. However, the connection does not always allow to give a further insightful analysis, since the Nakagami-q model is expressed as an equivalent Rayleigh model whose average power follows a non-classical distribution given in [23].

The scientific community has also been interested by the natural generalization of the Nakagami-q model: the η-μ fading model. The η-μ model is a general model only for non-line-of-sight (NLOS) scenarios and can be seen as a Nakagami-q model with more degree of freedoms, i.e., a sum in power of 2μ Hoyt RVs. With its two shape parameters η and μ which allow a better fit between measurements and theoretical results, the model can subsume the Nakagami-q, one-sided Gaussian, Rayleigh, and Nakagami-m models.

In general, the statistical characterization of the η-μ fading model poses

some challenges. For instance, the η-μ cdf expression involves a complicated special function, the confluent Lauricella function $\Phi_2^{(2)}$, which is not available in standard packages and needs a script to be computed [24]. Moreover, there is no tractable analysis of the ergodic capacity of systems subject to the η-μ fading in the literature. The ergodic capacity of such systems was only given in a very complicated form involving infinite sums of Meijer G-functions [25].

In the context of MIMO communications, the study of the Nakagami-q fading model requires the statistical characterization of a particular Wishart-type random matrix, defined as $\mathbf{W} = \mathbf{X}\mathbf{X}^\dagger$ (or $\mathbf{W} = \mathbf{X}^\dagger\mathbf{X}$), where $\mathbf{X}$ is a zero-mean noncircularly-symmetric complex Gaussian matrix, i.e., with unequal variance in the real and imaginary parts of its entries. These matrices have been referred to as the cross-over ensemble between the Laguerre unitary ensemble (LUE) and the Laguerre orthogonal ensemble (LOE) [26]. When the variances of the real and imaginary parts of the entries of $\mathbf{X}$ are equal, $\mathbf{W}$ is a central complex Wishart matrix (LUE); when one of these variances is zero, $\mathbf{W}$ is a central real Wishart matrix (LOE). Similar intermediate ensembles between the unitary and orthogonal groups have been a subject of interest in the context of (non Wishart-type) Gaussian ensembles, i.e. GUE and GOE, with applications to the study of energy-level spacings in nuclear physics [8].

Despite its cross-disciplinary interest, this intermediate ensemble is still an open problem of the literature. Although the cross-over ensemble between GUE and GOE has been analyzed in tractable form [27], previous works have shown how challenging it is extending those results to the case of Laguerre ensembles [26], [28].

The complexity and scarcity of results in [26], [28] are mainly due to the challenge posed by the asymmetric variance profile, which renders classical random matrix properties no longer applicable. In particular, results for the extreme eigenvalue distributions are not available thus far, even for a 2×2 matrix $\mathbf{X}$, and the implications of this real-imaginary variance asymmetry

remain largely unknown. It seems then necessary to explore other strategies to tackle the characterization of such noncircularly-symmetric Wishart-type matrices.

Classically, the analysis of these noncircularly-symmetric models for NLOS scenarios, both for SISO and MIMO applications, has been always separated from that of circularly-symmetric models for LOS scenarios, since there is no clear connection between those two sets of models which have arisen very differently. As a result, the analysis of the η-μ fading model has been always presented apart from that of its circularly-symmetric LOS brother, the κ-μ fading model [29]. A similar remark can be given for the statistical characterization of noncircularly-symmetric Wishart-type matrices. Previous approaches have not considered a connection with the simpler complex Wishart ensemble, since it does not seem possible in principle.

1.1 Focus of the Thesis

Among the vast literature related to fading models, the main focus of the thesis is to connect the analysis of a set of noncircularly-symmetric fading models with the analysis of the more tractable circularly-symmetric ones, both in SISO and MIMO contexts. The approach here presented needs to revisit a recently proposed and very general fading model for the univariate case (with SISO applications), the κ-μ shadowed model, as well as the statistical properties of the well-known complex Wishart ensemble for the multivariate case (with MIMO applications). In both cases, the derivations are based on a collection of new statistical properties, which are presented in Chapter 2.

Specifically, Chapter 3 briefly reviews the classical fading models, and some of their generalizations, as well as it presents a deep analysis of the κ-μ shadowed underlying model. Chapter 4 presents a general and unified

framework for all fading models presented in Chapter 3, which makes feasible to connect a set of noncircularly-symmetric models with that of very popular circularly-symmetric models. Moreover, the ergodic capacity analysis of these very different fading channels is unified with a simple formulation. Finally, Chapter 5 connects the noncircularly-symmetric Wishart-type ensemble with the well-known complex Wishart one, which facilitates the analysis of such matrices, as well as it gives further insights on the behavior of largest eigenvalue distribution when there is a power imbalance in the underlying Gaussian model.

1.2 Dissertation Overview

In this thesis, we have addressed the performance analysis of SISO and MIMO systems that considers a power imbalance between the in-phase and quadrature components of the received signal subject to fading. We have simplified the analysis of such noncircularly-symmetric fading models in both SISO and MIMO scenarios. We have also presented a strong unification of a vast number of fading distributions for SISO scenarios, leading to different contributions to the literature.

The main contributions of this thesis can be split into two categories: the ones derived from the analysis of SISO scenarios, and the ones corresponding to the analysis of MIMO scenarios.

In the context of SISO systems, we show that a particular LOS model, whose diffuse component is modeled with a circularly-symmetric Gaussian RV and its LOS component randomly fluctuates, is mathematically equivalent to a NLOS model with noncircularly-symmetric diffuse component. This has an important relevance in practice in the context of SISO performance analysis, since we can unify a multitude of classical and generalized fading models.

Moreover, we have simplified the ergodic capacity analysis of such vast set of models with a high signal-to-noise ratio (SNR) regime approach. The explicit solution involves a higher order hypergeometric function, which has been derived by taking the derivative of a Gauss hypergeometric function. Key of this approach is using first a well-known transformation, usually referred to as Euler relation, which makes easier to perform the derivative and then allows to identify the higher order hypergeometric function. This new result was essential to give a simple unification of the ergodic capacity analysis of the κ-μ and η-μ models, as well as the Rician shadowed, Rician, Nakagami-m, Nakagami-q, Rayleigh and one-sided Gaussian fading models.

In the context of MIMO systems, we have studied in depth the statistical properties of Hermitian matrices of the form $\mathbf{W} = \mathbf{X}\mathbf{X}^\dagger$ (or $\mathbf{W} = \mathbf{X}^\dagger\mathbf{X}$), where $\mathbf{X}$ has unequal variance in the real and imaginary parts of its entries. We have connected the statistical characterization of such matrices with that of the well-known noncentral complex Wishart matrices. By exploiting this novel method, we have provided, for the first time, exact expressions for the extreme eigenvalue distributions, as well as an asymptotic expansion (deep in the left-hand tail) for the largest eigenvalue distribution of $\mathbf{W}$.

Although the exact expressions are not simple, the simplicity of the asymptotic expression for the largest eigenvalue distribution here derived is quite remarkable, particularly when considering the complexity of the joint eigenvalue distribution derived in [26].

With these new expressions, we have studied the performance analysis of MIMO systems that employ the well-known beamforming principle [15] and are subject to Nakagami-q (Hoyt) fading, bringing new insights into the outage probability and outage data rate of such systems.

1.3 Additional Related Contributions

During the course of my Ph.D. studies, we develop other contributions which are not included in this thesis in order to preserve a consistent guiding thread. Their respective details can be found in the published papers listed in the next section.

The additional contributions include:

- Performance analysis of SISO systems subject to κ-μ Extreme (κ-μ-E) fading.
  - New cdf of the κ-μ-E fading envelope in terms of the Marcum Q-function. This allows to compute the probability density function (pdf) from it and derive an asymptotic expression of the right-hand tail distribution.
  - New method for generating κ-μ-E samples. From the new cdf expression, an inversion-based algorithm is applied for generating a set of κ-μ-E samples.
  - Ergodic capacity analysis in both low and high-SNR regimes. The expression in the high-SNR regime only involves the Exponential Integral function as special function. The slope of the capacity as a function of the logarithm of the average SNR is lower than the unit value for a finite product $\kappa \cdot \mu$. This is in contrast to the unified ergodic capacity analysis presented in this thesis, where the slope is equal to the unit value regardless of the parameter of each fading model.
- Joint parameter estimation for the Two-Wave with Diffuse Power (TWDP) fading model.
  - Estimation of the parameters K and Δ of the TWDP model from the sample moments of the received signal.

– Analysis of the performance of the proposed estimators for K and Δ. To that end, the asymptotic variance was computed, and compared to the Cramer-Rao Bound, which determines the minimum achievable variance of any unbiased estimator. Also, the effect of a finite number of observations was studied in details.

1.4 Publications

The following is a list of publications in refereed journals and conference proceedings produced during my Ph.D. candidature. In some cases the conference papers contain material overlapping with the journal publications.

1.4.1 International Journal Papers

- [30] L. Moreno-Pozas, F. J. Lopez-Martinez, S. L. Cotton, J. F. Paris, and E. Martos-Naya, "Comments on "Human body shadowing in cellular device-to-device communications: channel modeling using the shadowed κ-μ fading model"", *IEEE J. Sel. Areas Commun.*, vol. 35, no. 02, pp. 517–520, Feb. 2017.

- [31] L. Moreno-Pozas, F. J. Lopez-Martinez, J. F. Paris, and E. Martos-Naya, "The κ-μ shadowed fading model: unifying the κ-μ and η-μ distributions", *IEEE Trans. Veh. Technol.*, no. 12, pp. 9630–9641, Dec. 2016.

- [32] J. Lopez-Fernandez, L. Moreno-Pozas, F. J. Lopez-Martinez, and E. Martos-Naya, "Joint parameter estimation for the two-wave with diffuse power fading model", *Sensors*, vol. 16, no. 7, Jun. 2016.

- [33] F. J. Lopez-Martinez, L. Moreno-Pozas, and E. Martos-Naya, "Novel results for the κ-μ extreme fading distribution: generation of white samples and capacity analysis", *IEEE Commun. Lett.*, vol. 19, no. 9, pp. 1580–1583, Sep. 2015.

We must clarify that the main publications which gather the main contributions of this thesis referring to the analysis of SISO wireless systems are [30] and [31]. Also mention that the main contributions of this thesis referring to MIMO systems were developed in collaboration with Matthew R. McKay. The corresponding paper has not been included in this list since it has just been submitted to an IEEE journal for possible publication.

Finally, papers [32] and [33] correspond to the additional work developed during the Ph. D. studies and presented in Section 1.3.

1.4.2 International Conference Papers

- [34] J. Lopez-Fernandez, L. Moreno-Pozas, F. J. Lopez-Martinez, and E. Martos-Naya, "Moment-based parameter estimation for the two-wave with diffuse power fading model", in *2016 IEEE 83rd Vehicular Technology Conference (VTC Spring)*, Sep. 2016.

- [35] L. Moreno-Pozas and E. Martos-Naya, "On some unifications arising from the MIMO Rician shadowed model", in *2016 IEEE 83rd Vehicular Technology Conference (VTC Spring)*, May 2016, pp. 1–5.

1.4.3 National Conference Papers

- [36] L. Moreno-Pozas, F. J. Lopez-Martinez, J. F. Paris, and E. Martos-Naya, "The Nakagami-q fading distribution: a particular case of the Rician shadowed model", in *XXXI Simposium Nacional de la Unión Científica Internacional de Radio, URSI*, Sep. 2016 (**best student paper finalist**).

Chapter 2

New Univariate and Multivariate Statistical Properties

This chapter presents new statistical properties on the theory of random variables and finite-dimensional complex random matrices. These new results provide the essential tools for establishing the statistical connections between a multitude of random models. These will allow to unify the performance analysis of SISO and MIMO systems operating under a wide set of fading environments, including those which consider a power imbalance between the in-phase and quadrature components of the received signal.

To that end, necessary preliminary results and definitions are first introduced. Some classical distributions of the literature are revisited, as well as some properties of determinant and pfaffians.

This chapter is organized as follows. Firstly, we introduce the general notation that will be used throughout this thesis in Section 2.1. Secondly, we present some definitions and preliminary results associated with the univariate analysis of this thesis in Section 2.2. Then, we give the corresponding definitions and preliminary results which will be helpful regarding the multivariate analysis of this thesis in Section 2.3. Finally, the main results of this thesis are exposed in Sections 2.4 and 2.5.

2.1 General Notation

All vectors are defined as column vectors and designated with bold lower case. All matrices are given in bold upper case.

Notation for common sets

j	imaginary unit, $\sqrt{-1}$.
Re, Im	Real and imaginary parts.
$\mathbb{R}, \mathbb{C}$	Real and complex numbers.
$\mathbb{Z}, \mathbb{N}$	Integers and natural numbers.
$\mathbb{R}^+$, $\mathbb{Z}^*$	Positive real numbers and integers excluding 0.

Notation for common functions

$\log, e$	Natural logarithm, Euler's constant.
$\max, \min$	Maximum and minimum.
$\sup, \inf$	Supremum and infimum.
$\lim$	Limit.
$\forall$	For all.
$\triangleq$	Defined as.

Notation for probability and asymptotics

$\Pr(\cdot)$	Probability.
$\mathbb{E}[\cdot]$	Expectation operator.
$\sim$	Statistically distributed as.
$f_X(x)$	Pdf of the RV X.
$F_X(x)$	Cdf of the RV X.
$\mathcal{N}(m_x, \sigma^2)$	Real Gaussian RV with mean m_x and variance σ^2.
$\mathcal{CN}(m_x, \sigma^2)$	Complex Gaussian RV with mean m_x and variance σ^2.
$o(\cdot)$	$f(x) = o(g(x))$, $g(x) > 0$, states that $f(x)/g(x) \to 0$, as $x \to \infty$.

Matrix-vector notation

$\mathbb{R}^{m\times n}, \mathbb{C}^{m\times n}$	Real and complex $m \times n$ matrices.
$\mathbb{R}^{m}, \mathbb{C}^{m}$	Real and complex $m \times 1$ vectors.
$\{\mathbf{X}\}_{i,j}$	(i,j)th element of the matrix $\mathbf{X}$.
$\mathrm{tr}(\mathbf{X})$	Trace of the matrix $\mathbf{X}$.
$\mathrm{etr}(\mathbf{X})$	Shorthand for $e^{\mathrm{tr}(\mathbf{X})}$.
$\det(\mathbf{X})$	Determinant of the matrix $\mathbf{X}$.
$\mathrm{Pf}(\mathbf{X})$	Pfaffian of the matrix $\mathbf{X}$.
$\mathbf{I}_n$	$n \times n$ identity matrix.
$\mathbf{0}_n$	$n \times n$ matrix of all zeroes.
$\mathbf{0}_{n\times m}$	$n \times m$ matrix of all zeroes.
$(\cdot)^T, (\cdot)^\dagger$	Transpose, conjugate-transpose.
$\mathrm{diag}(a_1, \ldots, a_n)$	Square diagonal matrix with $a_1, \ldots, a_n$ on the diagonal.
$\mathbf{X} > 0$	Positive-definite matrix $\mathbf{X}$.
$\mathbf{X} \geq 0$	Positive semi-definite matrix $\mathbf{X}$.

2.2 Preliminaries of Univariate Analysis

The following sections provide some basic definitions and preliminary results, which will be useful when dealing with the univariate statistical analysis presented in this thesis.

2.2.1 Special Functions

Here, we introduce the special functions that are used throughout this thesis.

The Gamma Function

The Euler's integral of the second kind, also referred to as gamma function, is defined as [37, eq. (6.1.1)]

$$\Gamma(z) = \int_0^\infty t^{z-1} e^{-t} dt \tag{2.1}$$

with $\mathrm{Re}(z) > 0$. Alternative representations, special cases and other properties can be found in standard textbooks [37], [38].

The Digamma Function

The digamma function is defined in terms of the first derivative of the gamma function $\Gamma'(\cdot)$, such as [37, eq. (6.3.1)]

$$\psi(z) = \frac{\Gamma'(z)}{\Gamma(z)} \tag{2.2}$$

with $\mathrm{Re}(z) > 0$. The reader is referred to the same standard textbooks for alternative representations and other properties.

The Incomplete Gamma Function

The incomplete version of the integral in (2.1) is known as the incomplete gamma function. There are two definitions of the gamma function. Firstly, the lower-incomplete gamma function is defined as [37, eq. (6.5.2)]

$$\gamma(z, b) = \int_0^b t^{z-1} e^{-t} dt \tag{2.3}$$

with $\mathrm{Re}(z) > 0$ and $b \in \mathbb{R}^+$. Secondly, the upper-incomplete gamma function is defined as [37, eq. (6.5.3)]

$$\Gamma(z, a) = \int_a^\infty t^{z-1} e^{-t} dt \tag{2.4}$$

with $\mathrm{Re}(z) > 0$ and $a \in \mathbb{R}^+$. Again, we referred the reader to the same textbooks for alternative representations and other properties.

The Pochhammer Symbol

The Pochhammer symbol can be defined in terms of the gamma function such as [37, eq. (6.1.22)]

$$(z)_n = \frac{\Gamma(z+n)}{\Gamma(z)}. \tag{2.5}$$

The Pochhammer symbol is useful to define the next function.

The Generalized Hypergeometric Function

The generalized hypergeometric function of one scalar argument is defined as

$${}_p\mathcal{F}_q(a_1,\ldots,a_p;b_1,\ldots,b_q;x) = \sum_{r=0}^{\infty} \frac{(a_1)_r \ldots (a_p)_r}{(b_1)_r \ldots (b_q)_r} \frac{x^r}{r!}, \tag{2.6}$$

where $(a)_r$ is the Pochhammer symbol, $a_i \in \mathbb{C}$ and $b_j \in \mathbb{C}^* \backslash \mathbb{Z}^-$.

Among the multitude of hypergeometric functions properties, we must mention the well-known Kummer's relation or transformation, as well as the Euler's relation or transformation:

$${}_1\mathcal{F}_1(a;b;z) = e^z \, {}_1\mathcal{F}_1(b-a;b;-z), \tag{2.7}$$

$${}_2\mathcal{F}_1(a,b;c;z) = (1-z)^{c-a-b} \, {}_2\mathcal{F}_1(c-a,c-b;c;z). \tag{2.8}$$

The Incomplete Beta Function

The incomplete beta function is defined as [38, eq. (8.391)]

$$B_z(a,b) = \int_0^z t^{a-1}(1-t)^{b-1} \tag{2.9}$$

with $a, b \in \mathbb{R}^{+*}$.

We can relate this function with the Gauss hypergeometric function, such as

$$B_z(a,b) = \frac{z^a}{a}\,{}_2\mathcal{F}_1(a, 1-b; a+1; z). \tag{2.10}$$

The modified Bessel Function of the First Kind

The νth order modified Bessel function of the first kind with $\nu \in \{\mathbb{R} > -\frac{1}{2}\}$ can be defined as [37, eq. (9.6.18)]

$$I_\nu(z) = \frac{(\frac{1}{2}z)^\nu}{\pi^{\frac{1}{2}}\Gamma(\nu+\frac{1}{2})}\int_{-1}^{1}(1-t^2)^{\nu-\frac{1}{2}}e^{\pm zt}dt. \tag{2.11}$$

Particularly, this function can also be expressed in terms of the Bessel hypergeometric function ${}_0\mathcal{F}_1(\cdot;\cdot)$ [37, eq. (9.6.47)], such as

$$I_\nu(z) = \frac{1}{\Gamma(\nu+1)}\left(\frac{z}{2}\right)^\nu\,{}_0\mathcal{F}_1\left(\nu+1; \frac{z^2}{4}\right) \tag{2.12}$$

where $-\nu \notin \mathbb{N}^+$.

The Marcum Q-Function

The generalized Marcum Q-function is defined as [39]

$$Q_m(a,b) = \int_b^\infty x\left(\frac{x}{a}\right)^{m-1}e^{-\frac{x^2+a^2}{2}}I_{m-1}(ax)dx \tag{2.13}$$

where $a \in \mathbb{R}^+$, $b \in \mathbb{R} < \infty$, and $m \in \mathbb{Z}^+$. When $m = 1$, we find the standard Marcum Q-function.

The Marcum Q-function is used, e.g., to express the cdf for the noncentral chi-squared distribution [12, eq. (2-1-124)].

The Nuttall Q-Function

The Nuttall Q-function is defined as [40]

$$Q_{m,n}(a,b) = \int_b^\infty x^m e^{-\frac{x^2+a^2}{2}} I_n(ax)dx \tag{2.14}$$

where $a \in \mathbb{R}^{+*}$, $b \in \mathbb{R} < \infty$, and $m, n \in \mathbb{Z}^+$.

When $m+n$ —or, equivalently $(m-n)$—is odd, we can express the Nuttall Q-function in terms of finite sum of generalized Marcum Q-functions and modified Bessel function of first kind, such as [41, eq. (8)]

$$\begin{aligned} Q_{n+2k+1,n}(a,b) = &\sum_{l=1}^{k+1} c_{k,l} a^{n+2(l-1)} Q_{n+l}(a,b) \\ &+ e^{-\frac{a^2+b^2}{2}} \sum_{r=1}^{k} P_{k,r}(b^2) a^{r-1} b^{n+r+1} I_{n+r-1}(ab) \end{aligned} \tag{2.15}$$

where

$$c_{k,l} = 2^{k-l+1} \frac{k!}{(l-1)!} \binom{k+n}{k-l+1} \tag{2.16}$$

and $P_{k,r}(b^2)$ is a polynomial of order $k-r$ in b^2, namely

$$P_{k,r}(b^2) = \sum_{j=0}^{k-r} d_{j,k,r} b^{2j} \tag{2.17}$$

with

$$d_{j,k,r} = 2^{k-r-j} \frac{(k-1-j)!}{(r-1)!} \binom{k+n}{k-r-j}. \tag{2.18}$$

2.2.2 Some Statistical Distributions

Here, we review some classical statistical distributions that will be used to connect some noncircularly-symmetric random models with a wide set of circularly-symmetric ones.

Uniform Distribution

The pdf of a RV X uniformly distributed in $[a, b]$ is given by

$$f_X(x) = \begin{cases} \frac{1}{b-a}, & a < x < b \\ 0, & \text{otherwise.} \end{cases} \tag{2.19}$$

Gaussian (Normal) Distribution

The pdf of a Gaussian or normally distributed RV X with mean m_x and variance σ^2, i.e. $X \sim \mathcal{N}(m_x, \sigma^2)$ is given by [12, eq. (2-1-92)]

$$f_X(x) = \frac{1}{\sqrt{2\pi}\sigma} e^{-\frac{(x-m_x)^2}{2\sigma^2}}. \tag{2.20}$$

Central Chi-Squared Distribution

Let $Y = X^2$, where $X \sim \mathcal{N}(0, \sigma^2)$. Thus, the pdf of Y is given by [12, eq. (2-1-105)]

$$f_Y(y) = \frac{1}{\sqrt{2\pi y}\sigma} e^{-\frac{y}{2\sigma^2}}, \qquad y \geq 0. \tag{2.21}$$

Central Chi-Squared Distribution with n Degrees of Freedom

Let $Y = \sum_{i=1}^{n} X_i^2$, where X_i, $i = 1, \ldots, n$ are independent and identically distributed (i.i.d.) $\mathcal{N}(0, \sigma^2)$. Thus, the pdf of Y is given by [12, eq. (2-1-110)]

$$f_Y(y) = \frac{1}{\sigma^n 2^{n/2} \Gamma\left(\frac{1}{2}n\right)} y^{\frac{n}{2}-1} e^{-\frac{y}{2\sigma^2}}, \qquad y \geq 0. \tag{2.22}$$

Gamma Distribution

Let W be a RV which statistically follows a gamma distribution with shape parameter α and rate parameter β, i.e, $W \sim \Gamma(\alpha, \beta)$, then its pdf is given by

$$f_W(w) = \frac{\beta^\alpha}{\Gamma(\alpha)} w^{\alpha-1} e^{-\beta w}, \tag{2.23}$$

where $\alpha, \beta \in \mathbb{R}^+$. If $W \sim \Gamma(m/2, 2/\sigma^2)$, then W follows a chi-squared distribution with m degrees of freedom.

Noncentral Chi-Squared distribution:

Let $Y = X^2$, where $X \sim \mathcal{N}(m_x, \sigma^2)$. Thus, the pdf of Y is given by

$$f_Y(y) = \frac{1}{\sqrt{2\pi y}\sigma} e^{-\frac{y+m_x^2}{2\sigma^2}} \cosh\left(\frac{\sqrt{y}m_x}{\sigma^2}\right), \qquad y \geq 0. \tag{2.24}$$

Noncentral Chi-Squared Distribution with n Degrees of Freedom

Let $Y = \sum_{i=1}^{n} X_i^2$, where X_i, $i = 1, \ldots, n$ are independent $\mathcal{N}(m_i, \sigma^2)$. Thus, the pdf of Y is given by [12, eq. (2-1-118)]

$$f_Y(y) = \frac{1}{2\sigma^2}\left(\frac{y}{s^2}\right)^{\frac{n-2}{4}} e^{-\frac{y+s^2}{2\sigma^2}} I_{\frac{n}{2}-1}\left(\sqrt{y}\frac{s}{\sigma^2}\right), \qquad y \geq 0 \tag{2.25}$$

where the noncentrality parameter s^2 is

$$s^2 = \sum_{i=1}^{n} m_i^2 \tag{2.26}$$

and $I_\nu(\cdot)$ is the νth order modified Bessel function of the first kind.

We must note that, although the set of central and noncentral chi-squared distributions is usually defined with $\sigma = 1$, we have used here the unnormalized definitions presented in the standard textbook [12].

2.3 Preliminaries of Multivariate Analysis

The following sections provide some basic definitions and preliminary results, which will be useful when dealing with the multivariate statistical analysis presented in this thesis.

2.3.1 Determinants

The determinant operator applied to square matrices is commonly found in the analysis of random matrix models. It can be defined as follows:
Let $\mathbf{X}$ be an $n \times n$ matrix. Then,

$$\det(\mathbf{X}) = \sum_{\{\beta\}} (-1)^{\mathrm{per}(\beta)} \prod_{k=1}^{n} \{\mathbf{X}\}_{k,\beta_k} \tag{2.27}$$

where $\beta = \{\beta_1, \ldots, \beta_n\}$ is a permutation of $\{1, \ldots, n\}$ with sign $(-1)^{\mathrm{per}(\beta)}$, and the sum is over all such permutations.

We must highlight the following lemmas, involving integrals of determinants.

Lemma 2.1 [42] *Let* $\mathbf{X}$ *and* $\mathbf{Y}$ *be two* $n \times n$ *matrices whose* (i,j)*th entries are, respectively,* $\{\mathbf{X}\}_{i,j} = f_i(w_j)$ *and* $\{\mathbf{Y}\}_{i,j} = g_j(w_i)$*, where* f_k *and* g_k*,* $k = 1, \ldots, n$*, are functions defined on* $\mathbb{R}^+$*, and* $w_1 > \ldots > w_n$*. Then, for* $b > a > 0$

$$\underbrace{\int_a^b \ldots \int_a^b}_{n-\text{fold}} \det(\mathbf{X}) \det(\mathbf{Y}) \prod_{i=1}^{n} w_i = \det(\mathbf{A}) \tag{2.28}$$

where $\mathbf{A}$ *is another* $n \times n$ *matrix whose* (i,j)*th entry is*

$$\{\mathbf{A}\}_{i,j} = \int_a^b f_i(x) g_j(x) dx. \tag{2.29}$$

■

Lemma 2.2 [43] *Let* $\mathbf{X}$ *be an* $n \times n$ *matrix whose* (i,j)*th entries are* $\{\mathbf{X}\}_{i,j} = f_i(w_j)$*, where* f_k*,* $k = 1, \ldots, n$*, are functions defined on* $\mathbb{R}^+$*, and* $w_1 > \ldots > w_n$*. Then, for* $b > a > 0$

$$\underbrace{\int_a^b \ldots \int_a^b}_{n-\text{fold}} \det(\mathbf{X}) \prod_{i=1}^{n} w_i = \mathrm{Pf}(\mathbf{B}) \tag{2.30}$$

where $\mathrm{Pf}(\cdot)$ *is a pfaffian, the properties of which can be found in next section, and* $\mathbf{B}$ *is an* $n \times n$ *matrix whose* (i,j)*th entry is given by*

$$\{\mathbf{B}\}_{i,j} = \int_a^b \int_a^b f_i(x) f_j(y) \mathrm{sgn}(y-x) dx dy. \tag{2.31}$$

■

The first lemma, which involves a n-dimensional integral of a product of two determinants, is useful when studying the extreme eigenvalue statistics of unitary ensembles [44]–[47]. The second result, which involves a n-dimensional integral of a single determinant, is useful when analyzing the extreme eigenvalue distributions of orthogonal ensembles [47], [48]. We here are interested in both results, since we will deal with an intermediate ensemble between the orthogonal and unitary ones.

2.3.2 Pfaffians

Pfaffians have been extensively studied in [49] and in [43]. We here present a brief summary of their properties, as well as the computation of pfaffians in the context of this thesis.

Definition and Properties

Usually pfaffians are defined for skew-symmetric matrices of even dimension as follows. If $\mathbf{X}$ is a skew-symmetric $2n \times 2n$ matrix, i.e., $\{\mathbf{X}\}_{i,j} = -\{\mathbf{X}\}_{j,i}$, $i,j = 1,\ldots,2n$, and $\{\mathbf{X}\}_{i,i} = 0$, then its pfaffian is defined by

$$\mathrm{Pf}(\mathbf{X}) = \frac{1}{2^n n!} \sum_{\{\beta\}} (-1)^{\mathrm{per}(\beta)} \prod_{k=1}^{n} \{\mathbf{X}\}_{\beta_{2k-1},\beta_{2k}} \tag{2.32}$$

where $\beta = \{\beta_1,\ldots,\beta_{2n}\}$ is a permutation of $\{1,\ldots,2n\}$ with sign $(-1)^{\mathrm{per}(\beta)}$, and the sum is over all such permutations. The next properties hold:

- *Property 1:* Let $\mathbf{P}$ is a $2n \times 2n$ arbitrary matrix, then

$$\mathrm{Pf}(\mathbf{P}\mathbf{X}\mathbf{P}^T) = \mathrm{Pf}(\mathbf{X})\det(\mathbf{P}) \tag{2.33}$$

- *Property 2:* If $\mathbf{X}$ is non-sigular, then

$$\mathrm{Pf}(\mathbf{X})^2 = \det(\mathbf{X}). \tag{2.34}$$

It may be remarked that $\mathrm{Pf}(\mathbf{X})$ can be also defined by (2.32) if $\mathbf{X}$ is not skew-symmetric. We cannot, however, consider this possibility, since $\mathrm{Pf}(\mathbf{X}) = \mathrm{Pf}((\mathbf{X} - \mathbf{X}^T)/2)$, and $\mathbf{X} - \mathbf{X}^T$ is skew-symmetric $\forall\ \mathbf{X}$.

Nonetheless, considering pfaffians of odd dimension matrices can be useful. Let $\mathbf{K}$ be a skew-symmetric $(n-1) \times (n-1)$ matrix, where n is odd. The $n \times n$ matrix $\mathbf{K}^+$ arises from $\mathbf{K}$ by adding an nth column consisting of $n-1$ elements of 1, an n th row consisting of $n-1$ elements of -1, whereas the element $\{\mathbf{K}^+\}_{n,n} = 0$. For this skew-symmetric matrix $\mathbf{K}^+$ of odd dimension, the next properties hold:

- *Property 3:* $\mathrm{Pf}(\mathbf{K}^+) = \mathrm{Pf}(\mathbf{K})$.

- *Property 4:* Let $a = \{a_1, \ldots, a_n\}$ be a set of ordered elements. If the (i,j)th element of the $n \times n$ matrix $\mathbf{A}$ is given by

$$\{\mathbf{A}\}_{i,j} = a_j - a_i, \tag{2.35}$$

then

$$\mathrm{Pf}(\mathbf{A}) = (-1)^{\mathrm{per}(a)}. \tag{2.36}$$

- *Property 5:* Let $p_1, \ldots, p_n$ be real or complex numbers, and let $\mathbf{Y}$ be a $n \times n$ matrix, such as

$$\{\mathbf{Y}\}_{i,j} = \mathrm{sgn}(a_j - a_i) + p_j - p_i \tag{2.37}$$

where $\mathrm{sgn}(\cdot)$ is the signum function and a_i, $i = 1, \ldots, n$ are the elements of the ordered set a defined in the previous property. Then,

$$\mathrm{Pf}(\mathbf{Y}) = (-1)^{\mathrm{per}(a)}. \tag{2.38}$$

- *Property 6:* Let $\mathbf{P}$ be an $(n+1) \times (n+1)$ matrix such as

$$\{\mathbf{P}\}_{i,j} = \begin{cases} 1, & i = j \\ p_i, & i = 1, \ldots, n; j = n+1 \\ 0, & \text{otherwise} \end{cases} \tag{2.39}$$

and consider $\mathbf{Y}$ defined in the previous property. Then, $\mathbf{Y}^+ = \mathbf{P}\mathbf{A}^+\mathbf{P}^T$. Hence,

$$\mathrm{Pf}(\mathbf{Y}) = \mathrm{Pf}(\mathbf{Y}^+) = \mathrm{Pf}(\mathbf{A}^+) = \mathrm{Pf}(\mathbf{A}) = (-1)^{\mathrm{per}(a)}. \tag{2.40}$$

Computation of Pfaffians in this Thesis

In this thesis, the pfaffians will appear as a result of applying Lemma 2.2. The pfaffian in (2.30) can be computed as [43]

$$\mathrm{Pf}(\mathbf{B}) = \sqrt{\det(\mathbf{C})} \tag{2.41}$$

where the definition of $\mathbf{C}$ depends on n, the dimension of $\mathbf{B}$. When n is even, $\mathbf{C}$ is an $n \times n$ matrix whose (i,j)th entry is given by the right-hand side of (2.31). When n is odd, $\mathbf{C}$ is an $(n+1) \times (n+1)$ matrix whose (i,j)th entry is

given by

$$\{\mathbf{C}\}_{i,j} = \begin{cases} \int_a^b \int_a^b f_i(x) f_j(y) \mathrm{sgn}(y-x) dx dy, & i,j = 1,\ldots,n \\ \int_a^b f_i(x) dx, & i = 1,\ldots,n+1, j = n+1 \\ -\int_a^b f_j(x) dx, & i = n+1, j = 1,\ldots,n+1 \\ 0, & i = j = n+1. \end{cases} \tag{2.42}$$

2.3.3 Complex Zonal (Schur) Polynomials

Zonal polynomials of a matrix argument are a fundamental building block in multivariate statistics, forming the basis of the hypergeometric functions of a matrix argument (see next subsection). We will use exclusively complex zonal polynomials of Hermitian matrix arguments (also known as Schur polynomials [50]), in order to present later an expression of the pdf of noncircularly-symmetric Wishart-type matrices.

Concept of Partition

Before presenting the definition of these polynomials, we must introduce the concept of a partition. Let $k \geq 0$; then $\kappa = (k_1, k_2, \ldots, k_p)$, such that $\sum_{l=1}^{p} k_l = k$, $k_1 \geq k_2 \geq \ldots k_p \geq 0$, is a partition of k into p parts.

Complex Zonal Polynomial Definition

Let $\mathbf{X}$ be an $n \times n$ Hermitian matrix. The complex zonal polynomial $\widetilde{C}_\kappa(\mathbf{X})$ is defined as [51, eq. (85)]

$$\widetilde{C}_\kappa(\mathbf{X}) \triangleq \chi_{[\kappa]}(1)\chi_{\{\kappa\}}(\mathbf{X}) \tag{2.43}$$

where $\chi_{\{\kappa\}}(\mathbf{X})$ is the character of the representation $\{\kappa\}$ of the linear group, given as a symmetric function of the eigenvalues $x_1, \ldots, x_n$ of $\mathbf{X}$ by

$$\chi_{\{\kappa\}}(\mathbf{X}) = \frac{\det(\{x_i^{k_j+n-j}\}_{i,j=1,\ldots,n})}{\det(\{x_i^{n-j}\}_{i,j=1,\ldots,n})} \tag{2.44}$$

and $\chi_{[\kappa]}(1)$ is the dimension of the representation $[\kappa]$ of the symmetric group given by

$$\chi_{[\kappa]}(1) = k! \frac{\prod_{i<j}^{n}(k_i - k_j - i + j)}{\prod_{i=1}^{n}\Gamma(n + k_i - i + 1)}. \tag{2.45}$$

Note that the traditional definition given above requires that $\mathbf{X}$ have all non-zero distinct eigenvalues, otherwise (2.44) yields an indetermination $0/0$.

Properties

- *Property 1:*

$$\widetilde{C}_\kappa(\mathbf{YX}) = \widetilde{C}_\kappa(\mathbf{Y}^{\frac{1}{2}}\mathbf{X}\mathbf{Y}^{\frac{1}{2}}) = \widetilde{C}_\kappa(\mathbf{XY}) \tag{2.46}$$

  where $\mathbf{Y}$ is an Hermitian positive define $n \times n$ matrix, and $\mathbf{Y}^{\frac{1}{2}}$ is its unique hermitian positive definite square root. Note that this property follows from the fact that $\widetilde{C}_\kappa(\cdot)$ is a symmetric homogeneous polynomial in the eigenvalues of the matrix argument.

- *Property 2:* Reproductive property

$$\int_{\mathbf{Y}=\mathbf{Y}^+>0} \mathrm{etr}(-\mathbf{ZY}) \det(\mathbf{Y}) \widetilde{C}_\kappa(\mathbf{XY})(d\mathbf{Y}) = \widetilde{\Gamma}_n(m)[m]_\kappa \frac{\widetilde{C}_\kappa(\mathbf{XZ}^{-1})}{\det(\mathbf{Z})^m} \tag{2.47}$$

  where $\mathrm{Re}(m) > n - 1$, $\mathbf{Z}$ is an $n \times n$ Hermitian positive definite matrix, $[\cdot]_\kappa$ is defined in (2.50) and $\widetilde{\Gamma}_n(m)$ is the complex multivariate Gamma function [51, eq. (83)], i.e.

$$\widetilde{\Gamma}_n(m) = \pi^{\frac{n(n-1)}{2}} \prod_{i=1}^{n} \Gamma(m - i + 1). \tag{2.48}$$

2.3.4 Hypergeometric Function of Matrix Arguments

This thesis will deal exclusively with complex hypergeometric functions of Hermitian matrix arguments, denoted ${}_p\widetilde{F}_q(\cdot)$, which are defined as follows:

Let $\mathbf{X}$ an $n \times n$ Hermitian matrix. The hypergeometric function of a matrix argument ${}_p\widetilde{F}_q(a_1, \ldots, a_p; b_1, \ldots, b_q; \mathbf{X})$ is defined as [48]

$$ {}_p\widetilde{F}_q(a_1, \ldots, a_p; b_1, \ldots, b_q; \mathbf{X}) \triangleq \sum_{k=0}^{\infty} \sum_{\kappa} \frac{[a_1]_\kappa \ldots [a_p]_\kappa}{([b_1]_\kappa \ldots [b_q]_\kappa)} \frac{\widetilde{C}_\kappa(\mathbf{X})}{k!} \tag{2.49} $$

where $\kappa = (k_1, \ldots, k_n)$ is a partition of k and $[\cdot]_\kappa$ is the complex multivariate hypergeometric coefficient

$$ [a]_\kappa = \prod_{l=1}^{n} (a - l + 1)_{k_l} \tag{2.50} $$

where $(b)_r$ is the Pochhammer symbol.

2.3.5 Real and Complex Wishart Distributions

We consider both real and complex Wishart Distributions. Although the real Wishart distribution does not directly apply in the performance analysis of MIMO systems, we will see that the central real Wishart matrix will play an important role in the analysis of noncircularly-symmetric Wishart-type matrices, and thus, in the performance analysis of MIMO systems in Hoyt-faded environments.

Central Real Wishart Distribution

Let $\mathbf{H}_R$ be a $p \times n$ ($p \geq n$) matrix whose entries are i.i.d. $\mathcal{N}(0, \sigma_R^2)$. The real Gram matrix $\mathbf{W}_R = \mathbf{H}_R^T \mathbf{H}_R$ follows a central real Wishart distribution with p degrees of freedom, covariance matrix $\sigma_R^2 \mathbf{I}_n$, i.e., $\mathbf{W}_R \sim \mathcal{W}_n(p, \sigma_R^2 \mathbf{I}_n, \mathbf{0}_n)$, if its

pdf is given by [51, eq. (55)]

$$f_{\mathbf{W}_R}(\mathbf{W}) = \frac{\text{etr}\left(-\frac{1}{2}\sigma_R^{-2}\mathbf{W}\right)\det(\mathbf{W})^{\frac{p-n-1}{2}}}{2^{\frac{1}{2}pn}\sigma_R^{pn}\pi^{\frac{n(n-1)}{4}}\prod_{i=1}^{n}\Gamma(\frac{p}{2}-\frac{1}{2}(i-1))}. \tag{2.51}$$

Noncentral Complex Wishart Distribution

Let $\mathbf{H}_C$ be a $p \times n$ ($p \geq n$) matrix statistically, whose entries are independent, such as $\{\mathbf{H}_C\}_{i,j} \sim \mathcal{CN}(\{\bar{\mathbf{H}}_C\}_{i,j}, \sigma_C^2)$, where $\bar{\mathbf{H}}_C \in \mathbb{C}^{p\times n}$ is the mean matrix. The complex Gram matrix $\mathbf{W}_C = \mathbf{H}_C^\dagger\mathbf{H}_C$ follows a noncentral complex Wishart distribution with p degrees of freedom, covariance matrix $\sigma_C^2\mathbf{I}_n$ and noncentrality matrix $\mathbf{\Theta} = \sigma_C^{-2}\bar{\mathbf{H}}_C^\dagger\bar{\mathbf{H}}_C$, i.e., $\mathbf{W}_C \sim C\mathcal{W}_n(p, \sigma_C^2\mathbf{I}_n, \mathbf{\Theta})$, if its pdf is given by [51, eq. (99)]

$$f_{\mathbf{W}_C}(\mathbf{W}) = \frac{\text{etr}(-\sigma_C^{-2}\mathbf{W})\det(\mathbf{W})^{p-n}}{\sigma_C^{2pn}\pi^{\frac{n(n-1)}{2}}\prod_{i=1}^{n}\Gamma(p-i+1)}\text{etr}(-\mathbf{\Theta})\,{}_0\widetilde{F}_1(p;\sigma_C^{-2}\mathbf{\Theta}\mathbf{W}) \tag{2.52}$$

where ${}_0\widetilde{F}_1(\cdot;\cdot)$ is the complex Bessel hypergeometric function of matrix argument [51].

2.4 New Univariate Statistical Properties

Armed with the definitions and preliminary results from the previous section, we can then present our main contributions to the univariate analysis field.

First, we expose new general underlying Gaussian models which will allow new statistical connections between very different univariate models. This will be used in Chapter 4 to create a general framework that unify the analysis of SISO systems which are subject to a multitude of fading environments. Then, we give a new result involving the Gauss hypergeometric function, which will be also used in Chapter 4 to analyze the ergodic capacity of systems which belong to that general framework.

2.4.1 New General Underlying Gaussian Models

The following two propositions will be used in Chapter 4 to build a general framework that jointly analyze SISO systems subject to all classical and their most popular generalized fading environments.

Proposition 2.3 *Let A be a RV defined as*

$$A = \sum_{i=1}^{n} |Z_i + \xi\rho_i|^2 \tag{2.53}$$

where $Z_i = X_i + jY_i$, with X_i and Y_i, $i = 1, \ldots, n$, i.i.d. $\mathcal{N}(0, \sigma^2)$; ρ_i, $i = 1, \ldots, n$ are complex deterministic constants; and $|\xi|^2$ is a gamma RV such as $|\xi|^2 \sim \Gamma(m, m)$. The pdf of A is then given by

$$f_A(a) = \frac{1}{(2\sigma^2)^n \Gamma(n) \left(1 + \frac{s^2}{2m\sigma^2}\right)^m} a^{n-1} e^{-\frac{a}{2\sigma^2}} \, {}_1\mathcal{F}_1\left(m; n; \frac{s^2}{2\sigma^2(s^2 + 2m\sigma^2)} a\right) \tag{2.54}$$

where $s^2 = \sum_{i=1}^{n} |\rho_i|^2$.

Proof: The RV A, conditioned to the RV $|\widetilde{\xi}|^2$, follows a noncentral chi-square distribution with $2n$ degrees of freedom, such as

$$f_{A|\xi}(a, \xi) = \frac{1}{2\sigma^2} \left(\frac{a}{|\xi|^2 s^2}\right)^{\frac{n-1}{2}} e^{-\frac{a+s^2}{2\sigma^2}} I_{n-1}\left(\sqrt{a}\frac{|\xi| s}{\sigma^2}\right). \tag{2.55}$$

Moreover, since $|\xi|^2 \sim \Gamma(m, m)$, then $|\xi|^2 \sum_{i=1}^{\mu} |\rho_i|^2 \sim \Gamma(m, m/\sum_{i=1}^{\mu} |\rho_i|^2)$. We obtain the result by averaging (2.55) over $|\xi|$, similarly as in [52]. ■

Proposition 2.4 *Let B be a RV defined as*

$$B = \sum_{i=1}^{n} |Z_i + \xi_i\rho|^2 \tag{2.56}$$

where $Z_i = X_i + jY_i$, with X_i and Y_i, $i = 1, \ldots, n$, i.i.d. $\mathcal{N}(0, \sigma^2)$; ρ is a complex deterministic constant; and $|\xi_i|^2$, $i = 1, \ldots, n$, are i.i.d. RVs $\sim \Gamma(\hat{m}, \hat{m})$. The pdf of B is also given by (2.54) with $s^2 = n|\rho|^2$.

Proof: The RV B, conditioned to the sum of the i.i.d. RVs ξ_i, $i = 1, \ldots, n$, $P = |\rho|^2 \sum_{i=1}^{\mu} |\xi_i|^2$, follows the distribution in (2.55) when substituting $|\xi|^2 s^2$ by P. Moreover, since $|\xi_i|^2 \sim \Gamma(\hat{m}, \hat{m})\ \forall i$, then $P \sim \Gamma(m, \hat{m}/|\rho|^2)$, where $m = \sum_{i=1}^{\mu} \hat{m} = \mu \cdot \hat{m}$. We obtain then the result by averaging (2.55) over P, similarly as in [52]. ■

2.4.2 New Particular Cases

The following corollaries are used in Chapter 4 to show how the general framework embraces different fading environments.

Related to the RV A

Corollary 2.5 *If $m \to \infty$, then A follows the noncentral chi-squared distribution in (2.25) with $2n$ degrees of freedom and noncentrality parameter s^2.*

Proof: By taking the limit $m \to \infty$ in (2.54) and applying the following properties

$$\lim_{a \to \infty} {}_1\mathcal{F}_1\left(a; b; \frac{1}{a} z\right) = {}_0\mathcal{F}_1\left(b; z\right) \tag{2.57}$$

$$\lim_{a \to \infty} \left(1 + \frac{1}{a} x\right)^{-a} = e^{-x} \tag{2.58}$$

where (2.58) is the well-known limit that defines the exponential function, we obtain result. ■

Corollary 2.6 *If $s \to 0$, then $A \sim \Gamma(n, 1/(2\sigma^2))$.*

Proof: By taking the limit $s \to 0$ in (2.54) and applying the property

$$\lim_{c \to 0} {}_p\mathcal{F}_q\left(a_1 \ldots a_p; b_1 \ldots b_q; cz\right) = 1 \tag{2.59}$$

we straightforwardly obtain the result.

Notice that eq. (2.59) can be carried out by simply exploiting the series expression of the hypergeometric function of scalar argument, where the first term has the unit value and the rest of the terms are powers of the scalar argument [37, eq. (13.1.2)], so that they become zero when taking the limit.

■

Related to the RV B

Corollary 2.7 *If $m = n/2$, then the pdf of B is given by*

$$\begin{aligned} f_B(b) =& \frac{\sqrt{\pi}(1+\eta)^{\frac{n+1}{2}}\left(\frac{n}{2}\right)^{\frac{n+1}{2}}}{2n\sigma^2\Gamma\left(\frac{n}{2}\right)\sqrt{\eta}(1-\eta)^{\frac{n-1}{2}}}\left(\frac{b}{2n\sigma^2}\right)^{\frac{n-1}{2}} \\ & \times e^{-\frac{n(1+\eta)^2 b}{4\eta b}} I_{\frac{n-1}{2}}\left(\frac{n(1-\eta^2)}{8n\eta\sigma^2}b\right) \end{aligned} \tag{2.60}$$

where $\eta = (n\sigma^2)/(s^2 + n\sigma^2)$.

Proof: When $m = n/2$, we can apply in (2.54) the following property [37, eq. (9.6.47)]

$${}_1\mathcal{F}_1\left(a; 2a; z\right) = 2^{2a-1}\Gamma\left(a+\frac{1}{2}\right) z^{\frac{1}{2}-a} \mathrm{e}^{z/2} I_{a-\frac{1}{2}}\left(\frac{z}{2}\right). \tag{2.61}$$

This leads to the result after some simple algebraic manipulations. ■

The previous corollary will be essential to connect the statistical analysis of noncentral and noncircularly-symmetric fading models in Chapter 4.

Corollary 2.8 *If $m = n$, then the pdf of $B \sim \Gamma(n, n/(s^2 + 2n\sigma^2))$*

Proof: The result is straightforward by applying in (2.54) the property

$${}_1\mathcal{F}_1\Big(a; a; z\Big) = e^z. \tag{2.62}$$

■

2.4.3 New Result Involving Moments

The following theorem is useful since it involves the moments of the RV A defined previously and their derivatives. In particular, this derivative will be employed in Chapter 4 to analyze the capacity of a multitude of fading channels, with a similar approach as in [53].

Theorem 2.9 *Let A defined as in Proposition (2.3). Then,*

$$\mathbb{E}[A^t] = \frac{\Gamma(n+t)}{\Gamma(n)} \left(\frac{s^2+2m\sigma^2}{m}\right)^t {}_2\mathcal{F}_1\left(n-m,-t;n;\frac{s^2}{s^2+2m\sigma^2}\right) \tag{2.63}$$

and

$$\begin{aligned}\frac{d}{dt}\mathbb{E}[A^t]|_{t=0} =& -\psi(n) - \log\left(\frac{s^2+2m\sigma^2}{m(s^2+2n\sigma^2)}\right) \\ &+ \frac{s^2(n-m)}{n(s^2+2m\sigma^2)} \\ &\times {}_3\mathcal{F}_2\Big(1,1,n-m+1;2,n+1;\frac{s^2}{s^2+2m\sigma^2}\Big),\end{aligned} \tag{2.64}$$

where $\psi(\cdot)$ the digamma function and ${}_3\mathcal{F}_2(\cdot)$ a generalized hypergeometric function of one scalar argument.

Proof: We first compute the tth order moment of A, i.e.

$$\begin{aligned}\mathbb{E}[A^t] \triangleq& \int_0^{+\infty} a^t f_A(a)da \\ =& \frac{1}{(2\sigma^2)^n\Gamma(n)\left(1+\frac{s^2}{2m\sigma^2}\right)^m} \\ &\times \int_0^{+\infty} a^{n+t-1}e^{-\frac{a}{2\sigma^2}} {}_1\mathcal{F}_1\left(m;n;\frac{s^2}{2\sigma^2(s^2+2m\sigma^2)}a\right)da.\end{aligned} \tag{2.65}$$

Observing that the remaining integral corresponds to a Laplace transform evaluated in $s = 1/(2\sigma^2)$, we then have [54, eq. (4.23.17)]

$$\mathbb{E}[A^t] = \frac{\Gamma(n+t)}{\Gamma(n)} \frac{(2n\sigma^2)^t}{n^t(1+\frac{s^2}{2m\sigma^2})^m} {}_2\mathcal{F}_1\left(m;n+t;n;\frac{s^2}{s^2+2m\sigma^2}\right) \tag{2.66}$$

where ${}_2\mathcal{F}_1(\cdot)$ is the Gauss hypergeometric function of scalar argument [37, eq. (15.1.1)].

Invoking the Euler relation in (2.8), we obtain

$$\mathbb{E}[A^t] = \frac{\Gamma(n+t)}{\Gamma(n)} \left(\frac{s^2+2m\sigma^2}{m}\right)^t {}_2\mathcal{F}_1\left(n-m,-t;n;\frac{s^2}{s^2+2m\sigma^2}\right). \tag{2.67}$$

Expressing the Gauss hypergeometric function in series form, the derivative of the tth order moment with respect to t is then obtained with the product rule. Since the derivative of a Pochhammer symbol can be given by a difference of digamma functions $\psi(\cdot)$, we obtain

$$\begin{aligned}\frac{d}{dt}\mathbb{E}[A^t] =& \frac{\Gamma(n+t)}{\Gamma(n)} \left(\frac{s^2+2m\sigma^2}{m}\right)^t \left\{ \left[\psi(n+t) + \log\left(\frac{s^2+2m\sigma^2}{m}\right)\right] \right. \\ & \times {}_2\,\mathcal{F}_1\Big(n-m,-t;n;\frac{s^2}{s^2+2m\sigma^2}\Big) \\ & \left. - \sum_{r=1}^{+\infty} \frac{(n-m)_r(-t)_r}{(n)_r}(\psi(-t+r)-\psi(-t))\frac{\left(\frac{s^2}{s^2+2m\sigma^2}\right)^r}{r!} \right\}\end{aligned} \tag{2.68}$$

where the infinite sum starts at $r = 1$ because the first term equals zero. Setting the moments order $t = 0$, we get

$$\frac{d}{dt}\mathbb{E}[A^t]|_{t=0} = -\psi(n) - \log\left(\frac{s^2+2m\sigma^2}{m}\right) + \sum_{r=1}^{+\infty} \frac{(n-m)_r(1)_{r-1}}{(n)_r} \frac{\left(\frac{s^2}{s^2+2m\sigma^2}\right)^r}{r!}. \tag{2.69}$$

By applying some algebraic manipulations, we finally obtain

$$\begin{aligned}\frac{d}{dt}\mathbb{E}[A^t]|_{t=0} =& -\psi(n) - \log\left(\frac{s^2+2m\sigma^2}{m}\right) + \frac{s^2(n-m)}{ns^2+2nm\sigma^2} \\ & \times \sum_{r=1}^{+\infty} \frac{(n-m+1)_{r-1}(1)_{r-1}(1)_{r-1}}{(n+1)_{r-1}(2)_{r-1}} \frac{\left(\frac{s^2}{s^2+2m\sigma^2}\right)^{r-1}}{(r-1)!}\end{aligned} \tag{2.70}$$

where the infinite sum can be expressed in terms of the generalized hypergeometric function ${}_3\mathcal{F}_2(\cdot)$ and so we have the result. ■

Notice that this result gives a simple new expression for the derivative of the Gauss hypergeometric function ${}_2\mathcal{F}_1(a, b; c, z)$ with respect to a or b, when this same parameter a or b equals zero. The derivative is expressed in terms of the generalized hypergeometric function ${}_3\mathcal{F}_2(\cdot)$, instead of the more complicated form in terms of a Kampé de Fériet function proposed in [55].

2.5 New Random Matrix Theory Results

We here present new statistical expressions for noncircularly-symmetric Wishart-type matrices, i.e., Gram matrices generated from complex Gaussian matrices with unequal variance in the real and imaginary parts of their entries.

2.5.1 New Random Matrix Pdf

The following proposition presents, for the first time, an expression of the joint distribution of the entries of noncircularly-symmetric Wishart-type matrices, which will be used in Chapter 5.

Proposition 2.10 *Let* $\mathbf{W}$ *be an Hermitian matrix of the form:*

$$\mathbf{W} = \begin{cases} \mathbf{X}\mathbf{X}^\dagger, & p \leq n \\ \mathbf{X}^\dagger\mathbf{X}, & p > n \end{cases} \tag{2.71}$$

with

$$\mathbf{X} = \mathbf{X}_C + \mathbf{X}_R \tag{2.72}$$

where the matrices $\mathbf{X}_C \in \mathbb{C}^{p\times n}$ *and* $\mathbf{X}_R \in \mathbb{R}^{p\times n}$ *are mutually independent with zero-mean i.i.d. entries. The entries* $[\mathbf{X}_C]_{ij}$ *are circularly-symmetric* $\mathcal{CN}(0, \sigma_C^2)$*, while* $[\mathbf{X}_R]_{ij} \sim \mathcal{N}(0, \sigma_R^2)$*. Let* $s = \min(p, n)$ *and* $t = \max(p, n)$*. When* $\sigma_C, \sigma_R > 0$*,*

the pdf of $\mathbf{W}$ *can be given by*

$$\begin{aligned} f_{\mathbf{W}}(\mathbf{W}) =& K_{s,t}\text{etr}\left(-\sigma_C^{-2}\mathbf{W}\right)\det(\mathbf{W})^{t-s}\sum_{k=0}^{+\infty}\sum_{\kappa}\frac{1}{[p]_\kappa k!}\left(\frac{2\sigma_C^{-2}\sigma_R^2}{\sigma_C^2+2\sigma_R^2}\right)^k \\ &\times\int_{\mathbf{V}^T=\mathbf{V}>0}\text{etr}(-\mathbf{V})\det(\mathbf{V})^{\frac{t-s-1}{2}}\widetilde{C}_\kappa(\mathbf{V}\mathbf{W})(d\mathbf{V}) \end{aligned} \tag{2.73}$$

where $\widetilde{C}_\kappa(\cdot)$ *is the complex zonal polynomial and*

$$K_{s,t} = \frac{\pi^{-\frac{3s(s-1)}{4}}\left(\frac{\sqrt{2}\sigma_R}{\sigma_C^2+2\sigma_R^2}\right)^{st}}{\prod_{i=1}^{s}\Gamma\left(\frac{t}{2}-\frac{1}{2}(i-1)\right)\Gamma(t-i+1)}. \tag{2.74}$$

Proof: Define $\mathbf{W}_R = \mathbf{X}_R\mathbf{X}_R^\dagger$ if $p \leq n$ or $\mathbf{W}_R = \mathbf{X}_R^\dagger\mathbf{X}_R$ otherwise. When conditioned on $\mathbf{W}_R \in \mathbb{R}^{s\times s}$, $\mathbf{W}$ follows a noncentral complex Wishart distribution with t degrees of freedom and real noncentrality matrix $\mathbf{W}_R$, i.e., $\mathbf{W}|\mathbf{W}_R \sim \mathcal{CW}_s(t, \sigma_C^2\mathbf{I}_s, \mathbf{W}_R)$. The pdf of the $\mathbf{W}$ is carried out from the following integration over the space of real positive definite matrices, such as

$$f_{\mathbf{W}}(\mathbf{W}) = \int_{\mathbf{W}_R^T=\mathbf{W}_R>0} f_{\mathbf{W}|\mathbf{W}_R}(\mathbf{W}|\mathbf{W}_R)\cdot f_{\mathbf{W}_R}(\mathbf{W}_R)(d\mathbf{W}_R) \tag{2.75}$$

where $\mathbf{W}|\mathbf{W}_R \sim \mathcal{CW}_s(t, \sigma_C^2\mathbf{I}_s, \sigma_C^{-2}\mathbf{W}_R)$ and $\mathbf{W}_R \sim \mathcal{W}_s(t, \sigma_R^2\mathbf{I}_s, \mathbf{0}_s)$, so that

$$\begin{aligned} f_{\mathbf{W}}(\mathbf{W}) =& \frac{\pi^{-\frac{3s(s-1)}{4}}\text{etr}(-\sigma_C^{-2}\mathbf{W})\det(\mathbf{W})^{t-s}}{2^{pn/2}\sigma_C^{2pn}\sigma_R^{pn}\prod_{i=1}^{s}\Gamma\left(\frac{t}{2}-\frac{1}{2}(i-1)\right)\Gamma(t-i+1)} \\ &\times\int_{\mathbf{W}_R^T=\mathbf{W}_R>0}\text{etr}\left(-\left(\sigma_C^{-2}+\frac{1}{2}\sigma_R^{-2}\right)\mathbf{W}_R\right)\det\left(\mathbf{W}_R\right)^{\frac{t-s-1}{2}} \\ &\times_0\widetilde{F}_1(p;\sigma_C^{-4}\mathbf{W}_R\mathbf{W})(d\mathbf{W}_R). \end{aligned} \tag{2.76}$$

Naming $\sigma_{eq}^2 = \sigma_C^{-2} + \frac{1}{2}\sigma_R^{-2}$, we make the change of variables $\mathbf{V} = \sigma_{eq}^2 \mathbf{W}_R$, so that $(d\mathbf{V}) = \sigma_{eq}^{s\frac{s+1}{2}} (d\mathbf{W}_R)$ [56, Theorem 2.1.6], and we use the series representation of the hypergeometric function to obtain

$$\begin{aligned} f_{\mathbf{W}}(\mathbf{W}) =& K_{s,t} \mathrm{etr}(-\sigma_C^{-2}\mathbf{W}) \det(\mathbf{W})^{t-s} \sigma_{eq}^{-st} \\ & \times \sum_{k=0}^{+\infty} \sum_{\kappa} \frac{1}{[t]_\kappa k!} \int_{\mathbf{V}^T=\mathbf{V}>0} \mathrm{etr}(-\mathbf{V}) \det(\mathbf{V})^{\frac{t-s-1}{2}} \widetilde{C}_\kappa(\mathbf{V}\mathbf{T})(d\mathbf{V}) \end{aligned} \tag{2.77}$$

where $K_{s,t}$ is given by (2.74) and $\mathbf{T} = \sigma_{eq}^{-2}\sigma_C^{-4}\mathbf{W}$. Finally, noting that $\widetilde{C}_\kappa(a\mathbf{W}) = a^k \widetilde{C}_\kappa(\mathbf{W})$, which follows easily from the definition of Schur polynomial in (2.43), we have the result. ■

2.5.2 New Exact Extreme Eigenvalue Distributions

In the following theorem, we give for the first time exact expressions for the extreme eigenvalue distributions of noncircularly-symmetric Wishart-type matrices. We present both largest and smallest eigenvalue distributions, although we will restrict ourselves in Chapter 5 to analyze MIMO systems where the largest eigenvalue distribution plays the lead role.

Theorem 2.11 *Consider* $\mathbf{W}$ *in (2.71), with* $\sigma_C, \sigma_R > 0$. *The cdf of the largest eigenvalue of* $\mathbf{W}$ *admits*

$$F_{\phi_{\max}}(x) = \frac{\mathrm{Pf}(\mathbf{\Xi}_1(x))}{\mathrm{Pf}(\mathbf{\Xi}_2)} \tag{2.78}$$

where $\mathrm{Pf}(\cdot)$ *denotes the matrix pfaffian operation,* $\mathbf{\Xi}_1(x)$ *is* $s \times s$ *with entries*

$$\{\mathbf{\Xi}_1(x)\}_{i,j} = \int_0^\infty \int_0^\infty f_i(x,u) f_j(x,z) \mathrm{sgn}(z-u) du dz \tag{2.79}$$

with $\mathrm{sgn}(\cdot)$ *the signum function, and*

$$\begin{aligned} f_k(x,y) =& \sqrt{\frac{e^{-y/\sigma_R^2}}{(\sigma_C^2/2)^{2k}y}}\Bigg[Q_{s+t-2k+1,t-s}\left(\sqrt{2y/\sigma_C^2},0\right) \\ & - Q_{s+t-2k+1,t-s}\left(\sqrt{2y/\sigma_C^2},\sqrt{2x/\sigma_C^2}\right)\Bigg] \end{aligned} \tag{2.80}$$

where $Q_{\cdot,\cdot}(\cdot,\cdot)$ *is the Nuttall* Q*-function. The matrix* $\mathbf{\Xi}_2$ *is* $s \times s$ *with entries*

$$\{\mathbf{\Xi}_2\}_{i,j} = \int_0^{+\infty}\int_0^{+\infty} g_i(u)g_j(z)\mathrm{sgn}(z-u)dudz \tag{2.81}$$

where

$$g_k(y) = \sqrt{\frac{e^{-y/\sigma_R^2}}{(\sigma_C^2/2)^{2k}y}}Q_{s+t-2k+1,t-s}\left(\sqrt{2y/\sigma_C^2},0\right). \tag{2.82}$$

Proof: Let $\tau = t - s$. Conditioned on $\mathbf{W}_R$, the cdf of the largest eigenvalue $\phi_{\max}$ of $\mathbf{W}$ is given by [45]

$$\begin{aligned} F_{\phi_{\max}|\mathbf{W}_R}(x) \triangleq& \Pr(\phi_{\max} \le x|\mathbf{W}_R) \\ =& \frac{\sigma_C^{2s(s-1)-2st}\prod_{i=1}^s e^{-\sigma_C^{-2}w_i}}{(\tau!)^s\prod_{i<j}^s(w_i-w_j)}\det(\mathbf{\Lambda}(x)) \end{aligned} \tag{2.83}$$

where $w_1 > \ldots > w_s > 0$ are the eigenvalues of $\mathbf{W}_R$. The entries of $\mathbf{\Lambda}(x)$ are given in [45, eq. (50)] as a difference between a confluent hypergeometric function and a Nuttall Q-function. Here, for computational reasons, we use the alternative form [57, eq. (20)]

$$\begin{aligned} \{\mathbf{\Lambda}(x)\}_{i,j} =& \frac{\tau!\sigma_C^{3t-s+2i+2}2^{i-s}}{(2w_j)^{\tau/2}e^{-w_j/\sigma_C^2}}\Bigg[Q_{s+t-2i+1,\tau}\left(\sqrt{2w_j/\sigma_C^2},0\right) \\ & - Q_{s+t-2i+1,\tau}\left(\sqrt{2w_j/\sigma_C^2},\sqrt{2x/\sigma_C^2}\right)\Bigg]. \end{aligned} \tag{2.84}$$

Since (2.83) only depends on the eigenvalues of $\mathbf{W}_R$, we remove the conditioning by averaging with respect to $f_{w_1,\ldots,w_s}(w_1,\ldots,w_s)$, the jpdf of $w_1 > \ldots > w_s$, which corresponds to the eigenvalue jpdf of a central real Wishart matrix [51, eq. (58)]. This gives

$$F_{\phi_{\max}}(x) = c^{-1} \int_{\mathcal{L}} \det(\mathbf{\Lambda}(x)) \prod_{i=1}^{s} w_i^{\frac{\tau-1}{2}} e^{-\sigma_{eq}^2 w_i} dw_1 \ldots dw_s \tag{2.85}$$

where $\mathcal{L} = \{0 < w_s < \ldots < w_1 < \infty\}$, $\sigma_{eq}^2 = \sigma_C^{-2} + \sigma_R^{-2}/2$ and c is a normalization constant. Using Lemma 2.2, the multiple integral is expressed as

$$F_{\phi_{\max}}(x) = c^{-1}\mathrm{Pf}(\mathbf{\Xi}_1(x)) \tag{2.86}$$

where the elements of $\mathbf{\Xi}_1(x)$ are given by (2.79). Moreover, from (2.86), it is clear that $c = \lim_{x\to\infty} \mathrm{Pf}(\mathbf{\Xi}_1(x))$, which can be also expressed as $c = \mathrm{Pf}(\mathbf{\Xi}_2)$, with the elements of $\mathbf{\Xi}_2$ given in (2.81), since the second Nuttall Q-function in (2.80) vanishes when $x \to \infty$. ■

Theorem 2.12 *Consider* $\mathbf{W}$ *in (5.1), with* $\sigma_C, \sigma_R > 0$. *The cdf of the smallest eigenvalue of* $\mathbf{W}$ *admits*

$$F_{\phi_{\min}}(x) = 1 - \frac{\mathrm{Pf}(\mathbf{\Upsilon}(x))}{\mathrm{Pf}(\mathbf{\Xi}_2)} \tag{2.87}$$

where $\mathrm{Pf}(\cdot)$ *denotes the matrix pfaffian operation,* $\mathbf{\Upsilon}(x)$ *is* $s \times s$ *with entries*

$$\{\mathbf{\Upsilon}(x)\}_{i,j} = \int_0^\infty \int_0^\infty v_i(x,u) v_j(x,z) \mathrm{sgn}(z-u) du dz \tag{2.88}$$

and

$$v_k(x,y) = \sqrt{\frac{e^{-y/\sigma_R^2}}{(\sigma_C^2/2)^{2k} y}} Q_{s+t-2k+1,t-s}\left(\sqrt{2y/\sigma_C^2}, \sqrt{2x/\sigma_C^2}\right). \tag{2.89}$$

The matrix $\mathbf{\Xi}_2$ *is* $s \times s$ *with entries given in (2.81).*

Proof: Conditioned on $\mathbf{W}_R$, the cdf of the smallest eigenvalue $\phi_{\min}$ of $\mathbf{W}$ is given by

$$\begin{aligned} F_{\phi_{\min}|\mathbf{W}_R}(x) \triangleq & 1 - \Pr(\phi_{\min} > x|\mathbf{W}_R) \\ = & 1 - \frac{\sigma_C^{2s(s-1)-2st} \prod_{i=1}^{s} e^{-\sigma_C^{-2} w_i}}{(\tau!)^s \prod_{i<j}^{s} (w_i - w_j)} \det(\mathbf{\Psi}(x)) \end{aligned} \tag{2.90}$$

where $w_1 > \ldots > w_s > 0$ are the eigenvalues of $\mathbf{W}_R$. The entries of the $s \times s$ matrix $\mathbf{\Psi}(x)$ are given by [57, eq. (16)]

$$\{\mathbf{\Psi}(x)\}_{i,j} = \frac{\tau! \sigma_C^{3t-s+2i+2} 2^{i-s}}{(2w_j)^{\tau/2} e^{-w_j/\sigma_C^2}} Q_{s+t-2i+1,\tau}\left(\sqrt{2w_j/\sigma_C^2}, \sqrt{2x/\sigma_C^2}\right). \tag{2.91}$$

Since (2.90) has a similar form as (2.83), we can follow the steps of the proof of Theorem 2.11 to obtain the result. ■

2.5.3 New Asymptotic Expansion (in the Tail) of the Largest Eigenvalue Distribution

The following theorem will be used in Chapter 5 to give a unified expression for the asymptotic expansions of the largest eigenvalues of noncentral and noncircularly-symmetric Wishart-type matrices. In addition, we use this theorem to give further insights on how the noncircular symmetry of the entries of $\mathbf{W}$ affects the distribution of its largest eigenvalue, as well as we simplify the analysis of the outage probability and outage data rate of Hoyt-faded MIMO communications.

Theorem 2.13 *As* $x \to 0$,

$$F_{\phi_{max}}(x) = h_{s,t}\, a_{s,t}^{\mathrm{CW}} x^{st} + o(x^{st}) \tag{2.92}$$

where

$$a_{s,t}^{\mathrm{CW}} = \prod_{i=1}^{s} \frac{(s-i)!}{(s+t-i)!} \tag{2.93}$$

and

$$h_{s,t} = \frac{1}{\left(\sigma_C \sqrt{2\sigma_R^2 + \sigma_C^2}\right)^{st}} \,. \tag{2.94}$$

Proof: When conditioned on $\mathbf{W}_R$, as $x \to 0$ we have [57, eq. (28)]

$$F_{\phi_{\max}|\mathbf{W}_R}(x) = \frac{\sigma_C^{-2st} \prod_{i=1}^{s}(s-i)!}{\prod_{i=1}^{s}(s+t-i)!} \prod_{i=1}^{s} e^{-\sigma_C^{-2} w_i} x^{st} + o(x^{st}). \tag{2.95}$$

Removing the conditioning as in the proof of Theorem 2.11, we get

$$\begin{aligned} F_{\phi_{\max}}(x) =& \frac{2^{-\frac{st}{2}} \pi^{\frac{s^2}{2}} \sigma_R^{-st} \sigma_C^{-2st} \prod_{i=1}^{s}(s-i)! x^{st}}{\prod_{i=1}^{s} \Gamma(\frac{t}{2}-i+1)\Gamma(\frac{s}{2}-i+1)(s+t-i)!} \\ & \times \int_{\mathcal{L}} \prod_{m=1}^{s} e^{-\sigma_{eq}^2 w_m} w_m^{\frac{\tau-1}{2}} \prod_{i<j}^{s}(w_i - w_j) \prod_{l=1}^{s} dw_l \\ & + o(x^{st}). \end{aligned} \tag{2.96}$$

Making the multiple change of variables $\lambda_m = \sigma_{eq}^2 w_m$, $m = 1, \ldots, s$, the remaining multiple integral can be identified with the Selberg integral for the central real Wishart matrix [51, eq. (58)]. This leads to the result. ■

2.6 Conclusions

This chapter has presented new results in both univariate and multivariate statistical analyses. Of important mention are the result involving the derivative of a Gauss hypergeometric function presented in Section 2.4.3, as well as the eigenvalue results in Sections 2.5.2 and 2.5.3, which will find direct application in the following chapters. It is important to note, however, that the class of complex random matrices considered in this chapter arises in a large number of different areas. Thus, it is expected, and hoped, that many of

these new results will find further application beyond the analysis of wireless communication systems considered in this thesis.

Chapter 3

Classical and Generalized Fading Models

The mathematical description of radiowave propagation through wireless channels poses some challenging issues. Since there are various effects which depend on the propagation environment, such as multipath and shadowing, this description is sometimes complicated and does not always allow any further insightful analysis of these effects on the performance of wireless systems. However, there is a flurry of papers that made considerable efforts to characterize these effects in a wide variety of scenarios.

Among the plethora of fading models in the literature, this chapter briefly reviews the classical fading models and their most popular generalizations. A more detailed explanation of these and other models can be found in [5], [29], [52], [58]. This chapter also introduces the notation regarding fading model parameters that will be used throughout the thesis.

This chapter is organized as follows. The classical LOS and NLOS fading distributions, usually adopted as models for frequency-flat fading channels, i.e. corresponding to narrowband transmission, are described in Section 3.1. Their most popular generalizations are introduced in Section 3.2. Finally, the κ-μ shadowed fading distribution, which has been recently proposed in [52], is analyzed in detail in Section 3.3.

3.1 Classical Fading Models

In a wireless communication link, there are three main effects that can degrade the received signal power: path loss, shadowing and multipath. Path loss is mainly caused by dissipation of the power radiated by the transmitter. Path loss models generally assume that the power loss in the received signal only depends on the distance between the transmitter and receiver antennas. Shadowing can be caused by objects which appear between the transmitter and receiver sides. Path loss and shadowing produce variations of the signal over relatively large distances when compared to the signal wavelength, and therefore, they are sometimes referred to as large-scale propagation effects. Multipath is due to the constructive and destructive combination of randomly delayed, reflected, scattered, and diffracted signal components [5]. It produces signal variations which occur over distances similar to the signal wavelength. That is the reason why multipath is also referred to as small-scale propagation effects.

The analysis of these propagation effects in wireless communication has been a subject of several contributions in the literature. Depending on the nature of the radio propagation environment, there are different models to describe the statistical behavior of the envelope of the received signal. We here consider only flat-fading models, i.e., models employed to describe fadings which affect narrowband wireless systems.

Let α be the fading amplitude, where α is a RV with $\mathbb{E}[\alpha^2] = \Omega$. When the narrowband signal propagates through the fading channel, the received carrier amplitude is modulated by α, whose statistical properties depend on the nature and conditions of the propagation environment. The signal is also perturbed at the receiver by additive white Gaussian noise (AWGN), which is typically assumed to be statistically independent of α, and which is characterized by a one-sided power spectral density N_0 Watts/Hz. Defining the

instantaneous SNR per symbol by $\gamma = \alpha^2 E_s/N_0$ and the average SNR per symbol by $\bar{\gamma} = \Omega E_s/N_0$, where E_s is the energy per symbol, the pdf of γ can be obtained by introducing the following change of variable in the pdf of α [5, eq. (2.3)]:

$$p_\gamma(\gamma) = \frac{p_\alpha\left(\sqrt{\frac{\Omega\gamma}{\bar{\gamma}}}\right)}{2\sqrt{\frac{\gamma\bar{\gamma}}{\Omega}}}. \tag{3.1}$$

We now present the classical models involved in performance analysis of SISO systems subject to different fading environments. Such models further assume that there are many objects in the environment that scatter the radio signal before it arrives at the receiver. Then the central limit theorem holds, such that the channel impulse response will be well-modeled as a Gaussian process irrespective of the distribution of the individual components.

3.1.1 Rayleigh

The Rayleigh model can be defined as the magnitude α of a two-dimensional Gaussian random vector $\boldsymbol{x}$, whose entries are $[\boldsymbol{x}]_i \sim \mathcal{N}(0, \Omega/2)$. The pdf of α is given by [5, eq. (2.6)]

$$p_\alpha(\alpha) = \frac{2\alpha}{\Omega} e^{-\frac{\alpha^2}{\Omega}}, \qquad \alpha > 0, \tag{3.2}$$

and hence, following (3.1), the instantaneous SNR per symbol γ is distributed as

$$f_\gamma(\gamma) = \frac{1}{\bar{\gamma}} e^{-\frac{\gamma}{\bar{\gamma}}}. \tag{3.3}$$

It is evident from (3.3) that the Rayleigh model is closely related to the central chi-squared model presented in Section 2.2.2. To better illustrate this, let $Y = X_1^2 + X_2^2$ where X_1 and X_2 are i.i.d. $\mathcal{N}(0, \sigma^2)$. It follows that Y is central chi-squared distributed with two degrees of freedom. Then, the pdf of $\sqrt{Y}$ is given by (3.2) with $\Omega = 2\sigma^2$.

The Rayleigh model is normally used in NLOS scenarios, where the in-phase and quadrature components of the received signal have the same average power and there is no dominant component, i.e., no LOS component.

Several contributions have employed this model to shed light on the performance of wireless systems. We can say that the Rayleigh model is the most employed NLOS fading model thanks to its simplicity. We find the Rayleigh model to study a wide variety of communication systems, which includes mobile systems [58] and ship-to-ship radio links [59].

3.1.2 One-sided Gaussian

The one-sided Gaussian model is defined as the magnitude α of a real Gaussian RV $\sim \mathcal{N}(0, \Omega)$. The one-sided Gaussian distribution is given by

$$f_\alpha(\alpha) = \frac{\sqrt{2}}{\sqrt{\pi\Omega}} e^{-\frac{\alpha^2}{2\Omega}}, \qquad \alpha \geq 0. \tag{3.4}$$

With (3.1), we obtain the pdf of instantaneous SNR per symbol of the channel as

$$p_\gamma(\gamma) = \sqrt{\frac{1}{2\pi\bar{\gamma}\gamma}} e^{-\frac{\gamma}{\bar{\gamma}}}, \qquad \gamma \geq 0. \tag{3.5}$$

Using the one-sided Gaussian distribution in fading modeling can generate an ample debate. The one-sided Gaussian model does not arise from a complex underlying model, which is the natural model when analyzing bandpass signals using their baseband equivalents.

However, some contributions have considered the analysis of wireless systems subject to this fading. The one-sided Gaussian model can be seen as the worst fading case, since we are losing one of the two signal components —the in-phase or the quadrature component. The significance of this model is then reflected in its theoretical interest as a limiting worst-case. This has relevance in practice since it can be useful in the design of wireless links

with applications that demand stringent qualities of service, such as financial transfers and confident data [60], [61].

3.1.3 Nakagami-m

The Nakagami-m model has in essence the same underlying Gaussian model as a central chi-squared distribution with $2m$ degrees of freedom. Given X a central chi-squared-distributed RV with $2m$ degrees of freedom and $\sigma = 1$, we obtain a Nakagami-m-distributed RV such as

$$\alpha = \sqrt{\Omega/(2m)X}. \tag{3.6}$$

The Nakagami-m distribution is then given by

$$p_\alpha(\alpha) = \frac{2m^m \alpha^{2m-1}}{\Omega^m \Gamma(m)} e^{-\frac{m\alpha^2}{\Omega}}, \qquad \alpha \geq 0 \tag{3.7}$$

where m is the shape parameter which ranges from 0.5 to ∞, and $\Omega = \mathbb{E}[\alpha^2]$ is a second parameter which controls the spread.

Applying (3.1), we obtain the SNR per symbol, which is distributed according to a central chi-squared (gamma) distribution, i.e.

$$p_\gamma(\gamma) = \frac{m^m \gamma^{m-1}}{\bar{\gamma}^m \Gamma(m)} e^{-\frac{m\gamma}{\bar{\gamma}}}, \qquad \gamma \geq 0. \tag{3.8}$$

The Nakagami-m model can be seen as the generalization of the Rayleigh and one-sided Gaussian models. From the Nakagami-m model, the Rayleigh model can be derived as a particular case by setting $m = 1$, while the one-sided Gaussian model is obtained when $m = 0.5$.

Many publications have used the Nakagami-m in very different NLOS scenarios. Since it is a more general model than the Rayleigh one, it can better fit experimental data. Actually, the original work by Nakagami, where

this model was introduced, does not explain any physical phenomena that could justify to employ this model. This model was just proposed from empirical observations of signals propagating through the ionosphere and the troposphere [13].

3.1.4 Nakagami-q (Hoyt)

The Nakagami-q fading model is defined as the magnitude α of a noncircularly-symmetric complex Gaussian RV, i.e., with unequal variances in its real and imaginary parts, such as

$$\alpha = |X + jY| \tag{3.9}$$

where X and Y are jointly independent real Gaussian RVs with arbitrary variances, i.e., $X \sim \mathcal{N}(0, \sigma_X^2)$ and $Y \sim \mathcal{N}(0, \sigma_Y^2)$. The Nakagami-$q$ fading distribution is given by

$$f_\alpha(\alpha) = \frac{1+q^2}{q\Omega}\alpha e^{-\frac{(1+q^2)^2}{4q^2\Omega}\alpha^2} I_0\left(\frac{1-q^4}{4q^2\Omega}\alpha^2\right), \qquad \alpha \geq 0 \tag{3.10}$$

where $I_0(\cdot)$ is the zero-th order modified Bessel function of first kind (see Section 2.2.1), and $q \in (0, 1]$ is the Nakagami-q parameter, which is defined as

$$q = \begin{cases} \frac{\sigma_X}{\sigma_Y}, & \sigma_X \leq \sigma_Y \\ \frac{\sigma_Y}{\sigma_X}, & \text{otherwise.} \end{cases} \tag{3.11}$$

Using (3.1), the instantaneous SNR per symbol is given by

$$f_\gamma(\gamma) = \frac{1+q^2}{2q\bar{\gamma}} e^{-\frac{(1+q^2)^2\gamma}{4q^2\bar{\gamma}}} I_0\left(\frac{(1-q^4)\gamma}{4q^2\bar{\gamma}}\right), \qquad \gamma \geq 0. \tag{3.12}$$

If $q = 1$, we obtain the Rayleigh distribution. When $q \to 0$, we have the one-sided Gaussian distribution.

The Nakagami-q model has been commonly employed in satellite-based communications [5], [10], [11] or, in general, when the fading conditions are more severe than those of a Rayleigh-faded environment.

3.1.5 Rician

The Rician model is also known as Nakagami-n model [13]. This model is defined as α being the magnitude of a non-zero mean complex Gaussian RV. The pdf of α is given by [62]

$$p_\alpha(\alpha) = \frac{2(1+K)e^{-K\alpha}}{\Omega} e^{-\frac{(1+K)\alpha^2}{\Omega}} I_0\left(2\alpha\sqrt{\frac{K(1+K)}{\Omega}}\right), \qquad \alpha \geq 0 \qquad (3.13)$$

where K is the Rician factor, which corresponds to the ratio of the power of the dominant component to the average power of the scattered component. When applying (3.1), the SNR per symbol of the channel is distributed according to a noncentral chi-squared distribution given by

$$p_\gamma(\gamma) = \frac{(1+K)e^{-K}\alpha}{\bar{\gamma}} e^{-\frac{(1+K)\gamma}{\bar{\gamma}}} I_0\left(2\sqrt{\frac{K(1+K)\gamma}{\bar{\gamma}}}\right), \qquad \gamma \geq 0. \qquad (3.14)$$

Therefore, the Rician model is related to the noncentral chi-squared model presented in Section 2.2.2. To better illustrate this, let $Y = X_1^2 + X_2^2$ where X_1 and X_2 are independent Gaussian RVs with means m_i, $i = 1, 2$, respectively, and common variance σ^2. It follows then that Y is noncentral chi-squared-distributed with two degrees of freedom and noncentrality parameter $s^2 = m_1^2 + m_2^2$. Then, the pdf of $\sqrt{Y}$ is given by (3.13) with $\Omega = 2\sigma^2$ and $K = s^2/2\sigma^2$.

The Rician model is the first model here presented for LOS scenarios, i.e. which considers a dominant component to the scattered component. Similarly as in the Rayleigh model case, it is the most employed model in LOS scenarios due it simplicity. It can be seen as the natural extension of the

Rayleigh model to LOS scenarios. Therefore, it can be applied to all propagation environments where the Rayleigh model was used and, in addition, to those on which there is a LOS between the transmitter and receiver antennas.

3.2 Generalized Fading Models

The scientific community has been greatly interested by generalizing these aforementioned classical models in order to have a higher accuracy when fitting experimental data. Many of these generalizations can be found in standard textbooks [5], [58], including the Weibull and Beckmann models which are not in the scope of this thesis, since they are not very tractable. The moment generating function (mgf) of the Weibull model involves a Meijer G-function, and there is no closed-form expresion for the pdf of the Beckmann model [5].

3.2.1 Rician Shadowed/Shadowed-Rice

In the literature, two different Rician Shadowed or Shadowed-Rice models were proposed. The original Rician shadowed model was presented in [63], where the dominant component of the Rician model suffers from shadowing. The shadowing component was chosen to follow a log-normal distribution, which is the natural distribution for large-scale perturbations [5], [15]. The presence of this shadowing in the model was justified from experimental observations of signals propagating through land-mobile satellite (LMS) fading channels. When traveling through sparsely wooded area, a light shadowing is observed. In turn, a heavy shadowing is experienced when traveling through densely wooden areas [64].

The channel model is defined as [63, eq. (1)]

$$\alpha = |ze^{j\phi_0} + we^{j\phi}|, \qquad z, w \geq 0 \tag{3.15}$$

where the phases ϕ_0 and ϕ are uniformly distributed between 0 and 2π, w has a Rayleigh distribution, and z is log-normally distributed, i.e.

$$f_z(z) = \frac{1}{\sqrt{2\pi d_0}z} e^{-\frac{(lnz-\bar{z})^2}{2d_0}} \tag{3.16}$$

where $d_0 = \mathbb{E}[z^2]$ and $\bar{z} = \mathbb{E}[z]$.

The pdf of the fading envelope α is then given by [63, eq. (6)]

$$p_\alpha(\alpha) = \frac{\alpha}{b_0\sqrt{2\pi d_0}} \int_0^\infty \frac{1}{z} e^{-\frac{(\ln z-\bar{z})^2}{2d_0} - \frac{(r^2+z^2)}{2b_0}} I_0\left(\frac{rz}{b_0}\right) dz \tag{3.17}$$

where $b_0 = \mathbb{E}[w^2]/2$.

This model has shown to have reasonably good agreement with measurements in LMS links, both in the presence of light and heavy shadowing [63], [64]. However, the analysis of wireless systems subject to this fading can be sometimes complicated, since the pdf in (3.17) is given in integral form.

In this context, a second Rician shadowed model was proposed in [65]. This new model preserves the underlying model in (3.15). The difference lies in the shadowing, which is no longer log-normally distributed, but Nakagami-m distributed. With this in mind, the pdf of the fading amplitude can be given in a simpler form than (3.17) without compromising the accuracy when fitting experimental data [65].

The pdf of the amplitude α for this new model is given by [65, eq. (3)]

$$p_\alpha(\alpha) = \left(\frac{2b_0 m}{2b_0 m + \rho^2}\right)^m \frac{\alpha}{b_0} e^{-\frac{\alpha^2}{2b_0}} \, {}_1\mathcal{F}_1\left(m, 1; \frac{\rho^2\alpha^2}{2b_0(2b_0 m + \rho^2)}\right), \qquad \alpha \geq 0 \tag{3.18}$$

where ρ^2 is the average power of the dominant component, $2b_0$ is the average power of the scattered component, and m is extended version of the Nakagami-m parameter, which now ranges between $(0, \infty)$. The function ${}_1\mathcal{F}_1(\cdot,\cdot;\cdot)$ is the confluent hypergeometric function of scalar argument (see Section 2.2.1).

Applying the transformation $S = \alpha^2$, the pdf of the fading power S associated with this model is

$$p_S(s) = \left(\frac{2b_0 m}{2b_0 m + \rho^2}\right)^m \frac{1}{2b_0} e^{-\frac{s}{2b_0}} \, {}_1\mathcal{F}_1\left(m, 1; \frac{\rho^2 s}{2b_0(2b_0 m + \rho^2)}\right), \qquad s \geq 0. \tag{3.19}$$

3.2.2 κ-μ

The κ-μ fading model was proposed by Yacoub in [29]. The κ-μ fading envelope α can be written in terms of the in-phase and quadrature components of the fading signal as [29, eq. (6)]

$$\alpha^2 = \sum_{i=1}^{\mu} (X_i + p_i)^2 + \sum_{i=1}^{\mu} (Y_i + q_i)^2 \tag{3.20}$$

where X_i and Y_i are mutually independent Gaussian processes with $\mathbb{E}(X_i) = \mathbb{E}(Y_i) = 0$, $\mathbb{E}[X_i^2] = \mathbb{E}[Y_i^2] = \sigma^2$; p_i and q_i are respectively the mean values of the in-phase and quadrature components of the multipath waves of cluster i; and μ is the number of clusters of multipath.

The physical justification of the model can be found in [29] and is as follows. The fading model for the κ-μ distribution considers a signal composed of clusters of multipath waves, propagating in a nonhomogeneous environment. Within any cluster, the phases of the scattered waves are random and have similar delay times, with delay-time spreads of different clusters being relatively large. The clusters of multipath waves are assumed to have scattered waves with identical powers, but within each cluster a dominant component is found, which presents an arbitrary power.

Despite Yacoub's effort to justify the model from a physical perspective, it is still not clear why the components of different clusters are summed in power at the receiver, as shown in (3.20), instead of in amplitude. Answering this question is, however, not necessary when seeing the good accuracy of

the κ-μ model when fitting experimental data [29]. With the two parameters κ and μ, the model has more flexibility when compared to classical models.

The κ-μ model can be seen as a generalization of the Rician model, which is obtained as a particular case when $\mu = 1$. This generalized model can be employed in all LOS scenarios where the Rician was used to increase the accuracy between theoretical results and measurements. Moreover, one could extend the parameter μ to take real values to further improve the accuracy of the model while fitting real data, despite the underlying model in (3.20) loses its significance.

In addition, the statistical characterization of the κ-μ fading envelope is as tractable as the Rician model one. The pdf of the fading amplitude α is given by [29, eq. (11)]

$$f_\alpha(\alpha) = \frac{2\mu(1+\kappa)^{\frac{\mu+1}{2}}}{\Omega\kappa^{\frac{\mu-1}{2}}e^{\mu\kappa}}\left(\frac{\alpha}{\Omega}\right)^{\mu} e^{-\mu(1+\kappa)\left(\frac{\alpha}{\Omega}\right)^2} I_{\mu-1}\left((2\mu\sqrt{\kappa(1+\kappa)}\frac{\alpha}{\Omega}\right) \tag{3.21}$$

where $\Omega = \mathbb{E}[\alpha^2]$, $I_\nu(\cdot)$ is the ν-th order modified Bessel function of first kind (see Section 2.2.1), and κ has a similar meaning as the Rician K-factor, i.e., it is the ratio of the average power of the total LOS power to the average power of the scattered component, such as

$$\kappa = \frac{\sum_{i=1}^{\mu} p_i^2 + q_i^2}{2\sigma^2\mu}. \tag{3.22}$$

Notice that the pdf of the Rician fading envelope was also given in terms of a modified Bessel function of the first kind. We must remark, however, that the distribution in (3.21) is not a new distribution and correspond to a noncentral chi-squared distribution with 2μ degrees of freedom. A similar remark was given in [66].

Applying (3.1), the instantaneous SNR per symbol of this channel is given by

$$f_\gamma(\gamma) = \frac{\mu(1+\kappa)^{\frac{\mu+1}{2}}}{\bar{\gamma}\kappa^{\frac{\mu-1}{2}}e^{\mu\kappa}}\left(\frac{\gamma}{\bar{\gamma}}\right)^{\frac{\mu-1}{2}} e^{-\frac{\mu(1+\kappa)\gamma}{\bar{\gamma}}} I_{\mu-1}\left(2\mu\sqrt{\frac{\kappa(1+\kappa)\gamma}{\bar{\gamma}}}\right). \tag{3.23}$$

With the two shape parameter κ and μ, the κ-μ model subsumes some of the classical fading distributions as particular cases, e.g., one-sided Gaussian, Rayleigh, Nakagami-m and Rician models. However, it does not include the Nakagami-q (Hoyt) as particular case.

3.2.3 η-μ

The η-μ fading model was also presented in [29], together with the κ-μ model. This model can be seen as a generalization of the Nakagami-q (Hoyt) model, in a similar fashion as the κ-μ is the generalization of the Rician model. Therefore, it can be employed in all NLOS scenarios where the Nakagami-q was employed to increase the accuracy between theoretical results and measurements.

The η-μ model may appear in two different formats, for which a different underlying model can be found in [29]. We here are interested in the so-called η-μ model format 1, for which the fading envelope can be expressed as [29, eq. (22)]

$$\alpha^2 = \sum_{i=1}^{2\mu}\left(X_i^2 + Y_i^2\right) \tag{3.24}$$

where X_i and Y_i are mutually independent Gaussian processes with $\mathbb{E}(X_i) = \mathbb{E}(Y_i) = 0$, $\mathbb{E}[X_i^2] = \sigma_X^2$ and $\mathbb{E}[Y_i^2] = \sigma_Y^2$. We must note that now the number of clusters is 2μ, which can be confusing for the reader since the κ-μ model was divided into μ clusters. However, we here use the original notation, which has been conventionally adopted in the literature.

A physical interpretation of this model, similar to the one given for the κ-μ model, can be found in [29]. We here are just interested in the flexibility of such model to accommodating to different fading conditions.

The pdf of the η-μ fading amplitude α is given by [29, eq. (27)]

$$f_\alpha(\alpha) = \frac{4\sqrt{\pi}\mu^{\mu+\frac{1}{2}}h^\mu}{\Omega\Gamma(\mu)H^{\mu-\frac{1}{2}}}\left(\frac{\alpha}{\Omega}\right)^{2\mu} e^{-2\mu h\left(\frac{\alpha}{\Omega}\right)^2} I_{\mu-\frac{1}{2}}\left(2\mu H\left(\frac{\alpha}{\Omega}\right)^2\right) \tag{3.25}$$

where $\Omega = \mathbb{E}[\alpha^2]$, $h = (2+\eta^{-1}+\eta)/4$ and $H = (\eta^{-1}-\eta)/4$. The parameter η indicates the scattered wave power ratio between the in-phase and quadrature components of each cluster, in a similar fashion that the Hoyt parameter q indicates the ratio between the typical deviation of these components. However, the range of η is $(0, \infty)$, since the parameter is uniquely defined as

$$\eta = \frac{\sigma_X^2}{\sigma_Y^2}. \tag{3.26}$$

The distribution in (3.25) yields identical values within the intervals $(0, 1)$ and $(1, \infty)$, i.e., the distribution is symmetrical around $\eta = 1$. This can be mathematically explained from (3.25), since $I_\nu(-z) = (-1)^\nu I_\nu(z)$. Therefore, as far as the envelope (or power) distribution is concerned, it suffices to consider η only within one of the ranges.

In contrast to the distribution of the κ-μ model, the distribution of the η-μ model belongs to a different class of distributions which cannot be related to the one presented in (2.2.2). Actually, it can be seen as a generalization of the central chi-squared distribution where the underlying Gaussian RVs can be divided into two sets: a set of Gaussian RVs with variance σ_X^2 and a set of Gaussian RVs with variance σ_Y^2.

Applying (3.1), the instantaneous SNR per symbol of this channel is given by

$$f_\gamma(\gamma) = \frac{\sqrt{\pi}(1+\eta)^{\mu+\frac{1}{2}}\mu^{\mu+\frac{1}{2}}}{\Gamma(\mu)\bar{\gamma}\sqrt{\eta}(1-\eta)^{\mu-\frac{1}{2}}}\left(\frac{\gamma}{\bar{\gamma}}\right)^{\mu-\frac{1}{2}} e^{-\frac{\mu(1+\eta)^2\gamma}{2\eta\bar{\gamma}}} I_{\mu-\frac{1}{2}}\left(\frac{\mu(1-\eta^2)}{2\eta}\frac{\gamma}{\bar{\gamma}}\right). \quad (3.27)$$

With the two shape parameters η and μ, this model subsumes some classical fading models, e.g, the one-sided Gaussian, Rayleigh, Nakagami-m and Nakagami-q models. However, it does not include the Rician model because of the inherent LOS nature of the latter.

3.3 The κ-μ Shadowed Fading Model

We here present in details the κ-μ shadowed fading model, since it will allow to connect the κ-μ and η-μ distributions in the next chapter of this thesis. To that end, we need to clarify a discrepancy between two underlying models which have appeared independently in the literature. We must mention that the work presented in this section was done in collaboration with S.L. Cotton, and can be found in [30].

3.3.1 Context

The κ-μ shadowed model was defined for the first time by Paris in [52] as a natural generalization of the popular κ-μ fading model originally proposed by Yacoub in [29]. The difference with respect to the κ-μ model appears in the dominant component of each cluster, which is no longer deterministic and can randomly fluctuate because of shadowing. Closed-form expressions for the pdf, cdf and the mgf of the signal power envelope were derived in [52], and validated using Monte Carlo simulations and field measurements in the context of underwater acoustic channels. Shortly after, in an independent work recently published in [67], a κ-μ shadowed distribution was proposed

in the context of device-to-device communications. Starting from an underlying statistical model which can be regarded as a generalization of the one proposed in (3.15), closed-form expressions for the pdf, moments and mgf of the fading envelope were given, and also validated with field measurements obtained for a range of different scenarios. Nonetheless, the author of [67] failed to provide Monte Carlo simulations of the proposed underlying statistical model which would have helped to identify the discrepancy between both contributions in [52] and [67]. We note that the analytical expressions presented in [52] and [67] have the same functional form, even though they have arisen from two evidently different statistical models.

3.3.2 Statistical Models in [52], [67] Revisited

Underlying Statistical Model in [52]

The κ-μ shadowed fading model was defined in [52], on which the received signal power (or squared envelope) can be expressed as

$$\alpha^2 = \sum_{i=1}^{\mu} (X_i + \xi p_i)^2 + (Y_i + \xi q_i)^2 \tag{3.28}$$

where X_i and Y_i are i.i.d. real Gaussian RVs with zero mean and variance σ^2; p_i and q_i are constants with $d^2 = \sum_{i=1}^{\mu} p_i^2 + q_i^2$; and ξ is the shadowing parameter which follows a Nakagami-m distribution with $\mathbb{E}[\xi^2] = 1$.

When conditioning to the shadowing parameter ξ, the model in (3.28) reduces to the κ-μ fading model in (3.20), and the pdf for the RVs $\gamma = \bar{\gamma}\alpha^2/\mathbb{E}[\alpha^2]$ representing the instantaneous SNR per symbol is given by

$$f_{\gamma|\xi}(\gamma, \xi) = \frac{\mu(1+\kappa)^{\frac{\mu+1}{2}}}{\bar{\gamma}\kappa^{\frac{\mu-1}{2}} e^{\xi^2 \mu\kappa}} \left(\frac{\gamma}{\xi^2 \bar{\gamma}}\right)^{\frac{\mu-1}{2}} e^{-\frac{\mu(1+\kappa)\gamma}{\bar{\gamma}}} I_{\mu-1}\left(2\mu\xi\sqrt{\frac{\kappa(1+\kappa)\gamma}{\bar{\gamma}}}\right) \tag{3.29}$$

where $\kappa = d^2/(2\mu\sigma^2)$. This is evident, as the κ-μ shadowed fading model in (3.28) arises as a natural generalization of (3.20) in scenarios on which the

line-of-sight component is subject to shadowing. The κ-μ shadowed pdf is then obtained by averaging (3.29) over all possible shadowing states, yielding the following closed-form expression:

$$f_\gamma(\gamma) = \frac{\mu^\mu m^m (1+\kappa)^\mu}{\Gamma(\mu)\bar{\gamma}(\mu\kappa+m)^m} \left(\frac{\gamma}{\bar{\gamma}}\right)^{\mu-1} e^{-\frac{\mu(1+\kappa)\gamma}{\bar{\gamma}}} \, {}_1\mathcal{F}_1\left(m;\mu;\frac{\mu^2\kappa(1+\kappa)}{\mu\kappa+m}\frac{\gamma}{\bar{\gamma}}\right). \quad (3.30)$$

Notice that if μ takes real values, (3.30) is still a valid pdf, although the underlying Gaussian model in (3.28) is no longer meaningful. It is important to extend the parameter μ from the integers to the real numbers in order to increase the flexibility of the model [29], [52].

Underlying Statistical Model in [67]

In a later and independent work, a different κ-μ shadowed model was defined in [67]. The following complex envelope model was proposed for the received signal in the presence of shadowed fading[1]

$$Re^{j\theta} = We^{j\phi} + \Delta e^{j\phi_0} \quad (3.31)$$

where W and Δ are independent and non-identically distributed Nakagami-m distributed RVs; ϕ follows the distribution defined in [68] and ϕ_0 is a deterministic phase. The distribution of the phase ϕ is given by [68], [69]

$$f_\phi(\phi) = \frac{\Gamma(\mu)|\sin(2\phi)|^{\mu-1}}{2^\mu \Gamma\left(\frac{1+p}{2}\mu\right)\Gamma\left(\frac{1-p}{2}\mu\right)|\tan(\phi)|^{p\mu}} \quad (3.32)$$

for $\phi \in (0, 2\pi)$ and $p \in [-1, 1]$.

After introducing (3.31), the author in [67] states: *If Δ is initially held constant, then the conditional pdf of R is given by ... that of the κ-μ distribution [29].* However, no explicit proof for this statement was given. As we will later see,

[1] For the sake of notational simplicity in the further comparison, we use α and R to denote the fading envelopes of the models in [52] and [67], respectively. We must also note that the pdfs of α and α^2 (or R and R^2) are related through a simple change of variables.

this statement is incorrect and therefore, as it stands, the unconditional pdf obtained when averaging over the distribution of Δ cannot be regarded as a κ-μ shadowed fading model.

In fact, we have been unable to derive a simple expression for the pdf of $R|\Delta$, let alone for the pdf of R. For this reason, we resort to compare both models in the next subsection by using the underlying RVs from which they are built.

3.3.3 Comparing both models

In order to better observe the difference between both models, let us express each model in terms of underlying Gaussian RVs.

First, we consider the κ-μ shadowed model originally defined in [52]. Expanding (3.28), the received signal power can be expressed as

$$\alpha^2 = \sum_{i=1}^{\mu} \left(X_i^2 + Y_i^2\right) + \xi^2 d^2 + 2\xi d \underbrace{\sum_{i=1}^{\mu} \left(X_i \tfrac{p_i}{d} + Y_i \tfrac{q_i}{d}\right)}_{Z_\alpha}. \tag{3.33}$$

where Z_α is defined for convenience of discussion, and will be of later use.

We now consider the received signal power in [67], denoted as R^2, which can be conveniently expressed as

$$R^2 = |We^{j(\phi-\phi_0)} + \Delta|^2. \tag{3.34}$$

After some algebraic manipulations, we obtain

$$R^2 = W^2 + \Delta^2 + 2W\Delta\cos(\phi - \phi_0). \tag{3.35}$$

Since W and Δ follow independent and non-identical Nakagami-m distributions, for integer values of μ we can explicitly express these RVs such

as

$$\Delta = \xi d, \tag{3.36}$$

$$W = \sqrt{X^2 + Y^2}, \tag{3.37}$$

where $X = (-1)^u \sqrt{\sum_{i=1}^{\mu} X_i^2}$ and $Y = (-1)^v \sqrt{\sum_{i=1}^{\mu} Y_i^2}$, with X_i, Y_i, d and ξ defined previously; u and v are binary RVs which can take the values $\{0, 1\}$ with the same probability. Notice that we have here implicitly considered the balanced condition defined in [68], [69] (i.e. $p = 0$ in (3.32)), since the number of real Gaussian RVs is equal in both the in-phase and quadrature signals.

Taking into account that the phase of the scattering component ϕ is given by [69]

$$\phi = \arctan \frac{Y}{X}, \tag{3.38}$$

we then identify $W\cos(\phi) = (-1)^u \sqrt{\sum_{i=1}^{\mu} X_i^2}$ and $W\sin(\phi) = (-1)^v \sqrt{\sum_{i=1}^{\mu} Y_i^2}$. Therefore, (3.35) becomes

$$R^2 = \sum_{i=1}^{\mu} \left(X_i^2 + Y_i^2\right) + \xi^2 d^2 + 2\xi d \underbrace{W\cos(\phi - \phi_0)}_{Z_R} \tag{3.39}$$

where Z_R is given by

$$Z_R = \left((-1)^u \cos(\phi_0) \sqrt{\sum_{i=1}^{\mu} X_i^2} + (-1)^v \sin(\phi_0) \sqrt{\sum_{i=1}^{\mu} Y_i^2} \right). \tag{3.40}$$

The difference between (3.33) and (3.39) remains in the last term of both expressions, and is encapsulated in the RVs Z_α and Z_R. Since for (3.33) Z_α is a sum of Gaussian RVs, when conditioned to the shadowing ξ, the last term follows a Gaussian distribution. This is a key aspect of the κ-μ fading model proposed by Yacoub [29], for which α^2 resembles a non-central chi-squared distribution. However, Z_R is evidently not Gaussian distributed for $\mu \neq 1$. Therefore, the underlying statistical model presented in [67] when

conditioned to a specific shadowing value does not follow a κ-μ distribution, and neither resembles a non-central chi-squared distribution.

In the very specific case of $\mu = 1$, the parameter Z_R in (3.39) can be expressed as

$$Z_R = (-1)^u \cos(\phi_0)|X_1| + (-1)^v \sin(\phi_0)|Y_1| \tag{3.41}$$

which now it is indeed Gaussian distributed. For this reason, the model presented in [67] is only coincident with the κ-μ shadowed distributed when $\mu = 1$, i.e. when it reduces to the Rician shadowed distribution [65]. This is coherent, since the underlying statistical models in [67] and [65] are in fact identical for $\mu = 1$. We note that for the imbalanced condition in (3.32), (i.e. $p \neq 0$) the conditional model in [67, eq. (2)] does not follow a κ-μ distribution even for $\mu = 1$. This is easily explained by observing (3.39) for $p \neq 0$: although W is Rayleigh distributed, the distribution of ϕ is other than the uniform distribution and hence Z_R is not Gaussian.

Instead of being equivalent to the κ-μ distribution, the conditional model [67, eq. (2)] belongs to a family of bimodal distributions similar to the one presented in [70] by Beaulieu and Saberali. This is consistent with the fact that these models only differ in the phase distribution of the scattering waves and LOS component, which are both considered to be uniformly distributed in [70].

A simple correction to the underlying statistical model in [67]

For completeness, in this subsection, we introduce a straightforward correction to (3.31) which ensures that all of the formulations presented therein are fully compliant with the κ-μ shadowed fading model. Following from the statistical model originally proposed by [52], to correct the underlying statistical model in [67], we rearrange (3.36) to express ξ in terms of Δ and d.

We then substitute this result into (3.28), so that the mean values of the in phase and quadrature components of each of the multipath clusters are now normalized to the the total power contributed by the dominant component, such that

$$R^2 = \sum_{i=1}^{\mu} (X_i + \frac{\Delta}{d} p_i)^2 + (Y_i + \frac{\Delta}{d} q_i)^2. \tag{3.42}$$

Now assuming that the formulation given in (3.42) is used as the underlying statistical model for [67], the conditional pdf given in [67, eq. (2)] and the subsequent statements and derivations comply fully with the κ-μ and κ-μ shadowed fading models. We will now provide numerical results which illustrate the key points discussed in this section.

3.3.4 Numerical Results

Conditioned Statistical Models

We first consider the statistical models analyzed in this paper, when conditioned to a particular shadowing state, i.e.

$$R|\Delta = |We^{j\phi} + \Delta e^{j\phi_0}|, \tag{3.43}$$

where Δ is held constant.

In Fig. 1, we represent the pdf of conditional RV in eq. (3.43) generated by Monte Carlo (MC) simulations for $\mu = 4$ and $\kappa = 2$. We compare it to the theoretical and simulated pdf of the κ-μ distribution [29]. We clearly observe that the conditional distribution (CD) considered in [67] does not follow a κ-μ distribution. While the κ-μ distribution is a unimodal function for every pair of (κ, μ) [29], i.e., it has only one local maximum, the conditional pdf of the model presented in [67] is clearly bimodal for $\kappa = 2$ and $\mu = 4$ since it has two local maxima.

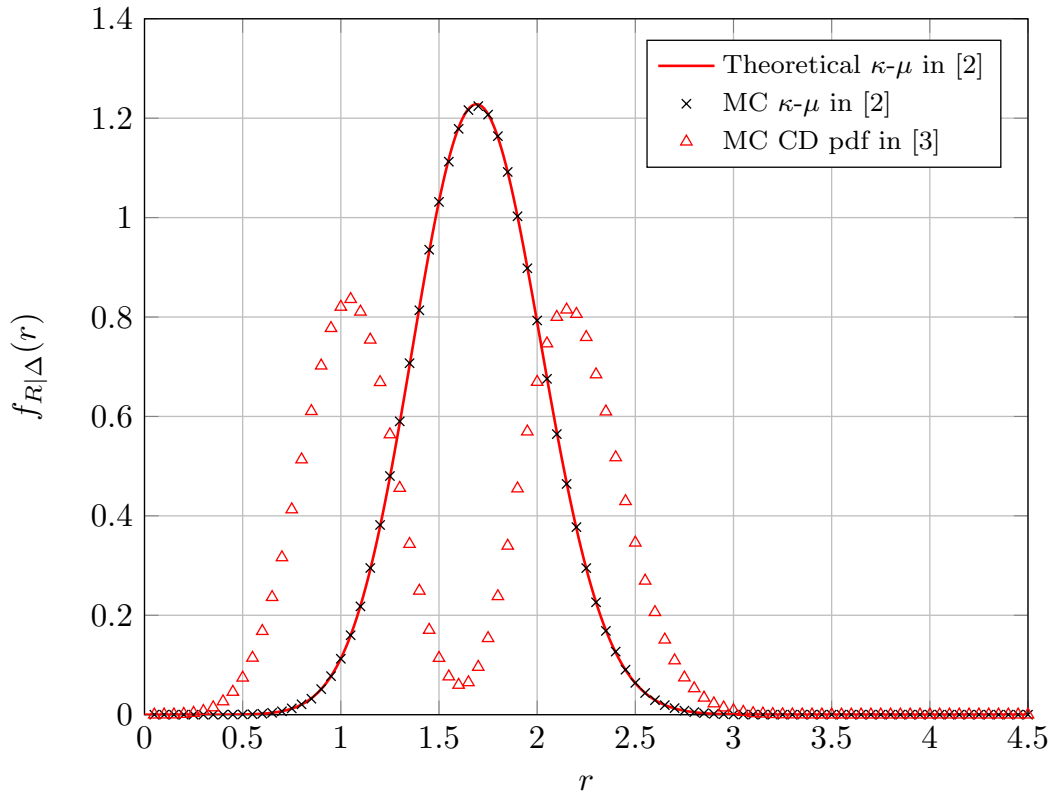

FIGURE 3.1: Comparison of the simulated CD pdf with $\kappa = 2$ and $\mu = 4$ with the κ-μ distribution.

Hence, we have shown that the distribution of the received signal amplitude R, when conditioned to a particular shadowing state, does not follow the κ-μ distribution.

Unconditioned Statistical Models

Despite having shown that the CD in [67] does not follow a κ-μ distribution, one could think of whether the resulting unconditional distribution (UD) obtained after averaging over all shadowing states in [67] could actually follow a κ-μ shadowed distribution. If we let the m parameter grow to infinity, then the Nakagami-m pdf is compressed and at the limit degenerates on a deterministic distribution, being its pdf the Dirac delta function. Therefore, for large but finite values of m the UD model in [67] is expected to have a shape similar to the conditioned case. This implies that the UD model in [67] will

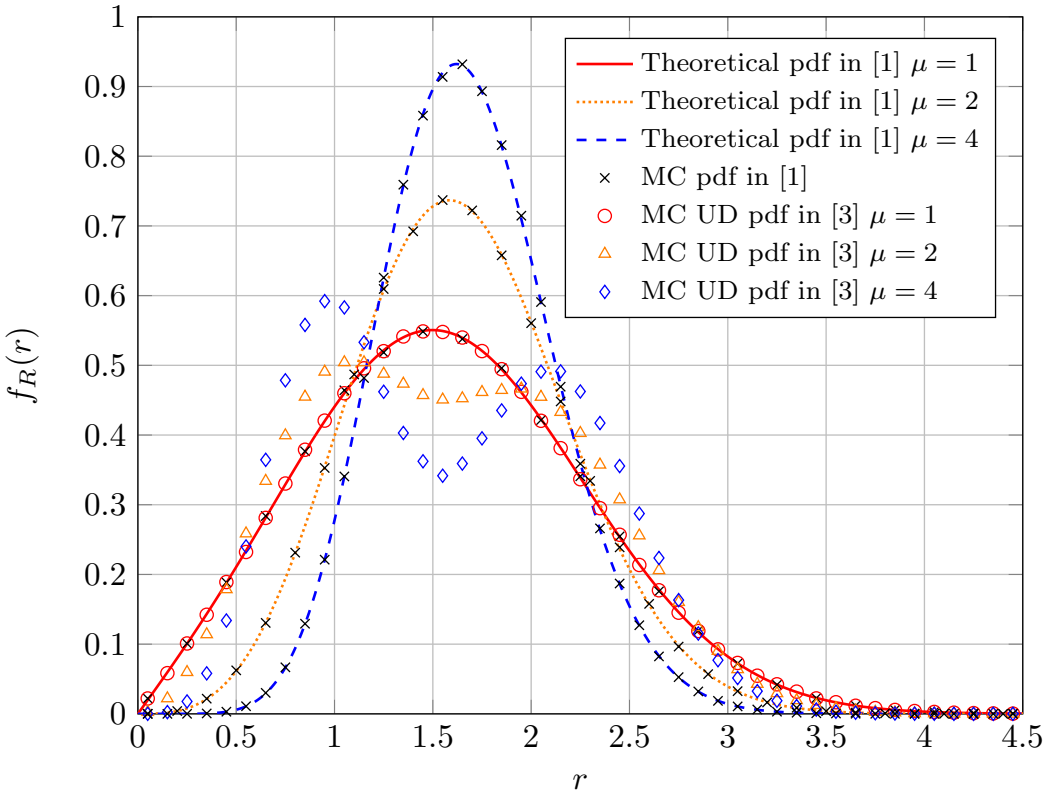

FIGURE 3.2: Comparison between the MC simulated UD in [67], the simulated original model presented in [52] and the theoretical pdf of the κ-μ shadowed distribution for different values of the parameter μ and fixed $\kappa = 2$, and $m = 4$.

also exhibit a bimodal behaviour, which is not the actual behavior of the κ-μ shadowed distribution.

In order to illustrate this aspect, we will now compare the pdfs arising from the statistical models in [67] and [52]. For generating the samples for the UD in [67], we follow the same steps as shown in the previous section, but now considering that Δ is a Nakagami-m RV.

In Fig. 2, we plot the pdf of the UD pdf for different values of the parameter μ, when the other parameters κ and m remain fixed. We observe that the UD pdf differs from the κ-μ shadowed model except for $\mu = 1$. This observation is consistent with the result presented in [65], and tackled in Section 3.3.2.

In Fig. 3, we now compare the evolution of both models with respect to the parameter κ. We observe that when the underlying statistical model is

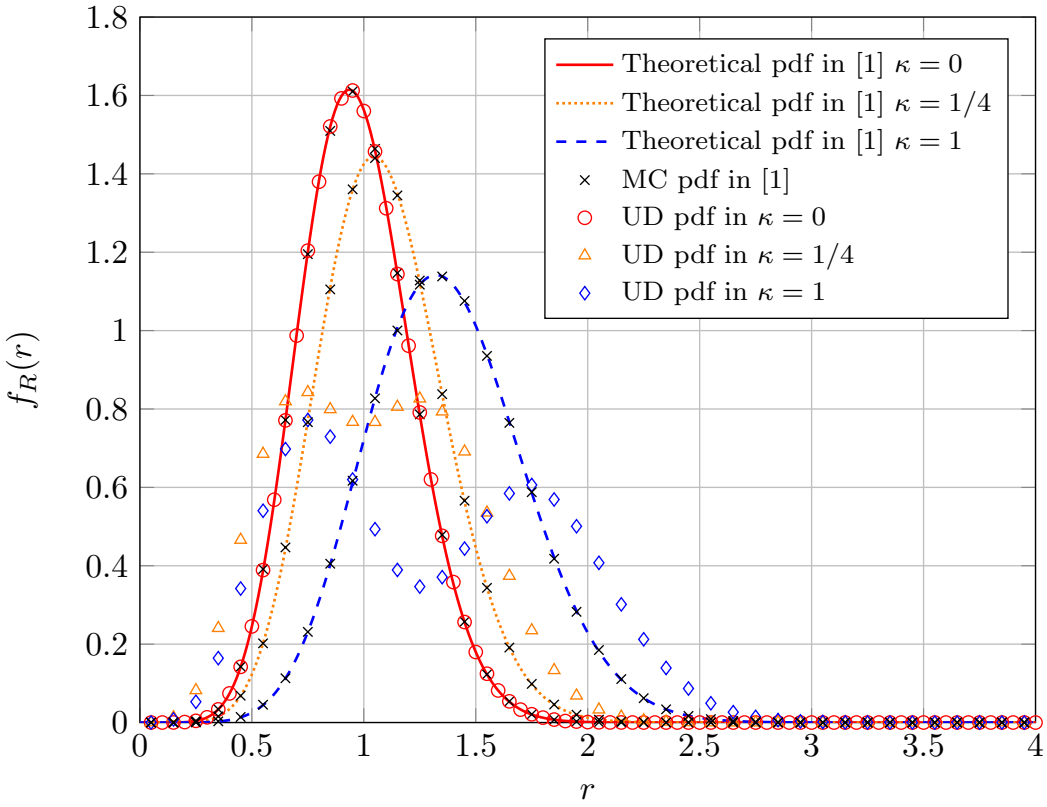

FIGURE 3.3: Comparison between the MC simulated UD in [67], the simulated original model presented in [52] and the theoretical pdf of the κ-μ shadowed distribution for different values of the parameter κ and fixed $\mu = 4$, $m = 4$.

assumed to be [67, eq. (1)], the UD is not the κ-μ shadowed distribution, except for the value $\kappa = 0$, which corresponds to the Nakagami-m case.

Note that when considering the correction described in Section 3.3.3, the results of the UD model in [67] and the original model in [52] would be equivalent.

Therefore, if the underlying statistical model presented in [67] is assumed, the subsequent pdf presented therein cannot be regarded as a κ-μ shadowed distribution, simply because the conditional statistical model from which it is derived does not follow the κ-μ distribution. In fact, the correct derivation of the κ-μ shadowed pdf can be found in [52], where a generalization of the Yacoub cluster model [29] is presented. Nonetheless, we point out that if the signal model proposed in [52] is used in place of [67, eq. (1)], the subsequent

derivations and statistics presented therein are completely correct and valid.

Some other relevant remarks arising from the results here presented are:

- The underlying statistical model originally proposed in [67] corresponds to another type of distribution which includes the Nakagami-m and the Rician shadowed models as particular cases, together with the Rayleigh, Rician and one-sided Gaussian, which are particular cases of the Rician shadowed model. However, the κ-μ shadowed distribution, whose pdf is defined in [52], [67], is not included in the statistical model in [67] and restated in (3.31).

- The underlying statistical model in [67] belongs to a family of bimodal distributions which are useful in many scenarios. Some examples are the generalized diffuse scatter plus LOS fading channel model [70], the Two-Wave with Diffuse Power fading model [71], the Generalized Two-Ray fading model [72], and the Fluctuating Two-Ray fading model [73].

- The derivation of the pdf for the statistical model proposed in [67] remains an open problem. Given that the pdfs of the models in [70]–[72] have complicated forms even in the absence of shadowing, it is expected that the pdf of interest has a very complicated form.

- We reiterate that the statistics presented in [67] can be made fully compliant with the κ-μ shadowed model provided that the model proposed in [52] is used as a starting point for defining the received signal amplitude.

- As a final note, it is worth highlighting that the works presented in [52] and [67] have both illustrated the significance of the κ-μ shadowed model. Through important empirical studies they have demonstrated the existence of this fading phenomena in real-life applications.

3.4 Conclusions

In this chapter, a brief overview of the fading channel models employed throughout this thesis has been provided. We have presented classical and generalized fading distributions, commonly used to characterize the small-scale variations of the signal, as well as the large-scale variations of the line-of-sight component. Also, the terminology and notation regarding the statistical functions for the characterization of these fading models have been introduced.

Besides, the κ-μ shadowed fading distribution [52], a recent and very general fading distribution which includes some classical distributions here presented as particular cases, as well as the generalized Rician shadowed [65] and κ-μ [29], has been introduced. Moreover, we have addressed a discrepancy between two underlying models that were available in the literature. We have shown that the underlying model proposed in [67] cannot be seen as a κ-μ shadowed model, but it belongs to a family of bimodal distributions similar to the one presented in [70] by Beaulieu and Saberali.

Chapter 4

Unifying the κ-μ and η-μ Fading Models

This chapter shows that the κ-μ shadowed distribution unifies the set of classical fading models associated with the κ-μ distribution, and strikingly, it also unifies set of classical fading models associated with the η-μ distribution. Particularly, it reveals that the Nakagami-q model can be obtained as a particular case of the Rician shadowed model proposed in [65], which may seem counterintuitive at first glance. In addition to a formal mathematical proof of how the chief probability functions introduced by Yacoub originate from the ones derived by Paris, we also establish new underlying Gaussian models for the κ-μ shadowed distribution that illustrate these mathematical derivations. In fact, we propose a novel method to derive the Nakagami-q and the η-μ distributions which consists of using the shadowing of the dominant components to recreate a power imbalance between the real and imaginary parts of the scattering components. This connection, which is here proposed for the first time in the literature, has important implications in practice: first, and contrary to the common belief, it shows that the κ-μ and η-μ fading distributions are connected. Hence we can jointly study the κ-μ and η-μ fading models by using a common approach instead of separately. Besides, it implies that when deriving any performance metric for the κ-μ shadowed fading model, we are actually solving the same problem for the κ-μ distribution

and, more importantly, for the η-μ distribution at no extra cost.

Leveraging our novel approach, we also derive here simple and closed-form asymptotic expressions for the ergodic capacity of communication systems operating under κ-μ shadowed fading in the high SNR regime, which can be evidently employed for the κ-μ and η-μ distributions. Unlike the exact analyses available in the literature which require the use of the Meijer G- and bivariate Meijer G-functions, our results allow for a better insight into the effects of the fading parameters on the capacity.

This chapter is organized as follows. Firstly, we introduce new underlying Gaussian models for the κ-μ shadowed model in Section 4.1. Secondly, we present the unification of the κ-μ and η-μ fading models in Section 4.2. Then, we unify the ergodic capacity analysis of the κ-μ shadowed, κ-μ and η-μ models, as well as their particular cases in Section 4.3. Finally, numerical results are provided in Section 4.4.

4.1 New κ-μ Shadowed Underlying Models

4.1.1 Generalized Model with the Same Shadowing for All the Clusters

Paris model in (3.28) clearly separates the real and imaginary scattering components, so that the model is defined by only using real RVs. If we use complex RVs, we can reformulate it as

$$\alpha^2 = \sum_{i=1}^{\mu} |Z_i + \xi\rho_i|^2, \tag{4.1}$$

where Z_i and ρ_i can be related to the variables of the previous model in form of $Z_i = X_i + jY_i$ and $\rho_i = p_i + jq_i$. Hence, $Z_i \sim \mathcal{CN}(0, 2\sigma^2)$ represents the scattering wave of the i-th cluster and $|\widetilde{\rho}_i|^2$ is the deterministic dominant power

of the ith cluster.

Observing (4.1), a straightforward generalization of the model in (3.28) is to consider a complex shadowing component, so that we obtain the following model

$$\Omega_1 = \sum_{i=1}^{\mu} |Z_i + \widetilde{\xi}\rho_i|^2, \tag{4.2}$$

where $\widetilde{\xi}$ is now a complex random variable, with $|\widetilde{\xi}|^2 \sim \Gamma(m, m)$ and arbitrary phase. Indeed, we are relaxing the assumption of the model in (3.28) because the real and imaginary parts of $\widetilde{\xi}$ do not need to be Nakagami-m distributed, but instead the power $|\widetilde{\xi}|^2$ has to be Gamma distributed, i.e., $|\widetilde{\xi}|$ has to be Nakagami-m distributed. This new model obviously represents a similar scenario as the model in (3.28), since all the clusters suffer from the same shadowing $\widetilde{\xi}$.

Let $\gamma_1 = \bar{\gamma}_1\Omega_1/\bar{\Omega}_1$, with $\bar{\gamma}_1 = \mathbb{E}[\gamma_1]$, be the instantaneous SNR per symbol of the model in (4.2). The pdf of γ_1 is derived thanks to Proposition 2.3, such as Ω_1 follows a κ-μ shadowed distribution, where $\kappa = \sum_{i=1}^{\mu} |\rho_i|^2/(2\sigma^2\mu)$. The parameter μ can be extended to the real numbers despite (4.2) loses its significance.

In fact, we have proved that the distribution of the model is independent of the phase of the shadowing component $\widetilde{\xi}$. In the next section, we propose another underlying model for the κ-μ shadowed distribution.

4.1.2 Generalized Model with I.I.D. Shadowing

In general, all the clusters could suffer from different shadowing effects, so the instantaneous received power can be expressed as

$$\Omega_2 = \sum_{i=1}^{\mu} |Z_i + \widetilde{\xi}_i\rho|^2, \tag{4.3}$$

where $Z_i \sim \mathcal{CN}(0, 2\sigma^2)$; $|\rho|^2$ is the power of each dominant component; and $\widetilde{\xi}_i$ is a complex random variable which represents the shadowing component of the i-th cluster, where $\widetilde{\xi}_i$ are i.i.d. $\sim \Gamma(\hat{m}, \hat{m})\ \forall i$.

Actually, these propagation conditions are likely to occur in real scenarios where the dominant components of different clusters could travel through different paths that are separated enough to suffer from independent large-scale propagation effects. However, our study is restricted to scenarios which present the same power ρ for each shadowed dominant component, since considering different dominant component powers for each cluster would lead to a distribution even more general than the κ-μ shadowed distribution. Moreover, this assumption allows us to connect the η-μ distribution with the κ-μ shadowed distribution, and is in accordance with the definition of η-μ channel, where every cluster exhibits the same ratio between the real and imaginary powers of the scattering waves [29].

Let $\gamma_2 = \bar{\gamma}_2 \Omega_2 / \bar{\Omega}_2$, with $\bar{\gamma}_2 = \mathbb{E}[\gamma_2]$, be the instantaneous SNR per symbol of the model in (4.3). Then, γ_2 is, by virtue of Proposition 2.4, κ-μ shadowed-distributed with $\kappa = |\rho|^2/(2\sigma^2)$, $m = \mu \cdot \hat{m}$. Again, μ can be extended to the real numbers.

The different shadowing components $\widetilde{\xi}_i$ do not have to be identically distributed to complete the proof. All that is needed is that the normalized rate parameter β_i/m_i of each shadowing power $|\widetilde{\xi}_i|^2$ must be equal $\forall i$. Although from a mathematical point of view this is a valid model, this scenario is hard to imagine in practical conditions. Therefore, we will restrict ourselves to the case with i.i.d. shadowing components.

Therefore, the SNRs of both underlying models presented in (4.2) and (4.3) follow a κ-μ shadowed distribution. The closed-form expressions for the cdf and the mgf can be found in [52].

4.2 κ-μ and η-μ Unification

In the previous section, we have introduced two different underlying models which lead to the κ-μ shadowed distribution. Now, we mathematically show how each of these models reduces to the general κ-μ and η-μ fading distributions, respectively. By doing so, we show that the κ-μ shadowed distribution can unify all classical fading models, both for scattering waves that have a perfect balance or an imbalance between their real and imaginary components, and their most general counterparts.

4.2.1 κ-μ Distribution and Particular Cases

The κ-μ distribution is employed in environments where the scattering for each cluster can be modeled with a circularly-symmetric random variable. The derivation of the κ-μ distribution from the κ-μ shadowed can be performed with the help of Corollary 2.5, when $m \to \infty$.

The κ-μ distribution is actually derived by completely eliminating the shadowing of each dominant component, which can be done by taking $m \to \infty$, so that the dominant component of each cluster becomes deterministic. As the parameter m grows, the pdf of each dominant component is gradually compressed and, at the limit $m \to \infty$, it becomes a Dirac delta function. Thus, the model is defined by a circularly symmetric complex random variable with some non-zero mean in each cluster, so that we obtain the κ-μ model, whereas in case that $\mu = 1$ we have the Rician fading model.

In turn, the Nakagami-m underlying model can be derived from (4.2) when $\kappa \to 0$ with the help of Corollary 2.6 and the change of variables $\gamma_1 = \bar{\gamma}_1 \Omega_1 / \bar{\Omega}_1$, with $\bar{\gamma}_1 = \mathbb{E}[\gamma_1]$, be the instantaneous SNR of the model in (4.2). We then get $\gamma_1 \sim \Gamma(\mu, \mu/\bar{\gamma}_1)$.

By tending $\kappa \to 0$, we eliminate all the dominant components of the model, regardless of the value of the shadowing parameter m, so that we only

have scattering components in each cluster, i.e., we obtain a model which follows a Nakagami-m distribution or one of its particular cases, Rayleigh or one-sided Gaussian models, depending on the value of μ.

4.2.2 η-μ Distribution and Particular Cases

The Nakagami-q (Hoyt) and the η-μ distributions are employed in propagation conditions environments where the scattering model is non-uniform and can be modeled by elliptical (or non-circularly symmetric) Gaussian RVs. At first glance, such scenario does not seem to fit with the κ-μ shadowed fading model. However, we can give a different interpretation to the cluster components of the model in (4.3): they can be interpreted as a set of uniform scattering waves with random averages. These random fluctuations in the average, which are different for each cluster, are responsible for modeling the non-homogeneity of the environment considered in [29] and ultimately lead to breaking the circular symmetry of the scattering model. We must note that a similar connection was inferred in [23], where the squared Nakagami-q distribution was shown to behave as an exponential distribution with randomly varying average power.

The circular symmetry of the model can be broken by using the result of Corollary 2.7, such as $\gamma_2 = \bar{\gamma}_2\Omega_2/\bar{\Omega}_2$, with $\bar{\gamma}_2 = \mathbb{E}[\gamma_2]$, being the instantaneous SNR of the model in (4.3), is η-μ-distributed when $m = \mu/2$, with parameter $\eta = 1/(2\kappa + 1)$.

Hence, we have shown that the η-μ fading distribution arises as a particular case of the more general κ-μ shadowed model. This is one of the main results of this thesis. Notice that, when $m = \mu/2 = 0.5$, we obtain the Nakagami-q model with shape parameter $q = \sqrt{\frac{1}{2\kappa+1}}$ since $\eta = q^2$ for η-μ format 1 [29][1]. Thus, the Nakagami-q model can be obtained from the Rician

[1]The η-μ fading model (format 1) is symmetrical for $\eta \in [0, 1]$ and $\eta \in [1, \infty]$. We have $q = \sqrt{\eta}$ or $q = 1/\sqrt{\eta}$ depending on the interval.

shadowed proposed in [65] by setting $m = 0.5$.

Although an interpretation of this result is not straightforward, it is clear, from a mathematical point of view, that if we fix the m parameter to half the value of the number of cluster μ in the κ-μ shadowed distribution, we obtain the η-μ distribution[2]. In order to give further insights of this result, we use the following example to illustrate what may happen in the model of (4.3) when $m = \mu/2$, i.e., when $\hat{m} = 0.5$. Let us consider that each shadowing component of the model in (4.3) can be expressed as $\widetilde{\xi}_i = x_i \cdot e^{j\phi}$, where $x_i \sim \mathcal{N}(0, 1)$, so that $|\widetilde{\xi}_i|^2 \sim \Gamma(1/2, 1/2)$, i.e., $\hat{m} = 0.5$. When we consider the simplest case on which the phase of $\widetilde{\xi}_i\rho$ is deterministic and set to zero, then $\widetilde{\xi}_i\rho$ becomes a real Gaussian random variable. Thus, in each cluster, we are adding the real Gaussian random variable $\widetilde{\xi}_i\rho$ to the complex Gaussian random variable Z_i, which is equivalent to have a unique complex Gaussian random variable with different power in its real and imaginary parts in each cluster, so that the circular symmetry of the model is broken. In the general case of an arbitrary phase for $\widetilde{\xi}_i\rho$, the circular symmetry would be broken in a direction of the complex plane different from the real axis.

Once m being fixed, the number of degree of freedoms is reduced by one and the following bi-unique relationship between κ and η is established,

$$\kappa = \frac{1 - \eta}{2\eta}. \tag{4.4}$$

This mathematical relationship between κ and η only has a clear meaning in the limit cases of the range where κ varies. For $\kappa = 0$, we obtain $\eta = 1$ from the (4.4), which actually corresponds to the Rayleigh case when there is only one cluster. For $\kappa \to \infty$, we have $\eta = 0$ from the (4.4), which is the one-sided Gaussian case when we again have one cluster. Therefore, while the κ-μ model in Section IV.A is obtained by totally eliminating the randomness

[2]We underline the fact that the number of clusters in the κ-μ model, and so in the κ-μ shadowed model, is μ, while 2μ is the number of clusters in the η-μ model [29].

of the shadowing component, this is not the case for the η-μ fading model.

The Nakagami-m model can be also deduced from the κ-μ shadowed model of (4.3) with a similar method, i.e., without eliminating directly the dominant component.

Let $\gamma_2 = \bar{\gamma}_2\Omega_2/\bar{\Omega}_2$, with $\bar{\gamma}_2 = \mathbb{E}[\gamma_2]$, be the instantaneous SNR of the model in (4.3). If $m = \mu$, we have $\gamma_2 \sim \Gamma(\mu, \mu/\bar{\gamma}_2)$ by virtue of Corollary 2.8.

Notice that by setting $m = \mu$, we transform the i.i.d. random dominant components of the (4.3) into scattering components. Since $m = \mu \cdot \hat{m}$, then we are setting $\hat{m} = 1$. For giving an intuitive explanation, let assume the particular case that the i-th random dominant component is a Gaussian random variable when $\hat{m} = 1$. Thus, we are adding two Gaussian RVs together in each cluster, which straightforwardly leads to an equivalent Gaussian random variable, so that the one-sided Gaussian, Rayleigh or Nakagami-m models are obtained depending on the number of clusters μ considered. Very interestingly, the model in (4.3) allows us to obtain the particular models aforementioned with a shadowing which may not be complex Gaussian distributed when $\hat{m} = 1$, or real Gaussian distributed when $\hat{m} = 0.5$, since the distribution of the model does not depend on the phase of the shadowing components, as we have proved in Proposition (2.3) and Proposition (2.4).

The table 4.1 summarizes all the models that are derived from the κ-μ shadowed fading model, where the κ-μ shadowed model parameters are underlined for the sake of clarity. When the κ-μ shadowed parameters are fixed to some specific real positive values or tend to some specific limits, we can obtain all the classical central models, i.e., the Rayleigh, one-sided Gaussian, Nakagami-q and Nakagami-m models, the classical noncentral Rician fading model, and their general counterparts, the Rician shadowed, κ-μ and η-μ fading models.

TABLE 4.1: Classical and Generalized Models Derived from the κ-μ Shadowed Fading

Channels	κ-μ Shadowed Parameters
One-sided Gaussian	a) $\underline{\mu} = 0.5$, $\underline{\kappa} \to 0$ b) $\underline{\mu} = 0.5$, $\underline{m} = 0.5$
Rayleigh	a) $\underline{\mu} = 1$, $\underline{\kappa} \to 0$ b) $\underline{\mu} = 1$, $\underline{m} = 1$
Nakagami-m	a) $\underline{\mu} = m$, $\underline{\kappa} \to 0$ b) $\underline{\mu} = m$, $\underline{m} = m$
Nakagami-q (Hoyt)	$\underline{\mu} = 1$, $\underline{\kappa} = (1-q^2)/2q^2$, $\underline{m}$ = 0.5
Rician with parameter K	$\underline{\mu} = 1$, $\underline{\kappa} = K$, $\underline{m} \to \infty$
κ-μ	$\underline{\mu} = \mu$, $\underline{\kappa} = \kappa$, $\underline{m} \to \infty$
η-μ	$\underline{\mu} = 2\mu$, $\underline{\kappa} = (1-\eta)/2\eta$, $\underline{m} = \mu$
Rician shadowed	$\underline{\mu} = 1$, $\underline{\kappa} = K$, $\underline{m} = m$

It is remarkable that there are two ways for deriving the one-sided Gaussian, Rayleigh and Nakagami-m models, depending on whether the approaches in Section 4.2.1 or Section 4.2.2 are used.

4.3 Ergodic Capacity Analysis

The characterization of the ergodic channel capacity in wireless systems subject to fading, defined as

$$\bar{C}[\text{bps/Hz}] \triangleq \int_0^{+\infty} \log_2(1+\gamma) f_\gamma(\gamma) d\gamma, \tag{4.5}$$

where γ is the instantaneous SNR at the receiver side, has been a matter of interest for many years [74]–[77]. While for the case of Rayleigh fading it is possible to obtain relatively simple closed-form expressions for the capacity,

the consideration of more general fading models [25], [77], [78] leads to very complicated expressions that usually require the use of Meijer G-functions.

In order to overcome the limitation of the exact characterization of κ-μ shadowed channel capacity due to its complicated closed-form [78], it seems more convenient to analyze the high-SNR regime. In this situation, the ergodic capacity can be approximated by [53, eq. (8)]

$$\bar{C}(\bar{\gamma})|_{\bar{\gamma}\Uparrow} = \log_2(\bar{\gamma}) - L, \tag{4.6}$$

which is asymptotically exact and where L is a constant value independent of the average SNR that can be given by

$$L = -\log_2(e)\frac{d}{dt}\frac{\mathbb{E}[\gamma^t]}{\bar{\gamma}^t}\Big|_{t=0}. \tag{4.7}$$

The parameter L can be interpreted as the capacity loss with respect to the AWGN case, since the presence of fading causes $L > 0$. When there is no fading, $L = 0$ and this reduces to the well-known Shannon result. Using this approach, we derive a simple closed-form expression for the asymptotic capacity of the κ-μ shadowed model, which is a new result in the literature.

Thanks to Theorem 2.9, the ergodic capacity of a wireless link subject to κ-μ shadowed fading can be accurately lower-bounded in the high-SNR regime by

$$\bar{C}_{\kappa\mu m}(\bar{\gamma})|_{\bar{\gamma}\Uparrow} = \log_2(\bar{\gamma}) - L_{\kappa\mu m}, \tag{4.8}$$

where $\log_2(\cdot)$ is the binary logarithm, $\bar{\gamma}$ is the average SNR at the receiver side, i.e. $\bar{\gamma} = \mathbb{E}[\gamma]$, and $L_{\kappa\mu m}$ can be expressed as

$$\begin{aligned} L_{\kappa\mu m} = &- \log_2(e)\psi(\mu) - \log_2\left(\frac{\mu\kappa + m}{\mu m(1+\kappa)}\right) \\ &+ \log_2(e)\frac{\kappa(\mu - m)}{\mu\kappa + m} \\ &\times_3 \mathcal{F}_2\Big(1, 1, \mu - m + 1; 2, \mu + 1; \frac{\mu\kappa}{\mu\kappa + m}\Big). \end{aligned} \tag{4.9}$$

Notice that when $\mu = 1$, we obtain the asymptotic ergodic capacity of the Rician shadowed channel proposed in [65].

As opposed to the exact analysis in [78], which requires for the evaluation of a bivariate Meijer G-function, Theorem 2.9 provides a very simple closed-form expression for the capacity in the high-SNR regime. More interestingly, since the κ-μ and η-μ fading models are but particular cases of the κ-μ shadowed distribution, we also obtain the capacity in these scenarios without the need of evaluating an infinite sum of Meijer G-functions as in [25]. This is formally stated as follow.

In the high-SNR regime, the ergodic capacity of a κ-μ channel can be accurately lower-bounded by

$$\bar{C}_{\kappa\mu}(\bar{\gamma})|_{\bar{\gamma}\Uparrow} = \log_2(\bar{\gamma}) - L_{\kappa\mu}, \tag{4.10}$$

where $L_{\kappa\mu}$ can be expressed as

$$\begin{aligned} L_{\kappa\mu} = &- \log_2(e)\psi(\mu) + \log_2(\mu) + \log_2(1+\kappa) \\ &- \kappa\log_2(e)\,{}_2\mathcal{F}_2\Big(1, 1; 2, \mu + 1; -\mu\kappa\Big). \end{aligned} \tag{4.11}$$

(4.11) is derived by applying the limit $m \to \infty$ in (4.9), so that the ${}_3\mathcal{F}_2(\cdot)$ collapses in a ${}_2\mathcal{F}_2(\cdot)$ hypergeometric function since

$$\lim_{c\to\infty}\ {}_3\mathcal{F}_2(a_1, a_2, c; b_1, b_2; \frac{z}{c}) = \ {}_2\mathcal{F}_2(a_1, a_2; b_1, b_2; z). \tag{4.12}$$

In the high-SNR regime, the ergodic capacity of an η-μ channel can be accurately lower-bounded by

$$\bar{C}_{\eta\mu}(\bar{\gamma})|_{\bar{\gamma}\Uparrow} = \log_2(\bar{\gamma}) - L_{\eta\mu}, \tag{4.13}$$

where $L_{\eta\mu}$ can be expressed as

$$\begin{aligned} L_{\eta\text{-}\mu} = &- \log_2(e)\psi(2\mu) + \log_2(\mu) + \log_2(1+\eta) \\ &+ \log_2(e)\frac{(1-\eta)}{2}\,{}_3\mathcal{F}_2\big(1,1,\mu+1;2,2\mu+1;1-\eta\big). \end{aligned} \tag{4.14}$$

We have obtain the η-μ asymptotic capacity loss from (4.9) by setting $\underline{m}=\mu$, $\underline{\mu}=2\mu$ and $\underline{\kappa}=\frac{1-\eta}{2\eta}$ as Table 4.1 indicates.

Hence, the expressions of the κ-μ and η-μ asymptotic capacities have been jointly deduced from the result in (4.10), which are also new results. Moreover, deriving the asymptotic capacity of the κ-μ shadowed has not been harder than deriving the κ-μ or η-μ asymptotic capacities directly, since the κ-μ and η-μ moments are expressed, like in the κ-μ shadowed case, in terms of a Gauss hypergeometric function [29]. Thus, we are hitting two (actually three) birds with one stone.

Using the equivalences in Table 4.1, we can obtain even simpler expressions for classical fading models which reduce to existing results in the literature, for Nakagami-m [53], Rician [72] and Hoyt [23]. For the sake of clarity, we omit the straightforward derivations of the rest of asymptotic capacities. Instead, we summarize in Table 4.2 their capacity losses with respect to the AWGN channel in the high-SNR regime, where $\Gamma(a,b)$ is the incomplete gamma function and γ_e is the Euler-Mascheroni constant, i.e., $\gamma_e \approx 0.5772$. It is also remarkable that, for the first time, we give the asymptotic capacity expression of the Rician shadowed proposed in [65], which is but a particular case of the κ-μ shadowed model when $\mu = 1$.

TABLE 4.2: Ergodic Capacity Loss in the High-SNR Regime for Different Channels

Channels	Ergodic capacity loss (L) [bps/Hz]
One-sided Gaussian	$1+\gamma_e \cdot \log_2(e) \approx 1.83$
Rayleigh	$\gamma_e \cdot \log_2(e) \approx 0.83$
Nakagami-m	$\log_2(m) - \log_2(e)\psi(m)$
Nakagami-q (Hoyt)	$1+\gamma_e \cdot \log_2(e) + \log_2\left(\frac{1+q^2}{(1+q)^2}\right)$
Rician with parameter K	$\log_2(1+1/K) - \log_2(e)\Gamma(0,K)$
κ-μ	$-\log_2(e)\psi(\mu) + \log_2(\mu) + \log_2(1+\kappa)$ $-\kappa\log_2(e)_2\mathcal{F}_2\Big(1,1;2,\mu+1;-\mu\kappa\Big)$
η-μ	$-\log_2(e)\psi(2\mu) + \log_2(\mu)$ $+\log_2(1+\eta) + \log_2(e)\frac{(1-\eta)}{2}$ $\times_3\mathcal{F}_2\big(1,1,\mu+1;2,2\mu+1;1-\eta\big)$
Rician shadowed	$\gamma_e \cdot \log_2(e)$ $-\log_2\left(\frac{K+m}{m(1+K)}\right) + \log_2(e)\frac{K(1-m)}{K+m}$ $\times_3\mathcal{F}_2\Big(1,1,2-m;2,2;\frac{K}{K+m}\Big)$

4.4 Numerical Results

We now study the evolution of the capacity loss for the κ-μ shadowed, κ-μ and η-μ fading models with respect to the AWGN case. We underline the fact that the different parameter values here presented do not come from real practical channels, but allow the theoretical expressions to be verified.

Depending on the propagation conditions, the parameters κ and μ can take very different values [52], [67], [79]–[81]. For instance, in some underwater acoustic communication scenarios [79], the channel parameters $\kappa \in [0.03 - 9.56]$, $\mu \in [0.90 - 1.27]$ and $m \in [1.32 - 18.01]$, while in some body centric communication scenarios [67], [80], [81], we have $\kappa \in [1.08 - 481]$, $\mu \in [0.01 - 3.22]$ and $m \in [0.04 - 2876]$.

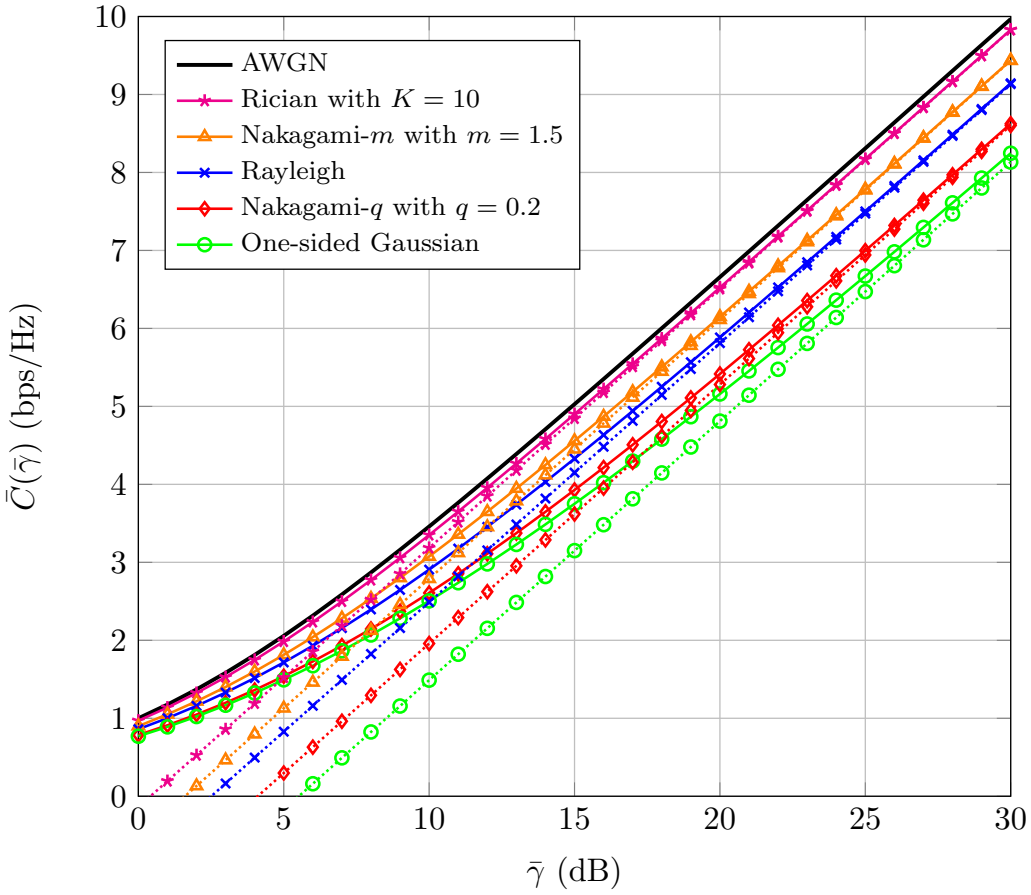

FIGURE 4.1: Comparison of classical channel ergodic capacities with their asymptotic values in the high-SNR regime.

In Fig. 4.1 and Fig. 4.2, we plot the exact theoretical expressions of the ergodic capacity of the classical and generalized fading models, respectively, which are readily available in the literature [25], [78], and we compare them to the asymptotic theoretical expressions obtained in (4.8-4.13).

We observe that all the models converge accurately to their asymptotic capacity values, remaining below the Shannon limit, i.e, the capacity of the AWGN channel. Therefore, the asymptotic ergodic capacity expression derived in (4.10) for the κ-μ shadowed model is here validated with the one-sided Gaussian, Rayleigh, Nakagami-m, Nakagami-q, Rician, Rician shadowed, κ-μ and η-μ ergodic capacities in the high-SNR regime.

In Figs. 4.3-4.6, we show the evolution of the κ-μ shadowed asymptotic capacity loss L defined in (4.7) when m grows. Note that this metric does not

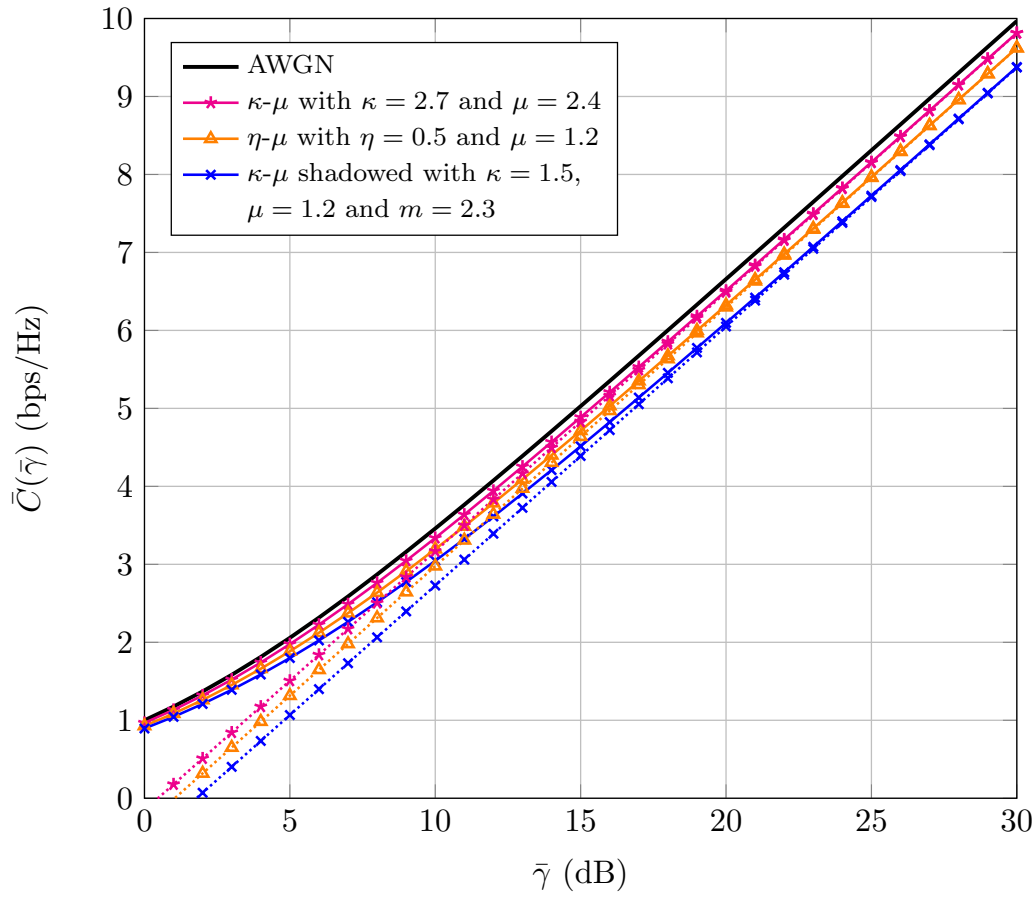

FIGURE 4.2: Comparison of generalized channel ergodic capacities with their asymptotic values in the high-SNR regime.

depend on the average received SNR $\bar{\gamma}$. When the shadowing cannot be negligible, i.e, in Figs. 4.3-4.5, having more power in the dominant components does not always improve the ergodic capacity, but sometimes raises considerably the capacity loss, especially for a great number of clusters. When $m \geq 20$, i.e., in Fig. 4.6, the shadowing can be neglected and the model actually tends to the κ-μ fading, where an increase in the power of the dominant components is obviously favorable for the channel capacity. Therefore, receiving more power through the dominant components does not always increase the capacity in the presence of shadowing. We observe two different behaviors in the capacity loss evolution with respect to the parameter κ. For $m < \mu$, increasing the parameter κ is detrimental for the capacity. Conversely, when $m > \mu$ the capacity is improved as κ is increased, i.e. in the

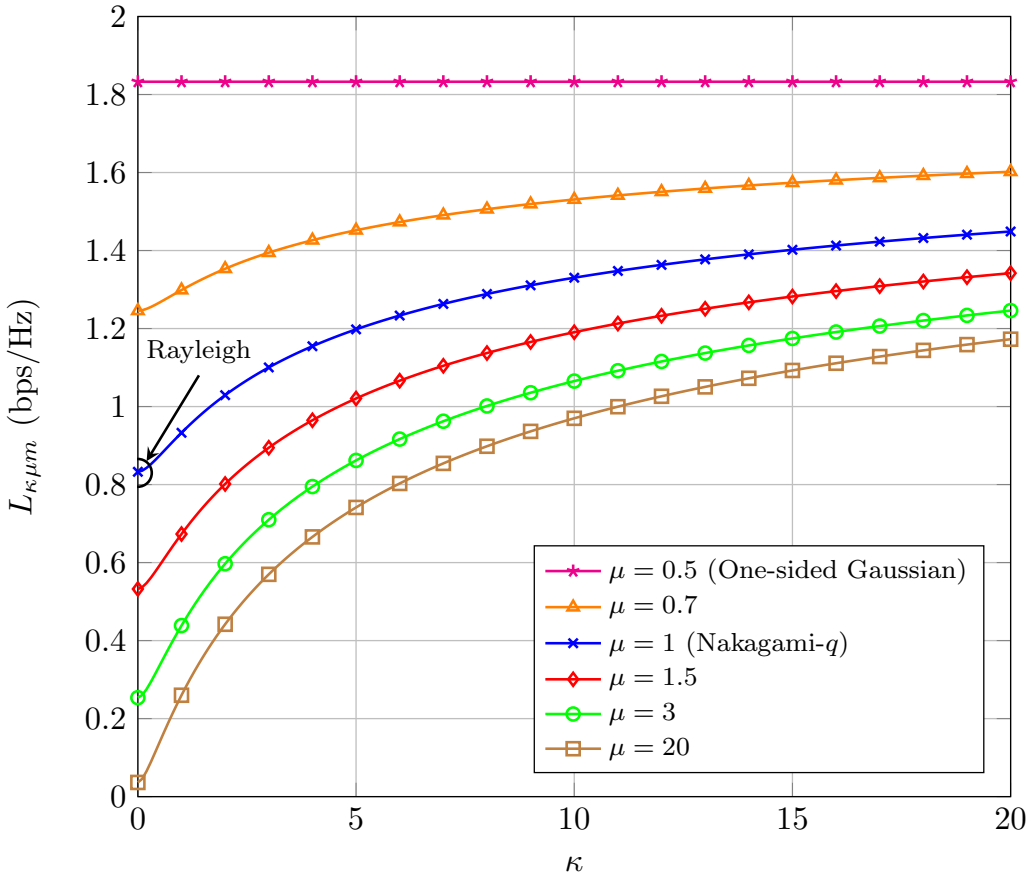

FIGURE 4.3: Evolution of the κ-μ shadowed ergodic capacity loss in the high-SNR regime for fixed $m = 0.5$.

presence of a stronger LOS component. In the limit case of $m = \mu$, we see that the capacity loss is independent of κ. We can explain this observation using again our model for i.i.d shadowing in (4.3), in a similar fashion as when the interpretation of the Corollary 2.7 and Corollary 2.8 was discussed. For $m = \mu$, we have $\hat{m} = 1$ since $m = \mu \cdot \hat{m}$. Let us assume that both the scattering and shadowed dominant components in each cluster are complex Gaussian RVs, which is the simplest possible case when $\hat{m} = 1$. We will obtain an equivalent Gaussian random variable whose power is not affected by the parameter κ. For $m > \mu$, the κ-μ shadowed model can be approximated by the κ-μ model for m sufficiently high, as Table 4.1 shows. In this case, it is straightforward to see that increasing the parameter κ implies decreasing the asymptotic capacity losses, since a higher LOS power implies improving

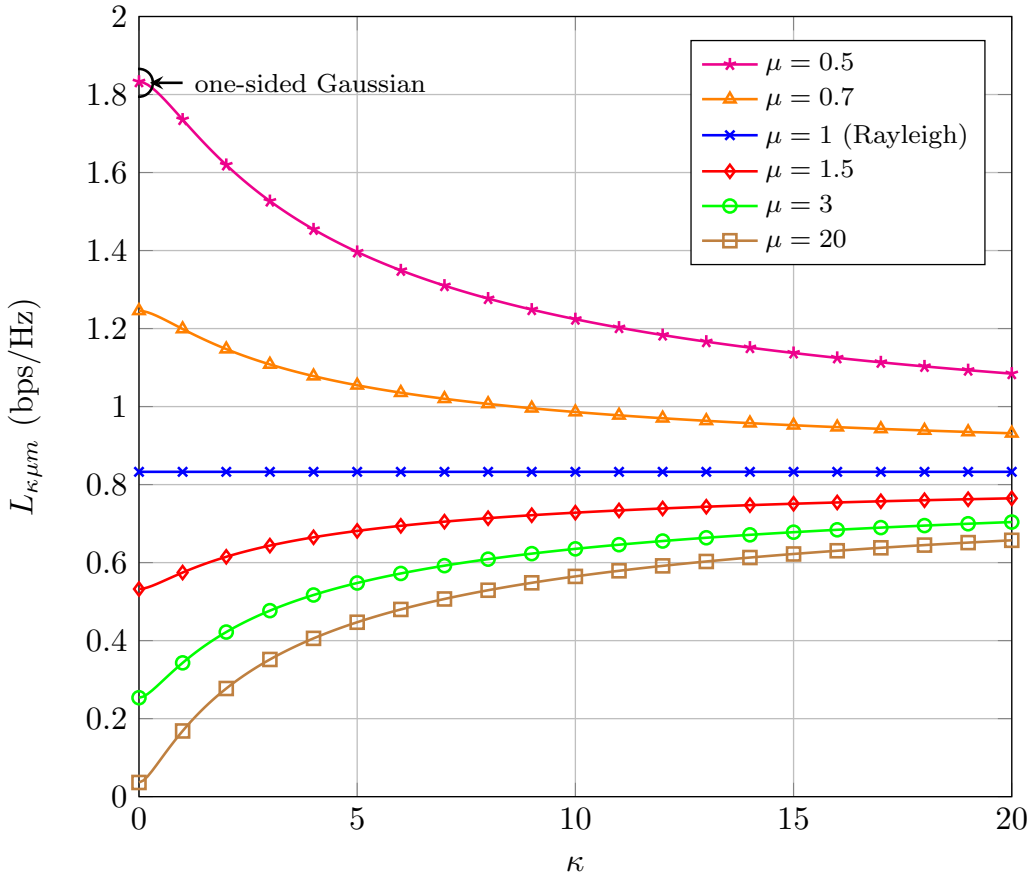

FIGURE 4.4: Evolution of the κ-μ shadowed ergodic capacity loss in the high-SNR regime for fixed $m = 1$.

the capacity of the κ-μ channel. Conversely, for $m < \mu$, the observation may seem counterintuitive at first glance. Let consider the particular case where $m = \mu/2$, which coincides with the η-μ case. In that case, increasing the parameter κ implies increasing the asymmetry of the non-circularly symmetric Gaussian underlying RVs of the model, which degrades the capacity. For the rest of cases where $m < \mu$, a similar justification can be done.

We also see that the capacity loss decreases as μ grows, since having a larger number of clusters reduces the fading severity of the small-scale propagation effects.

We have also marked in Figs. 4.3-4.6 some models that can be deduced from the κ-μ shadowed model. We can see them in the different legends and also at some specific points rounded by a circle in different curves.

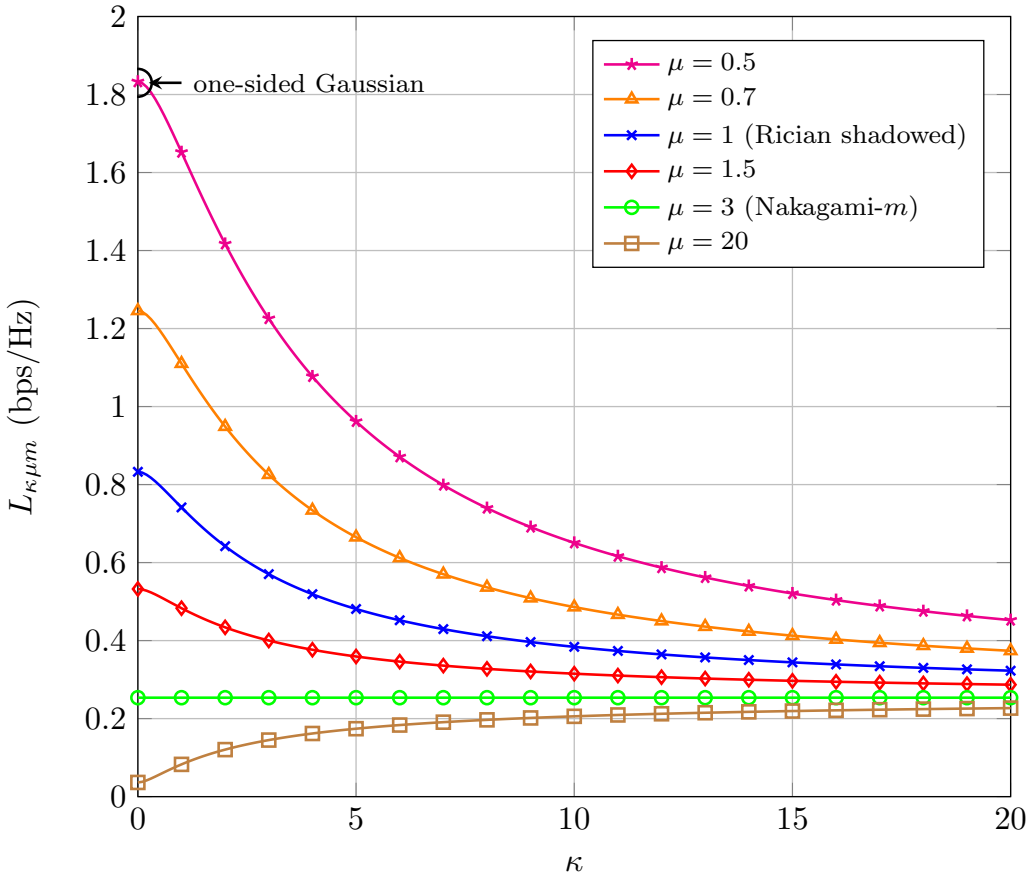

FIGURE 4.5: Evolution of the κ-μ shadowed ergodic capacity loss in the high-SNR regime for fixed $m = 3$.

Finally, Fig. 4.7 and Fig. 4.8 depict the asymptotic ergodic capacity loss for the κ-μ and η-μ fading models respectively. We observe that Fig. 4.7 is quite similar to Fig. 4.6 because, as mentioned before, the κ-μ shadowed model with $m \geq 20$ can be approximated by the κ-μ fading model. In Fig. 4.8, we see that, regardless of the number of clusters 2μ, there is a minimum in the channel capacity loss at $\eta = 1$ which divides in two symmetric parts the fading behavior as expected. It is also noticeable that in Fig. 4.8 we have specified the limit cases for $\eta \to 0$ and $\eta \to \infty$. When $\mu = 0.5$, the η-μ model collapses into the one-sided Gaussian model for $\eta = 0$ or $\eta \to \infty$, whereas for $\eta = 1$ it collapses into the Rayleigh model. When $\mu = 1$, the η-μ model is reduced to the Rayleigh one for $\eta = 0$ or $\eta \to \infty$. This is shown in the figure by including also the Rayleigh and one-sided Gaussian capacity loss values

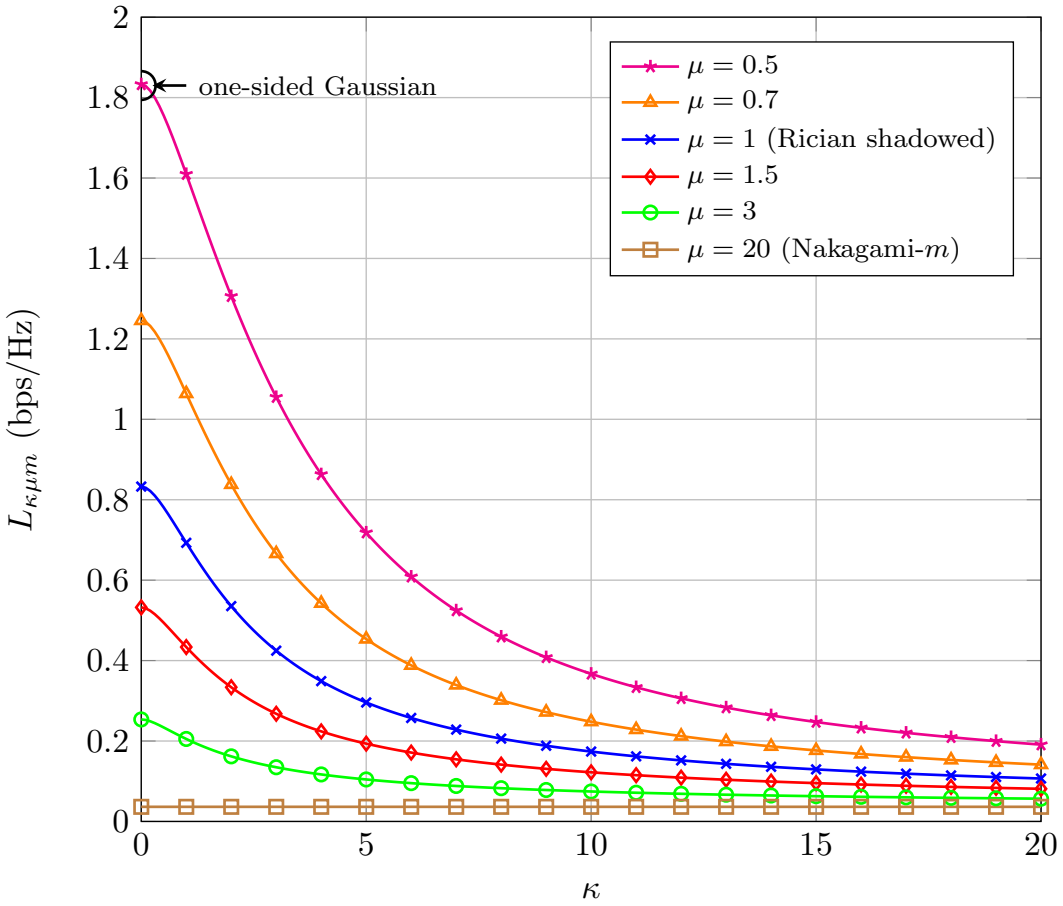

FIGURE 4.6: Evolution of the κ-μ shadowed ergodic capacity loss in the high-SNR regime for fixed $m = 20$.

with horizontal dotted and dashed lines respectively.

4.5 Conclusions

We have proved that the κ-μ shadowed model unifies the κ-μ and η-μ fading distributions. By a novel interpretation of the shadowing in the dominant components, we have shown that the κ-μ shadowed model can also be employed in scenarios where the scattering is modeled with noncircularly-symmetric complex Gaussian RVs, which gives the κ-μ shadowed distribution a stronger flexibility to model different propagation conditions than existing alternatives, when operating in wireless environments. Thus, the κ-μ shadowed model unifies all the classical fading models, i.e., the one-sided

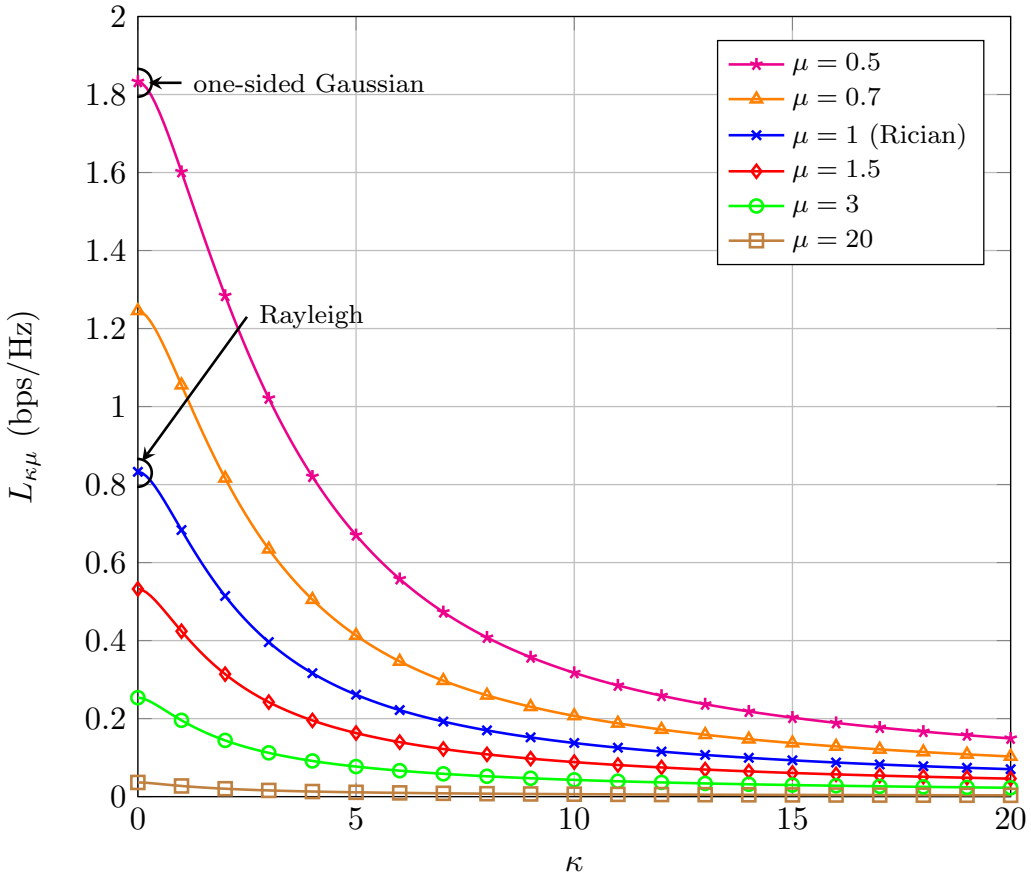

FIGURE 4.7: Evolution of the κ-μ ergodic capacity loss in the high-SNR regime.

Gaussian, Rayleigh, Nakagami-m, Nakagami-q and Rician fading channels, and their generalized counterparts, the κ-μ, η-μ and Rician shadowed fading models. Simple new closed-form expressions have been deduced to evaluate the ergodic capacity in the high-SNR regime for the κ-μ shadowed, and hence, using the connection here unveiled, for the simpler κ-μ, η-μ and Rician shadowed fading models, giving us clear insights into the contribution of the fading parameters on the capacity improvement or degradation.

As a closing remark, one can think of whether the name of κ-μ shadowed distribution is still appropriate for this model, since its flexibility transcends the original characteristics presented in [52].

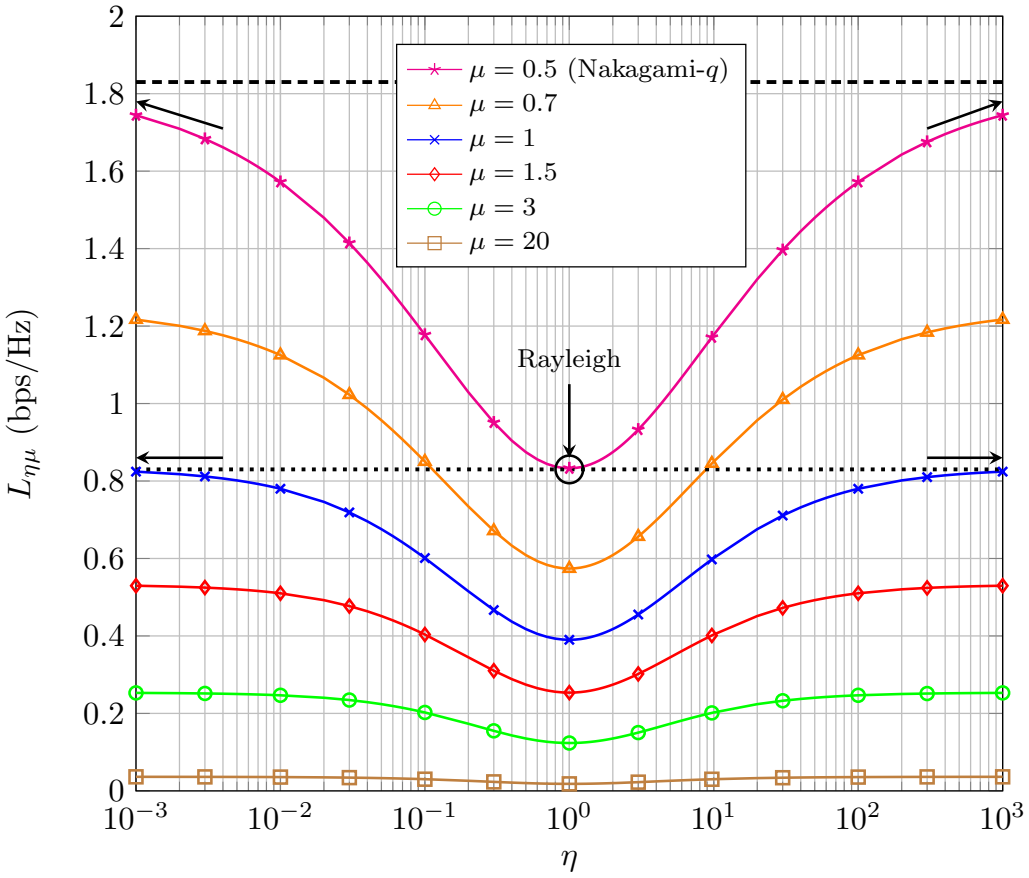

FIGURE 4.8: Evolution of the η-μ ergodic capacity loss in the high-SNR regime. The Rayleigh and the one-sided Gaussian capacity loss particular cases are also included in horizontal dotted and dashed lines respectively.

Chapter 5

Noncircularly-symmetric Wishart-type Matrices

When multiple antennas are present, the performance analysis of wireless systems becomes more challenging. The univariate analysis presented in this thesis does not hold. We must then employ a multivariate analysis which is framed in the theory of random matrices.

The study of the impact of MIMO diversity in the capacity of flat-fading NLOS channels was studied for a long while [82]–[84] and was finally analytically evaluated for single-side spatially correlated antennas in [85]. These analyses consider MIMO systems subject to the simplest possible fading environment, i.e., the Rayleigh fading, and require the statistical characterization of central complex Wishart matrices. MIMO systems subject to Rician fading environments were also deeply studied in the literature [86]–[88], showing that their performance analysis is much more complicated than those subject to Rayleigh fading, since they require the study of noncentral complex Wishart matrices.

However, in both Rayleigh and Rician environments, the scattering waves are considered to have a perfect power balance between the in-phase and the quadrature components. Considering a power imbalance between the in-phase and the quadrature components of the channel matrix is even more

challenging, since it requires the study of noncircularly-symmetric Wishart-type matrices, for which the way is not paved, and only few initial works are available [26], [28].

In this chapter, we propose a new approach to characterize noncircularly-symmetric Wishart-type matrices. By exploiting a novel statistical connection between these matrices and the well-known noncentral complex Wishart matrix, we derive an expression for the joint distribution of their entries, as well as exact expressions for the extreme eigenvalue distributions and an asymptotic expansion (in the tail) for the distribution of the largest eigenvalue, which provide new insights on the effects of the real-imaginary variance asymmetry of the underlying model of these matrices. We then use these expressions to study the performance of MIMO communication systems subject to Nakagami-q (Hoyt) fading. In particular, our analytical results explain the impact of the fading parameter q on the outage performance of MIMO systems with maximal ratio combining (MIMO-MRC).

This chapter is organized as follows. Firstly, we provide a context of the analysis of noncircularly-symmetric Wishart-type matrices in Section 5.1. Secondly, we present the novel statistically connection between these matrices and the well-known noncentral complex Wishart ones in Section 5.2. Thirdly, we present in Section 5.3 a new result for the pdf of noncircularly-symmetric Wishart-type matrices, as well as we discuss the derivation of the joint probability density function (jpdf) of the eigenvalues in [26]. Then, we give new exact expressions for the extreme eigenvalue distributions, as well as an asymptotic expansion in the left-hand tail for the largest eigenvalue distribution in Section 5.4. Finally, we analyze the outage performance of Hoyt-faded MIMO-MRC communications.

We must note that part of the work presented in this chapter has been done in collaboration with Matthew R. McKay, during my internship in HKUST. In particular, the study of the largest eigenvalue distribution has

been submitted to an IEEE journal for possible publication.

5.1 Context

Despite the rich characterization of the well-known complex and real Wishart matrices [4], [45], [47], [89], results for Wishart-type models generated from noncircularly-symmetric complex Gaussian matrices are far more scarce. In particular, we are interested in matrices of the form:

$$\mathbf{W} = \begin{cases} \mathbf{X}\mathbf{X}^{\dagger}, & p \leq n \\ \mathbf{X}^{\dagger}\mathbf{X}, & p > n \end{cases} \tag{5.1}$$

where $\mathbf{X} \in \mathbb{C}^{p \times n}$ has i.i.d. complex Gaussian entries with $\mathrm{Re}(\{\mathbf{X}\}_{i,j}) \sim \mathcal{N}(0, \sigma^2_{\mathrm{Re}})$ and $\mathrm{Im}(\{\mathbf{X}\}_{i,j}) \sim \mathcal{N}(0, \sigma^2_{\mathrm{Im}})$, i.e., with arbitrary variances in the real and imaginary parts, and where $\mathrm{Re}(\{\mathbf{X}\}_{i,j})$ and $\mathrm{Im}(\{\mathbf{X}\}_{i,j})$ are mutually independent.

The model in (5.1) has been referred to as the cross-over ensemble between the Laguerre unitary (LUE) and orthogonal (LOE) ensembles [26]. When both variances are equal, i.e. $\sigma^2_{\mathrm{Re}} = \sigma^2_{\mathrm{Im}}$, $\mathbf{W}$ is a central complex Wishart matrix (LUE); when one of the variances is zero, $\mathbf{W}$ is a central real Wishart matrix (LOE).

The works in [26] and [28] made initial progress to characterize the intermediate Wishart-type ensemble of (5.1). In [28], the analysis is restricted to a 2×2 matrix $\mathbf{X}$ and the jpdf of the eigenvalues of $\mathbf{W}$ is given in a very complicated form involving six integrals. In [26], the eigenvalue jpdf is derived for arbitrary dimensions by using Brownian motion properties with a fictitious time variable which is related to the ratio between the variances σ^2_{Re} and σ^2_{Im}. However, this expression is still complicated and does not allow for any further insightful analysis.

This context, where only two initial works analyze some statistics of $\mathbf{W}$, has pushed us to explore a novel approach, different from the ones given in [28] and [26], in order to facilitate the analysis of noncircularly-symmetric matrices. We explain this approach in the following section.

5.2 A Novel Statistical Connection

We first explain the reasons why the previous univariate statistical connection presented in this thesis and other related works cannot be directly extended to the multivariate case. Then, we present the novel statistical connection that will allow to tackle the statistical characterization of (5.1).

5.2.1 Can We Use Previous Univariate Connections?

Leveraging the statistical connections presented in Chapter 4 in the context of SISO communications, one first think to directly extend those results to the multivariate analysis, i.e., to connect the analysis of the Rician shadowed matrix model with that of the noncircularly-symmetric Wishart-type matrix defined in (5.1).

The Rician shadowed matrix model was studied in depth in [90] in the context of LMS communications, where fundamentally statistical results were provided for the so-called Gamma-Wishart matrices. Further results were presented in [91] to tackle the general double-correlated case. It seems then that we have a collection of results that could be helpful for the analysis of noncircularly-symmetric Wishart-type matrices, when one wants to extend the univariate analysis here presented to the multivariate case.

Nonetheless, in the context of random matrix theory, connecting noncircularly-symmetric underlying Gaussian models with the more tractable circularly-symmetric ones is not that simple. Denote $\mathbf{Z}$ the Gram matrix of a particular channel. The matrix $\mathbf{Z}$ is defined from the complex

channel matrix $\mathbf{H}$, such as $\mathbf{Z} = \mathbf{H}^{\dagger}\mathbf{H}$ or $\mathbf{Z} = \mathbf{H}\mathbf{H}^{\dagger}$, and represents a general Hermitian matrix whose diagonal elements are positive real RVs and off-diagonal elements are complex RVs. Since the work associated with the univariate analysis of this thesis only involves the norm or the square-norm of underlying Gaussian models, we can only provide a connection between the diagonal elements of $\mathbf{Z}$ and those of the well-known Gamma-Wishart matrix. Unfortunately, this partial connection does not allow to characterize noncircularly-symmetric Wishart-type matrices.

This same reason also discards the possibility of extending the univariate connection recently presented in [23], where a Nakagami-Hoyt RV can be generated from randomly perturbing the average power of a Rayleigh RV with a specific distribution [23].

5.2.2 A Non-Classical Multivariate Analysis: A Connection with the Complex Wishart Ensemble

In the model (5.1), it is convenient to rewrite $\mathbf{X}$ as

$$\mathbf{X} = \mathbf{X}_C + \mathbf{X}_R \tag{5.2}$$

where the matrices $\mathbf{X}_C \in \mathbb{C}^{p\times n}$ and $\mathbf{X}_R \in \mathbb{R}^{p\times n}$ are mutually independent with zero-mean i.i.d. entries. The entries $\{\mathbf{X}_C\}_{ij}$ are circularly-symmetric $\mathcal{CN}(0,\sigma_C^2)$, while $\{\mathbf{X}_R\}_{ij} \sim \mathcal{N}(0,\sigma_R^2)$ with the correspondence

$$\sigma_C^2 = 2\sigma_{\mathrm{Im}}^2\ , \qquad \sigma_R^2 = \sigma_{\mathrm{Re}}^2 - \sigma_{\mathrm{Im}}^2\ . \tag{5.3}$$

This redefinition of (5.1) will facilitate the subsequent analysis. Note that, albeit (5.2) imposes $\sigma_{\mathrm{Re}} \geq \sigma_{\mathrm{Im}}$, this does not imply any loss of generality regarding the eigenvalue statistics of $\mathbf{W}$, since replacing σ_{Re} with σ_{Im} and vice versa does not affect them.

For $\sigma_C^2 = 0$ or $\sigma_R^2 = 0$, $\mathbf{W}$ collapses to a central (real or complex) Wishart matrix, the properties of which have been studied extensively. However, with both $\sigma_C, \sigma_R > 0$, one deviates from such classical matrix models, and the statistical characterization becomes more challenging.

Key to our approach is to adopt a "condition and average" method which allows us to connect the statistical properties of $\mathbf{W}$ with those of non-central Wishart matrices, and to leverage existing results for such matrices. Specifically, let $\mathbf{W}_R = \mathbf{X}_R\mathbf{X}_R^\dagger$ if $p \leq n$ or $\mathbf{W}_R = \mathbf{X}_R^\dagger\mathbf{X}_R$ otherwise. Also, let

$$s \triangleq \min(p, n), \qquad t \triangleq \max(p, n). \tag{5.4}$$

When conditioned on $\mathbf{W}_R \in \mathbb{R}^{s\times s}$, $\mathbf{W}$ follows a non-central complex Wishart distribution with t degrees of freedom and real non-centrality parameter $\mathbf{W}_R$, i.e., $\mathbf{W}|\mathbf{W}_R \sim \mathcal{CW}_s(t, \sigma_C^2\mathbf{I}_s, \mathbf{W}_R)$. The statistics of $\mathbf{W}$ can be obtained by averaging that of $\mathbf{W}|\mathbf{W}_R$ over $\mathbf{W}_R$, which belongs to the space of real positive definite matrices.

One key advantage of this approach is that it does not need to follow the classical approach, where each random matrix statistic is derived from the joint density of the matrix entries. In particular, it circumvents the need to directly integrate over the joint eigenvalue density of $\mathbf{W}$ when deriving the extreme eigenvalue distributions. Such joint density is known for arbitrary s, t [26], however the expression is complicated, involving pfaffians of matrices whose entries contain double infinite series with terms involving products of generalized Laguerre polynomials. As such, it appears difficult to compute the extreme eigenvalue distributions by marginalizing the joint eigenvalue density in [26]. In the following, by exploiting the noncentral Wishart connection, we provide for the first time, an expression for the distribution of $\mathbf{W}$, as well as exact expressions for the extreme eigenvalue distributions and an asymptotic result for the largest eigenvalue distribution of $\mathbf{W}$.

5.3 Pdf and Eigenvalue Jpdf of W

5.3.1 Pdf of W

Thanks to Proposition 2.10, we give for the first time an expression of the pdf of $\mathbf{W}$:

$$\begin{aligned} f_{\mathbf{W}}(\mathbf{W}) =& K_{s,t}\mathrm{etr}\left(-\sigma_C^{-2}\mathbf{W}\right)\det(\mathbf{W})^{t-s}\sum_{k=0}^{+\infty}\sum_{\kappa}\frac{1}{[p]_\kappa k!}\left(\frac{2\sigma_C^{-2}\sigma_R^2}{\sigma_C^2+2\sigma_R^2}\right)^k \\ &\times\int_{\mathbf{V}^T=\mathbf{V}>0}\mathrm{etr}(-\mathbf{V})\det(\mathbf{V})^{\frac{t-s-1}{2}}\widetilde{C}_\kappa(\mathbf{V}\mathbf{W})(d\mathbf{V}) \end{aligned} \tag{5.5}$$

where $K_{s,t}$ is defined in 2.74.

This expression is particular interesting, since it allow us to show the peculiarities of the matrix $\mathbf{W}$. The expression involves an integral which is very similar to the integral of the reproduction property of zonal polynomials presented in (2.47). However, the integral here presented is defined over the space of real positive definite matrices, instead of the space of Hermitian positive definite matrices. This does not allow to give a simple result for this integral, which needs to define another class of matrix argument polynomials which are not known in the literature. Specifically, if one supposes that the integral was over the space of Hermitian positive definite matrices, the pdf of $\mathbf{W}$ could have been given in terms of a complex hypergeometric function of matrix argument. It is hoped that in the future a new class of hypergeometric functions would be defined to give a compact expression for this pdf.

Moreover, we clearly see the advantage of the approach presented in the previous section. If we follow the classical approach, we should derive the eigenvalue jpdf from (5.5) and, in turn, the extreme eigenvalue distributions from the eigenvalue jpdf. We here circumvent that and we can directly obtain those statistics by averaging those of the well-known noncentral complex Wishart matrix.

5.3.2 Eigenvalue Jpdf

Let $\Omega = \sigma_{\mathrm{Re}}^2 + \sigma_{\mathrm{Im}}^2$ and

$$\tau = \log\left(\frac{\sigma_{\mathrm{Re}}^2 + \sigma_{\mathrm{Im}}^2}{\sigma_{\mathrm{Re}}^2 - \sigma_{\mathrm{Im}}^2}\right). \tag{5.6}$$

The eigenvalue jpdf for arbitrary s, t is available in the literature in form of [26, eq. (10)]

$$f_{\phi_1,\ldots,\phi_s}(\phi_1,\ldots,\phi_s) = \frac{2^m e^{\frac{s(s-1)\tau}{2}}}{(2\Omega)^{\frac{s(s+1)}{2}}} C_s^{(0)} \mathrm{Pf}(\mathbf{F}(\tau)) \prod_{r=1}^{s} w_{\frac{t-s-1}{2}}\left(\frac{\phi_r}{2\Omega}\right) \prod_{i<j}^{s}(\phi_i - \phi_j) \tag{5.7}$$

where $w_a(x)$ is the associated Laguerre weight function, i.e.

$$w_a(x) = x^a e^{-x} \tag{5.8}$$

$C_s^{(0)}$ is the normalization constant, such as

$$C_s^{(0)} = \frac{\pi^{s/2}}{2^s} \prod_{i=1}^{s} \frac{1}{\Gamma(\frac{i}{2}+1)\Gamma(\frac{i}{2}+\frac{t-s}{2})} \tag{5.9}$$

and $\mathbf{F}(\tau)$ is a $2m$-dimensional antisymmetric matrix with $2m = s$ or $2m = s+1$, depending on whether s is even or odd. For even s,

$$\{\mathbf{F}(\tau)\}_{i,j} = \mathcal{G}_\tau\left(\frac{\phi_i}{2\Omega}, \frac{\phi_j}{2\Omega}\right). \tag{5.10}$$

For odd s, we have in addition

$$\{\mathbf{F}(\tau)\}_{i,s+1} = -\{\mathbf{F}(\tau)\}_{s+1,i} = f^{(\tau)}\left(\frac{\phi_i}{2\Omega}\right)(1 - \delta_{i,s+1}) \tag{5.11}$$

where $\delta_{i,j}$ is the Kronecker delta, $f_\tau(x)$ is given by

$$f^{(\tau)}(x) = w_{\frac{t-s+1}{2}} \sum_{\mu=0}^{\infty} \frac{e^{-2\mu\tau}\Gamma(\mu+\frac{1}{2})}{\Gamma(\mu+\frac{t-s}{2}+1)} L_{2\mu}^{(t-s)}(2x) \tag{5.12}$$

where $L_{\mu}^{(\alpha)}$ representing the associated Laguerre polynomials [37, eq. (22.2.12)] and

$$\begin{aligned}\mathcal{G}_{\tau}(x,y) =& 2w_{\frac{t-s+1}{2}}(x)w_{\frac{t-s+1}{2}}(y)\sum_{\mu=0}^{\infty}\sum_{\nu=0}^{\mu}e^{-(2\nu+2\mu+1)\tau}\kappa_{\nu,\mu}\left(\frac{t-s-1}{2}\right) \\ &\times\left[L_{2\nu}^{(t-s)}(2x)L_{2\mu+1}^{t-s}(2y)-L_{2\mu+1}^{(t-s)}(2x)L_{2\nu}^{t-s}(2y)\right]\end{aligned} \tag{5.13}$$

with

$$\kappa_{\mu,\nu}(a)=\frac{\Gamma\left(\mu+\frac{1}{2}\right)\Gamma(\nu+1)}{\Gamma\left(\mu+a+\frac{3}{2}\right)\Gamma(\nu+a+2)}. \tag{5.14}$$

To obtain this eigenvalue jpdf, the authors in [26] employed a complicated analysis. This cross-over ensemble was recreated with a Brownian motion process whose fictitious time τ is related to the variance imbalance.

Although the novel approach here proposed is easier to follow than the one given in [26], since we only need to average the eigenvalue jpdf of a noncentral complex Wishart, it would lead to a similar result than the one presented in [26] and reproduced in this section. Therefore, it is not interesting to explicitly employ our novel method for the analysis of the eigenvalue jpdf.

However, as commented before, our novel approach is very advantageous since it circumvents the need of manipulating the complicated result in (5.7) to derive the extreme eigenvalue distributions. For these reasons, we move directly to the study of the extreme eigenvalue distributions.

5.4 Extreme Eigenvalue Distributions

The analysis of the extreme eigenvalue distributions plays an important role in wireless communications [45], [90]. While most of contributions gives applications for the largest eigenvalue distribution, the smallest eigenvalue distribution is also used to analyze, e.g., MIMO systems which considers a linear zero-forcing receiver [92]. We here present statistical expressions for both extreme eigenvalues.

5.4.1 Smallest Eigenvalue Distribution

By virtue of Theorem 2.12, the cdf of the smallest eigenvalue admits

$$F_{\phi_{\min}}(x) = 1 - \frac{\mathrm{Pf}(\boldsymbol{\Upsilon}(x))}{\mathrm{Pf}(\boldsymbol{\Upsilon}(0))} \tag{5.15}$$

where $\boldsymbol{\Upsilon}(x)$ is an $s \times s$ matrix whose entries can be given by (2.88). The specific computation of the pfaffians in (5.15) depends on whether the matrix dimension s is even or odd. In either case, however, they may be evaluated as the square root of a matrix determinant, as detailed in Section 2.3.2.

We can compare the result in (5.15) with that of the smallest eigenvalue of noncentral Wishart matrix in [57]. We see that both results can be written in terms of a ratio, however, of different objects. While the smallest eigenvalue distribution of noncentral complex Wishart proposed in [57, eq. (15)] involves a ratio of determinants, here we have a ratio of pfaffians. Furthermore, the elements of the arguments of those objects can be also compared. While in the case of the noncentral Wishart matrix these elements can be given in terms of a Nuttall Q-function [57, eq. (16)], the elements of $\boldsymbol{\Upsilon}(x)$ can be expressed in terms of a double integral involving a Nuttall Q-function, as shown in (2.88).

Let $\psi = t - s + 1$, the elements of the matrix $\boldsymbol{\Upsilon}(x)$ also admits a series representation, such as

$$\begin{aligned}\{\boldsymbol{\Upsilon}(x)\}_{i,j} =& \sigma_C^{-2i-2j} e^{-2x/\sigma_C^2} \sum_{l=0}^{\infty}\sum_{m=0}^{\infty} \beta_{l,m}^{i,j}(t,\psi) f_{t-i+l+1}(x/\sigma_C^2) f_{t-j+m+1}(x/\sigma_C^2) \\ &\times \frac{(\sqrt{2}\sigma_{eq}\sigma_C)^{-2l}}{l!} \frac{(\sqrt{2}\sigma_{eq}\sigma_C)^{-2m}}{m!} \\ &\times \Big(B_{\frac{1}{2}}(l+\psi, m+\psi) - B_{\frac{1}{2}}(m+\psi, l+\psi) \Big).\end{aligned} \tag{5.16}$$

where $\sigma_{eq}^2 = \sigma_C^{-2} + \sigma_R^{-2}/2$, $B_z(a,b)$ is the incomplete beta function,

$$\beta_{l,m}^{i,j}(p,\psi) = 2^{l+m+2\psi} \frac{\Gamma(l+m+2\psi)\Gamma(p-i+l+1)\Gamma(p-j+m+1)}{\Gamma(l+2\psi)\Gamma(m+2\psi)}, \tag{5.17}$$

and

$$f_n(y) = \sum_{r=0}^{n-1} \frac{y^r}{r!}. \tag{5.18}$$

The derivation of this series representation of the elements of the matrix $\boldsymbol{\Upsilon}(x)$ can be found in Appendix A. This representation is of similar complexity than the expression of the elements of the matrix $\mathbf{F}(\tau)$, which is the pfaffian argument expression of the eigenvalue jpdf of $\mathbf{W}$ presented in [26] and here reproduced in Section 5.3.2.

Although this expression is exact, it does not give insight into how the smallest eigenvalue distribution behaves when the variance imbalance between the real and imaginary parts of $\mathbf{X}$ changes. With this in mind, one could think of establishing a simplified tail expansion for this distribution, similarly as other works did for the smallest eigenvalue of central and noncentral complex Wishart matrices [57], [93]. However, the corresponding result for noncentral complex Wishart matrices given in [57, eq. (28)] is already complicated and lacks insight. We believe that, when deriving the corresponding noncircularly-symmetric result from it, we will obtain a result

even more difficult to interpret. Therefore, we will skip such derivation and jump directly into the study of the largest eigenvalue distribution, since its asymptotic expansion is prone to be very simple, when one observes that of the noncentral Wishart case in [57, eq. (28)].

5.4.2 Largest Eigenvalue Distribution

By virtue of Theorem 2.11, we can give an exact expression of the cdf of the largest eigenvalue $F_{\phi_{\max}}(x)$ of $\mathbf{W}$:

$$F_{\phi_{\max}}(x) = \frac{\mathrm{Pf}(\boldsymbol{\Xi}(x))}{\mathrm{Pf}(\boldsymbol{\Upsilon}(0))} \tag{5.19}$$

where $\boldsymbol{\Xi}(x)$ is an $s \times s$ matrix whose entries can be given by (2.79).

This result also admits a comparison with the corresponding result for noncentral Wishart matrices, which is similar as the one given for the smallest eigenvalue case. Also, the elements of $\boldsymbol{\Xi}(x)$ have a similar representation in series as the elements of $\boldsymbol{\Upsilon}(x)$ in the previous section.

We then give an asymptotic expansion in the left-hand tail of the distribution thanks to Theorem 2.13. As $x \to 0$,

$$F_{\phi_{\max}}(x) = h_{s,t}\, a_{s,t}^{\mathrm{CW}} x^{st} + o(x^{st}) \tag{5.20}$$

where

$$a_{s,t}^{\mathrm{CW}} = \prod_{i=1}^{s} \frac{(s-i)!}{(s+t-i)!} \tag{5.21}$$

and

$$h_{s,t} = \frac{1}{\left(\sigma_C \sqrt{2\sigma_R^2 + \sigma_C^2}\right)^{st}} \,. \tag{5.22}$$

In the expression above, $a_{s,t}^{\mathrm{CW}}$ corresponds to the expansion coefficient for the largest eigenvalue distribution of a central complex Wishart matrix [57], [93]. Hence, in the left-hand tail, the effect of the unbalanced variances of the

real and imaginary components of $\mathbf{X}$ is clearly revealed, and is decoupled into the function $h_{s,t}$ in (5.22). This simplicity is quite remarkable, particularly when considering the complexity of the exact largest eigenvalue distribution (2.78), as well as that of the joint eigenvalue distribution derived in [26].

To better interpret the result in (5.20), we express the function $h_{s,t}$ in terms of the original variances σ^2_{Re} and σ^2_{Im}, while we fix the total variance as $\sigma^2_{\mathrm{Re}} + \sigma^2_{\mathrm{Im}} = 1$. Then,

$$h_{s,t} = \frac{1}{\left(4\sigma^2_{\mathrm{Re}}(1-\sigma^2_{\mathrm{Re}})\right)^{st/2}} \,. \tag{5.23}$$

From (5.23), $h_{s,t}$ is clearly minimized at the "balanced" case, $\sigma^2_{\mathrm{Re}} = 1/2$, for which $h_{s,t} = 1$, as it should. One observes a significant deviation, however, as the variances of the real and imaginary components become more unbalanced. That is, the higher the imbalance, the slower the decay of the left-hand tail of $F_{\phi_{\max}}(x)$.

5.5 Outage performance of MIMO-MRC systems in Nakagami-q (Hoyt) environments

We here provide an application example for the derived results. Consider a communication link between a transmitter, equipped with N_t antennas, and a receiver with N_r antennas. The multi-antenna link is subject to Nakagami-q (Hoyt) fading, typically assumed in satellite-based communications [5] or, in general, when the fading conditions are more severe than those of a Rayleigh-faded environment. The channel is modeled by $\mathbf{H} \in \mathbb{C}^{N_r \times N_t}$ with zero-mean i.i.d. entries $\{\mathbf{H}\}_{i,j}$ representing the complex gain between the j-th transmit and the i-th receive antennas, where $\mathrm{Re}(\{\mathbf{H}\}_{i,j}) \sim \mathcal{N}(0, \sigma^2_{\mathrm{Re}})$ and $\mathrm{Im}(\{\mathbf{H}\}_{i,j}) \sim \mathcal{N}(0, \sigma^2_{\mathrm{Im}})$ are mutually independent, $\sigma^2_{\mathrm{Re}} = 1/(1+q^2)$, $\sigma^2_{\mathrm{Im}} =$

$q^2/(1+q^2)$, and $q \in (0,1)$ denotes the Hoyt fading parameter, which defines the power imbalance between the real and imaginary channel components. Invoking the redefinition in (5.2),

$$\mathbf{H} = \sqrt{\frac{2q^2}{1+q^2}}\mathbf{H}_C + \sqrt{\frac{1-q^2}{1+q^2}}\mathbf{H}_R \tag{5.24}$$

where the entries of $\mathbf{H}_C$ are circularly-symmetric $\mathcal{CN}(0,1)$, while those of $\mathbf{H}_R$ are $\mathcal{N}(0,1)$. Define $\mathbf{W}_{\mathrm{H}} = \mathbf{H}\mathbf{H}^\dagger$, if $N_r \leq N_t$, or $\mathbf{W}_{\mathrm{H}} = \mathbf{H}^\dagger\mathbf{H}$ otherwise.

We further assume that the receiver has perfect knowledge of $\mathbf{H}$ while the transmitter, with only partial knowledge, uses the well-known beamforming (BF) principle [15] to send data with a total fixed power P. The noise at each receive antenna is assumed independent $\mathcal{CN}(0,1)$ and we define the transmit SNR as $\bar{\gamma} \triangleq P$. The received signal vector $\mathbf{r} \in \mathbb{C}^{N_r}$ can then be expressed as

$$\mathbf{r} = \sqrt{\bar{\gamma}}\mathbf{H}\mathbf{w}x + \mathbf{n} \tag{5.25}$$

where x is the transmitted symbol with $\mathbb{E}[|x|^2] = 1$, $\mathbf{n}$ is the noise vector, and $\mathbf{w}$ is the BF vector with $||\mathbf{w}|| = 1$. The detection of x is optimal when $\mathbf{w}$ equals the eigenvector corresponding to the largest eigenvalue of $\mathbf{W}_{\mathrm{H}}$ and when the MRC principle is applied to the received signal $\mathbf{r}$, which yields a post-processing SNR [15]

$$\gamma = \bar{\gamma}\lambda_{\max} \tag{5.26}$$

where $\lambda_{\max}$ denotes the largest eigenvalue of $\mathbf{W}_{\mathrm{H}}$.

Defining γ_{th} as the minimum required SNR for a reliable communication (i.e., with x reliably detected), the outage probability is exactly obtained from Theorem 2.11 as

$$P_{\mathrm{out}} = \Pr(\gamma \leq \gamma_{\mathrm{th}}) = F_{\phi_{\max}}\left(\frac{\gamma_{\mathrm{th}}}{\bar{\gamma}}\right) \tag{5.27}$$

with $\sigma_C^2 = 2q^2/(1+q^2)$, $\sigma_R^2 = (1-q^2)/(1+q^2)$, $s = \min(N_t, N_r)$ and $t = \max(N_t, N_r)$.

To give further insight, we approximate P_{out} by leveraging the asymptotic characterization of Theorem 2.13. In practice, we are interested in small outage probabilities, i.e., implying small values of $\gamma_{\text{th}}/\bar{\gamma}$. From Theorem 2.13, as $\gamma_{\text{th}}/\bar{\gamma} \to 0$,

$$P_{\text{out}} \approx \hat{P}_{\text{out}} = a_{s,t}^{\text{CW}} \left(\frac{\gamma_{\text{th}}}{\theta(q)\bar{\gamma}} \right)^{st} \tag{5.28}$$

where $\theta(q) = 2q/(1+q^2)$ and $q > 0$. This explicitly reveals that the power gain one gets by steering the signal along the top channel eigenmode decreases as the real and imaginary channel components get more imbalanced. Specifically, the effect of such imbalance can be seen as a reduction in the average SNR—with respect to the perfectly balanced case (Rayleigh fading, $q = 1$)—by a factor of $\theta(q) < 1$. The outage probability is then degraded (increased) by a factor of $\theta(q)^{-st}$, which can be approximated by $(2q)^{-st}$ for small q. Remark that this degradation is exponentially accentuated as the number of antennas increases.

Fig. 5.1 depicts the outage probability as a function of the SNR $\bar{\gamma}$ for 2×2 and 2×3 MIMO systems, operating in three different fading conditions ($q = 1$, $q = 0.5$ and $q = 0.3$). For each q, we plot: (i) the empirical probability—obtained from Monte-Carlo simulations (10^6 realizations), (ii) the exact P_{out} in (5.27)—where we compute $F_{\phi_{\max}}(x)$ from (5.19) numerically[1], and (iii) the asymptotic outage probability $\hat{P}_{\text{out}}$ in (5.28). We observe a good agreement between (exact) analytical and simulated results in all cases and, as expected, the asymptotic result coverges to the exact one as P_{out} gets smaller. As anticipated, P_{out} degrades significantly as q decreases, with such degradation being

[1]To compute (2.79) and (2.81), we use the Gauss-Laguerre integration method, where the Nuttall Q-functions are computed as finite sums of Marcum Q-functions, since the difference of their orders is odd.

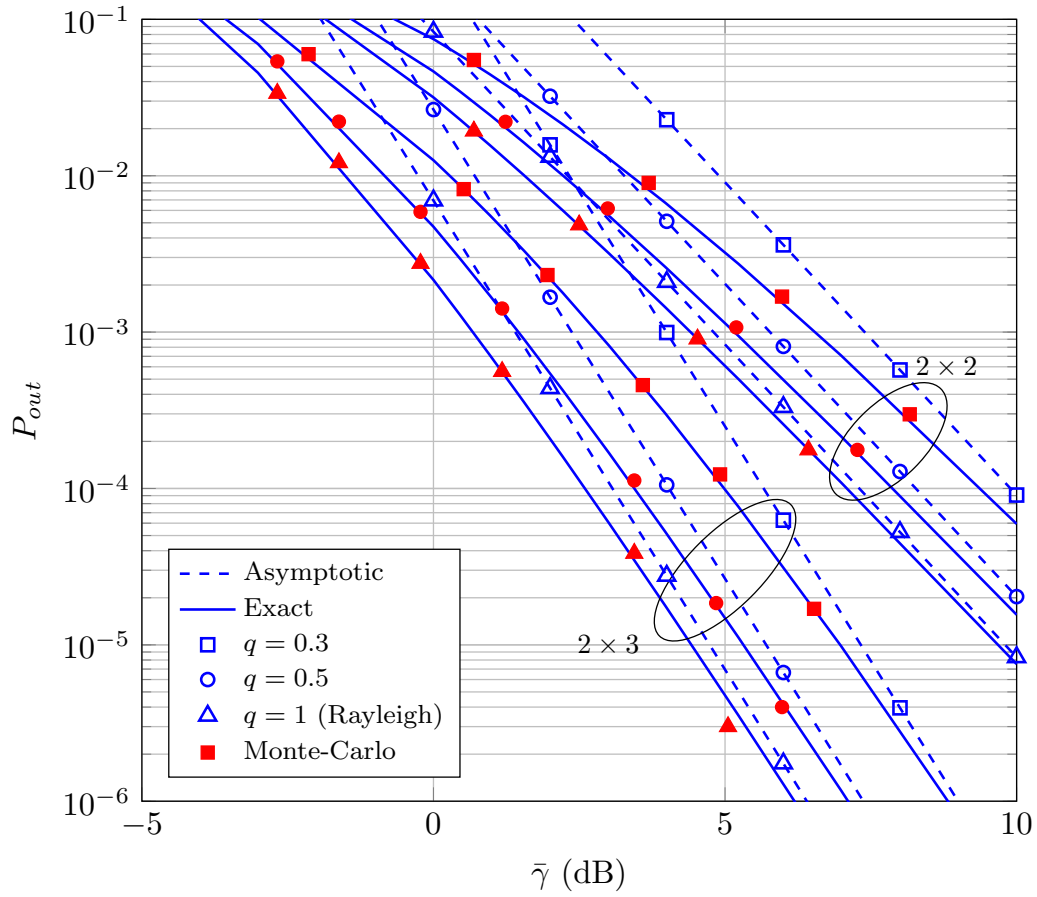

FIGURE 5.1: Outage probabilities of 2×2 and 2×3 MIMO-MRC systems under Nakagami-q (Hoyt) fading for different values of q; $\gamma_{\text{th}} = 0$ dB.

more pronounced in the 2×3 setting. Even for a dual-antenna (2×2) system, this degradation at $\bar{\gamma} = 10$ dB is approximately one order of magnitude for the case $q = 0.3$ (90% of the channel gain in the real part and 10% in the imaginary part, or vice versa) with respect to the case $q = 1$ (Rayleigh). This is consistent with the analytical prediction above, where the P_{out} degradation was given by the factor $\theta(q)^{-st}$ as $\gamma_{\text{th}}/\bar{\gamma} \to 0$. For $q = 0.3$ and $st = 4$, this factor yields ~ 10.9.

We are also interested in the outage data rate, defined as the largest transmission rate (in bits/s/Hz) that can be reliably guaranteed at least

$(1-\epsilon)\times 100\%$ of the time, i.e.

$$R_{\text{out}}(\epsilon) = \sup_{R\geq 0}(R : P_{\text{out}}(R) < \epsilon) \tag{5.29}$$

where ϵ is the maximum outage level and $P_{\text{out}}(R)$ is the outage probability for a given data rate R, i.e.

$$\begin{aligned} P_{\text{out}}(R) \triangleq &\Pr\left(\log_2(1+\gamma) \leq R\right) \\ =&F_{\phi_{\text{max}}}((2^R-1)/\bar{\gamma}). \end{aligned} \tag{5.30}$$

Thus,

$$R_{\text{out}}(\epsilon) = \log_2(1+\bar{\gamma}F^{-1}_{\phi_{\text{max}}}(\epsilon)) \tag{5.31}$$

where $F^{-1}_{\phi_{\text{max}}}(\cdot)$ denotes the inverse function of $F_{\phi_{\text{max}}}(\cdot)$. Again, Theorem 2.13 allows us to approximate $R_{\text{out}}(\epsilon)$ for small values of ϵ by a compact and insightful expression; as $\epsilon \to 0$,

$$R_{\text{out}}(\epsilon) \approx \hat{R}_{\text{out}}(\epsilon, q) = \log_2\left(1+\theta(q)\bar{\gamma}\left(\frac{\epsilon}{a^{\text{CW}}_{s,t}}\right)^{1/st}\right) \tag{5.32}$$

where, once more, we see the effect of the Nakagami-q fading through the isolated factor $\theta(q)$ which, for $q<1$, causes a reduction in the "effective" average SNR. To better illustrate the proportional outage rate degradation with respect to the Rayleigh case ($q=1$), we define the (approximated) fractional rate loss

$$\hat{RL}(\%) \approx \frac{\hat{R}_{\text{out}}(\epsilon,1) - \hat{R}_{\text{out}}(\epsilon,q)}{\hat{R}_{\text{out}}(\epsilon,1)} \times 100. \tag{5.33}$$

Table 5.1 shows the approximated $\hat{RL}$ along with the exact RL, computed with (5.31) by numerically inverting $F_{\phi_{\text{max}}}(\cdot)$, for a 2×2 setting with a maximum outage level of $\epsilon = 10^{-3}$ and $\bar{\gamma} = 10$ dB. The numbers reveal a substantial rate degradation as q gets smaller, up to $\sim 37\%$ loss ($q=0.2$).

TABLE 5.1: Data rate loss of a 2×2 MIMO system at $\bar{\gamma} = 10$ dB, $\epsilon = 10^{-3}$

q	0.5	0.4	0.3	0.2
RL	9%	17%	26%	37%
$\hat{RL}$	9%	18%	27%	43%

5.6 Conclusions

We have simplified the study of noncircularly-symmetric Wishart-type matrices, which has allowed to give, for the first time, results regarding the pdf of such matrices, as well as the extreme eigenvalue distributions. Particularly, we have studied in depth their largest eigenvalue distribution by connecting the statistics of those matrices and that of the well-known noncentral complex Wishart matrices. Although the exact largest eigenvalue distribution does not allow to give any further insightful analysis, the asymptotic expansion in the tail clearly translates the effect of a power imbalance between the real and imaginary parts of the model into a simple decoupled factor.

These results have been applied to 2×2 and 2×3 MIMO systems under different Nakagami-q (Hoyt) fading severity levels. We have seen that the presence of an imbalance between the real and imaginary channel components significantly degrades the outage performance. This effect is exponentially accentuated for large numbers of antennas at both the transmitter and receiver sides. We also have observed that the asymptotic results, despite being very simple, are remarkably tight to the exact ones, even for extreme fading cases (q small).

Chapter 6

Summary and Future Work

There were two main topics addressed in this thesis, which are summarized as follows:

- An investigation of the statistical connection between noncircularly-symmetric fading models, such as the η-μ model and its particular case, the Nakagami-q (Hoyt) model, with the more tractable circularly-symmetric models.
- An investigation of a novel approach that facilitates the analysis of noncircularly-symmetric Wishart-type matrices.

6.1 Summary

The performance analysis given throughout this thesis is based on different univariate and multivariate statistical results, which were presented and derived in Chapter 2. The key utility of these results is that, in contrast to many existing results associated with application to fading modeling, they unify the statistical analysis of a multitude of models and, therefore, future analyses of these models will not be performed separately as usual so far. We must underline the fact that, in addition to the vast model unification performed between noncircularly-symmetric and noncentral models in the univariate

case, the multivariate analysis of noncircularly-symmetric-Wishart type matrices was clearly simplified, with a novel connection with the statistical analysis of noncentral complex Wishart matrices.

In Chapter 3, we have resolved a controversy between two different underlying models for the recently proposed κ-μ shadowed model, which was essential to build all the model connections presented in Chapter 4. Indeed, we have proved that the κ-μ shadowed model unifies the set of noncentral models associated with the κ-μ model, and, strikingly, it also unifies the set of noncircularly-symmetric models associated with the η-μ model. In other words, the analysis of the five classical fading models, i.e., the one-sided Gaussian, Rayleigh, Nakagami-m, Nakagami-q and Rician models, and their most popular generalizations, i.e., the Rician shadowed, the κ-μ, η-μ and κ-μ shadowed models, can be jointly performed exclusively with only that of the latter one, since the rest of aforementioned models can be seen as its particular cases.

Finally, in Chapter 5, we have tackled the statistical analysis of the noncircularly-symmetric Wishart-type matrices. We have derived for the first time an expression for the pdf of those matrices, as well as for the extreme eigenvalue distributions. Of particular mention is the analysis of the largest eigenvalue distribution provided in this thesis, since it gives rich insight on how the variance imbalance of the underlying model affect this distribution.

6.2 Future Work

The univariate analysis provided in Chapter 2-4 unifies the analysis of NLOS noncircularly-symmetric fading models with that of LOS circularly-symmetric ones. An interesting topic for future work is the extension of these results for LOS noncircularly-symmetric fading models, i.e., underlying models that consider non-zero mean in their Gaussian RVs, such as the

Beckmann model [45].

The results of Chapter 5 showed that there are many different investigating paths to follow in the future. Associated with the new pdf of noncircularly-symmetric Wishart-type matrices, new polynomials of matrix arguments are needed. Referring to the smallest eigenvalue distribution of those matrices, it seemed necessary to first simplify the corresponding asymptotic result of noncentral complex Wishart matrices. Then, we also propose to derive from it an asymptotic expansion in the tail for the smallest eigenvalue distribution of noncircularly-symmetric Wishart-type matrices to shed some light on how the variance asymmetry affects it. Finally, we could apply this distribution to study the outage performance of MIMO systems which employ a linear zero-forcing receiver.

Appendix A

Series Representation of the Elements of $\boldsymbol{\Psi}(x)$

Proof: From (2.88), we remove the signum function such as

$$\begin{aligned}\{\boldsymbol{\Upsilon}(x)\}_{i,j} =& \left(\frac{2}{\sigma_C^2}\right)^{i+j} \\ &\times \left[\int_0^{+\infty}\int_0^{z} t^{-\frac{1}{2}} e^{-\frac{1}{2\sigma_R^2}t} Q_{s+t-2i+1,t-s}\left(\sqrt{\frac{2}{\sigma_C^2}t}, \sqrt{\frac{2}{\sigma_C^2}x}\right)\right. \\ &\times z^{-\frac{1}{2}} e^{-\frac{1}{2\sigma_R^2}z} Q_{s+t-2j+1,t-s}\left(\sqrt{\frac{2}{\sigma_C^2}z}, \sqrt{\frac{2}{\sigma_C^2}x}\right) dtdz \\ &- \int_0^{+\infty}\int_z^{+\infty} t^{-\frac{1}{2}} e^{-\frac{1}{2\sigma_R^2}t} Q_{s+t-2i+1,t-s}\left(\sqrt{\frac{2}{\sigma_C^2}t}, \sqrt{\frac{2}{\sigma_C^2}x}\right) \\ &\left.\times z^{-\frac{1}{2}} e^{-\frac{1}{2\sigma_R^2}z} Q_{s+t-2j+1,t-s}\left(\sqrt{\frac{2}{\sigma_C^2}z}, \sqrt{\frac{2}{\sigma_C^2}x}\right) dtdz\right]\end{aligned} \tag{A.1}$$

Using the series representation of the Nuttall Q-function [94, eq. (5)], i.e.,

$$Q_{2c+k+1,k}(a,b) = \sum_{l=0}^{\infty} \frac{a^{2l+k} e^{-\frac{a^2}{2}} \Gamma\left(c+k+l+1, \frac{b^2}{2}\right)}{l!\Gamma(k+l+1)2^{l-c}} \tag{A.2}$$

we have

$$
\begin{aligned}
\{\boldsymbol{\Upsilon}(x)\}_{i,j} = & \left(\frac{2}{\sigma_C^2}\right)^{i+j+t-s} \\
& \times \left[\sum_{l=0}^{\infty} \frac{\Gamma\left(t-i+l+1, \frac{1}{\sigma_C^2}x\right)\left(\frac{2}{\sigma_C^2}\right)^l}{l!\Gamma(t-s+l+1)2^{l+i-s}}\right. \\
& \times \sum_{m=0}^{\infty} \frac{\Gamma\left(t-j+m+1, \frac{1}{\sigma_C^2}x\right)\left(\frac{2}{\sigma_C^2}\right)^m}{m!\Gamma(t-s+m+1)2^{m+j-s}} \\
& \times \int_0^{+\infty} \int_0^z t^{l+\frac{t-s-1}{2}} e^{-\sigma_{eq}^2 t} z^{m+\frac{t-s-1}{2}} e^{-\sigma_{eq}^2 z} dt dz \qquad \text{(A.3)} \\
& - \sum_{l=0}^{\infty} \frac{\Gamma\left(t-i+l+1, \frac{1}{\sigma_C^2}x\right)\left(\frac{2}{\sigma_C^2}\right)^l}{l!\Gamma(t-s+l+1)2^{l+i-s}} \\
& \times \sum_{m=0}^{\infty} \frac{\Gamma\left(t-j+m+1, \frac{1}{\sigma_C^2}x\right)\left(\frac{2}{\sigma_C^2}\right)^m}{m!\Gamma(t-s+m+1)2^{m+j-s}} \\
& \left. \times \int_0^{+\infty} \int_z^{+\infty} t^{l+\frac{t-s-1}{2}} e^{-\sigma_{eq}^2 t} z^{m+\frac{t-s-1}{2}} e^{-\sigma_{eq}^2 z} dt dz \right].
\end{aligned}
$$

In both incomplete integrals, we identify the the lower- and upper-incomplete gamma functions. After some simplifications, we have

$$
\begin{aligned}
\{\boldsymbol{\Upsilon}(x)\}_{i,j} =& \left(\frac{2}{\sigma_C^2}\right)^{i+j+t-s} \sigma_{eq}^{s-t-1} \\
&\times \Bigg[\sum_{l=0}^{\infty} \frac{\Gamma\Big(t-i+l+1, \frac{1}{\sigma_C^2}x\Big)(\sigma_{eq}\sigma_C)^{-2l}}{l!\Gamma(t-s+l+1)2^{i-s}} \\
&\times \sum_{m=0}^{\infty} \frac{\Gamma\Big(t-j+m+1, \frac{1}{\sigma_C^2}x\Big)\Big(\frac{1}{2\sigma_C^2}\Big)^m}{m!\Gamma(t-s+m+1)2^{m+j-s}} \\
&\int_0^{+\infty} z^{m+\frac{t-s-1}{2}} e^{-\sigma_{eq}^2 z} \gamma\left(l+\frac{t-s+1}{2}, \sigma_{eq}^2 z\right) dz \\
&- \sum_{l=0}^{\infty} \frac{\Gamma\Big(t-i+l+1, \frac{1}{\sigma_C^2}x\Big)(\sigma_{eq}\sigma_C)^{-2l}}{l!\Gamma(t-s+l+1)2^{i-s}} \\
&\times \sum_{m=0}^{\infty} \frac{\Gamma\Big(t-j+m+1, \frac{1}{\sigma_C^2}x\Big)\Big(\frac{2}{\sigma_C^2}\Big)^m}{m!\Gamma(t-s+m+1)2^{m+j-s}} \\
&\int_0^{+\infty} z^{m+\frac{t-s-1}{2}} e^{-\sigma_{eq}^2 z} \Gamma\left(l+\frac{t-s+1}{2}, \sigma_{eq}^2 z\right) dz\Bigg].
\end{aligned}
\tag{A.4}
$$

The remaining integrals of incomplete gamma functions can be compute thanks to [38, eq. (6.455.1)] and [38, eq. (6.455.2)], and after some simplifications we have,

$$
\begin{aligned}
\{\boldsymbol{\Upsilon}(x)\}_{i,j} =& 2^{2s-i-j}\left(\frac{2}{\sigma_C^2}\right)^{i+j-1} (\sigma_C\sigma_{eq})^{2s-2t-2} \\
&\times \Bigg[\sum_{l=0}^{\infty} \frac{\Gamma\Big(t-i+l+1, \frac{1}{\sigma_C^2}x\Big)(\sigma_{eq}\sigma_C)^{-2l}}{l!\Gamma(t-s+l+1)2^{l}} \\
&\times \sum_{m=0}^{\infty} \frac{\Gamma\Big(t-j+m+1, \frac{1}{\sigma_C^2}x\Big)(\sigma_{eq}\sigma_C)^{-2m}}{m!\Gamma(t-s+m+1)2^{m}} \\
&\times \Gamma(l+m+t-s+1)\left(\frac{{}_2\mathcal{F}_1\big(1, l+m+t-s+1, l+\frac{t-s+3}{2}, \frac{1}{2}\big)}{l+\frac{t-s+1}{2}}\right. \\
&\left.- \frac{{}_2\mathcal{F}_1\big(1, l+m+t-s+1, m+\frac{t-s+3}{2}, \frac{1}{2}\big)}{m+\frac{t-s+1}{2}}\right)\Bigg].
\end{aligned}
\tag{A.5}
$$

Using (2.10) we finally obtain the result. ■

Appendix B

Resumen en Castellano

B.1 Prefacio

Según la normativa española, se puede escribir la memoria de la tesis completamente en inglés para solicitar la mención "Doctor Internacional". Sin embargo, se requiere escribir un breve resumen (de al menos cinco mil palabras) en castellano. Se ha de tener en cuenta que este anexo no es el propio manuscrito de la tesis, sino que es sólo un resumen para mostrar los resultados más relevantes.

B.2 Introducción y Motivación

Las variables aleatorias (VAs) gaussianas complejas son ampliamente utilizadas para modelar fluctuaciones aleatorias en diferentes áreas, como la óptica [1], la física nuclear [2], el procesamiento de señal [3], [4], y las comunicaciones inalámbricas [5], por nombrar algunas. En todas estas áreas, se suele suponer (por lo general implícitamente) que estas VAs son circularmente simétricas, es decir, con igual varianza en sus partes real e imaginaria. Esta suposición realmente simplifica el análisis de una multitud de problemas a expensas de disminuir la exactitud de los resultados.

Sin embargo, hay muchos otros casos en los que el supuesto de circularidad es incluso inapropiado. En óptica, la rugosidad de las superficies transmisoras o reflectoras afecta desigualmente las varianzas de las partes real e imaginaria del campo lejano de la componente dispersiva, que ya no puede ser modelada con VAs gaussianas circularmente simétricas [6], [7]. En física nuclear, el estudio de los espaciamientos de los saltos energéticos requiere el análisis de matrices aleatorias Gaussianas no-circularmente simétricas (o impropias) [8]. En el procesamiento de señal, el desequilibrio entre las ramas en fase y en cuadratura (I/Q) debido a desajustes I/Q hace que la señal recibida sea impropia [9]. En las comunicaciones inalámbricas, los modelos gaussianos subyacentes no-circularmente simétricos son convenientes cuando un ensombrecimiento severo o un fuerte centelleo ionosférico están presentes en las comunicaciones móviles por satélite e inter-satélite [5], [10], [11].

A pesar del gran número de aplicaciones, el análisis de los modelos no-circularmente simétricos es mucho más escaso que el de los circularmente simétricos. Considerar un desequilibrio entre partes real e imaginaria presenta un desafío significativo ya que las propiedades clásicas de variable aleatoria son a menudo no aplicables.

En este contexto, el objetivo principal de esta tesis es simplificar el análisis de modelos derivados de VAs gaussianas no-circularmente simétricas en un contexto de comunicación inalámbrica. Particularmente, esta tesis establece nuevas conexiones estadísticas entre los modelos de desvanecimiento no-circularmente simétricos y auquellos que son circularmente simétricos. Éstos se emplearán para estudiar el rendimiento de los sistemas *single-input single-output* (SISO) y *multiple-input multiple-output* (MIMO) sujetos a desvanecimientos que consideran un desequilibrio entre las componentes en fase y en cuadratura de la señal.

B.3 Unificando los Modelos κ-μ y η-μ

Esta sección demuestra que la distribución κ-μ con ensombrecimiento unifica el conjunto de modelos clásicos de desvanecimiento asociados con la distribución κ- μ, y sorprendentemente, también unifica el conjunto de modelos clásicos de desvanecimiento asociados Con la distribución mbox η-μ. Particularmente, revela que el modelo de Nakagami-q se puede obtener como un caso particular del modelo Rician con ensombrecimiento propuesto en [65], lo que puede parecer contraintuitivo a primera vista. Se propone un método novedoso para derivar las distribuciones Nakagami- q y η-μ que consiste en utilizar el fenómeno de ensombrecimiento de las componentes dominantes para recrear un desequilibrio de potencia entre las partes real e imaginaria de las componentes difusas. Esta conexión, que aquí se propone por primera vez en la literatura, tiene implicaciones importantes en la práctica: en primer lugar, y en contra de la creencia común, muestra que los modelos κ-μ y η-μ están conectados. Por lo tanto, podemos estudiar conjuntamente dichos modelos usando un enfoque común en lugar de por separado. Además, implica que al derivar cualquier métrica de rendimiento para el modelo de desvanecimiento κ-μ con ensombrecimiento, en realidad estamos resolviendo el mismo problema para la distribución κ-μ y, lo que es más importante, para la distribución η-μ sin costo adicional.

Aprovechando nuestro enfoque novedoso, también derivamos aquí expresiones asintóticas simples y de forma cerrada para la capacidad ergódica de sistemas de comunicación que operan bajo un desvanecimiento κ-μ con ensombrecimiento en el régimen de relación señal-ruido alta, pudiendo ser evidentemente empleado para las distribuciones κ-μ y η-μ. A diferencia de los análisis exactos disponibles en la literatura que requieren el uso de las funciones Meijer G univariables y bivariables, nuestros resultados permiten una mejor comprensión de los efectos de los parámetros de desvanecimiento

en la capacidad.

B.3.1 Modelo κ-μ con Ensombrecimiento

El modelo κ-μ con ensombrecimiento fue definido por primera vez por Paris en [52] como una generalización natural del modelo popular κ-μ originalmente propuesto por Yacoub en [29]. La diferencia con respecto al modelo κ-μ aparece en la componente dominante de cada clúster, que ya no es determinista y puede fluctuar aleatoriamente debido al fenómeno de ensombrecimiento. Las expresiones cerradas para la función densidad de probabilidad, la función de distribución y la función generadora de momentos de la envolvente de potencia de señal se obtuvieron en [52] y se validaron mediante simulaciones de tipo Monte-Carlo y mediciones de campo en el contexto de canales acústicos subacuáticos.

La función densidad de probabilidad del modelo κ-μ con ensombrecimiento viene dada por la siguiente expresión cerrada [52]:

$$f_\gamma(\gamma) = \frac{\mu^\mu m^m (1+\kappa)^\mu}{\Gamma(\mu)\bar{\gamma}(\mu\kappa+m)^m} \left(\frac{\gamma}{\bar{\gamma}}\right)^{\mu-1} e^{-\frac{\mu(1+\kappa)\gamma}{\bar{\gamma}}} \, {}_1\mathcal{F}_1\left(m;\mu;\frac{\mu^2\kappa(1+\kappa)}{\mu\kappa+m}\frac{\gamma}{\bar{\gamma}}\right) \quad \text{(B.1)}$$

donde γ es la relación señal-ruido instantánea y $\bar{\gamma}$ es su media.

B.3.2 Distribución κ-μ y sus Casos Particulares

La distribución κ-μ se emplea en entornos donde la componente difusa para cada clúster puede ser modelada con una variable aleatoria circularmente simétrica. La derivación de la distribución κ-μ a partir de la distribución κ-μ con ensombrecimiento se puede realizar tomando el límite $m \to \infty$ en (B.1) y aplicando las siguientes propiedades

$$\lim_{a\to\infty} \, {}_1\mathcal{F}_1\Big(a;b;\frac{1}{a}z\Big) = \, {}_0\mathcal{F}_1\Big(b;z\Big) \quad \text{(B.2)}$$

$$\lim_{a\to\infty}\left(1+\frac{1}{a}x\right)^{-a}=e^{-x}. \tag{B.3}$$

En realidad, la distribución κ-μ se obtiene eliminando completamente el sombreado de cada componente dominante, lo que puede hacerse tomando $m \to \infty$, de manera que la componente dominante de cada clúster se convierta en determinista. A medida que el parámetro m crece, la distribución de cada componente dominante se comprime gradualmente y, en el límite $m \to \infty$, se convierte en una función delta de Dirac. Por lo tanto, el modelo se define por una variable aleatoria compleja gaussiana circularmente simétrica con una media no nula en cada clúster, de modo que obtenemos el modelo κ-μ, mientras que en el caso de que $\mu = 1$ se obtiene el modelo de Rician con ensombrecimiento.

A su vez, el modelo subyacente de Nakagami- m puede derivarse del modelo κ-μ con ensombrecimiento cuando $\kappa \to 0$ en (B.1) y aplicando la propiedad

$$\lim_{c\to 0}\ {}_p\mathcal{F}_q\left(a_1\dots a_p; b_1\dots b_q; cz\right)=1. \tag{B.4}$$

Al tender $\kappa \to 0$, eliminamos todas los componentes dominantes del modelo, independientemente del valor del parámetro de ensombrecimeinto m, de modo que sólo tenemos componentes de dispersión en cada clúster, es decir, obtenemos un modelo que sigue una distribución de Nakagami-m o uno de sus casos particulares, es decir el modelo Rayleigh o el modelo gaussiano unilateral, dependiendo del valor de μ.

B.3.3 Distribución η-μ y sus Casos Particulares

Las distribuciones de Nakagami- q (Hoyt) y η-μ se emplean en entornos de propagación donde las componentes difusas son no uniformes y pueden ser modeladas por varaibles gaussianas elípticas (o no-circularmente simétricas).

A primera vista, este escenario no parece encajar con el modelo κ-μ con ensombrecimiento. Sin embargo, podemos dar una interpretación diferente a los componentes del clúster de este modelo: pueden interpretarse como un conjunto de ondas difusas uniformes con medias aleatorias. Estas fluctuaciones aleatorias en las medias, que son diferentes para cada clúster, son responsables de modelar la no homogeneidad del entorno considerado en [29] y finalmente rompen la simetría circular del modelo. Debemos resaltar que una conexión similar se presentó recientemente en [23], donde se mostró que la distribución de una variable Nakagami- q se comporta como una distribución Rayleigh con una potencia media aleatoriamente variable.

La simetría circular del modelo se puede romper fijando $m = \mu/2$. La distribución η-μ surgiría como un caso particular de la distribución más general κ-μ con ensombrecimiento, donde el parámetro $\eta = 1/(2\kappa+1)$. Este es uno de los principales resultados de esta tesis. Obsérvese que cuando $m = \mu/2 = 0.5$, se obtiene el modelo de Nakagami- q con el parámetro $q = \sqrt{1/(2\kappa + 1)}$ ya que $\eta = q^2$ para el modelo η-μ con formato 1 [29] [1]. Por lo tanto, el modelo de Nakagami- q puede obtenerse del modelo Rician con ensombrecimiento propuesto en [65] estableciendo $m = 0.5$.

Aunque una interpretación de este resultado no es directa, está claro, desde un punto de vista matemático, que si fijamos el parámetro m a la mitad del valor del número de clúster μ en el modelo κ-μ μ con ensombrecimiento[2].

Una vez fijado m, el número de grados de libertad del modelo resultante se reduce en uno y se establece la siguiente relación bi-única entre los parámetros κ y η,

$$\kappa = \frac{1 - \eta}{2\eta}. \tag{B.5}$$

[1] El modelo η- μ es simétrico para $\eta \in [0, 1]$ y $\eta \in [1, \infty]$. Se tiene $q = \sqrt{\eta}$ o $q = 1/\sqrt{\eta}$ dependiendo del intervalo.

[2] Se ha de subrayar el hecho de que el número de clusters en el modelo κ - μ, y por lo tanto en el modelo κ-μ shadowed, es μ, mientras que 2μ es el número de clusters en el modelo η-μ model [29].

Esta relación matemática entre κ y η sólo tiene un claro significado físico en los casos límite del rango donde κ varía. Para $\kappa = 0$, se obtiene $\eta = 1$ a partir de (B.5), que en realidad corresponde al caso Rayleigh cuando sólo hay un cluster. Para $\kappa \to \infty$, se obtiene $\eta = 0$ de la (B.5), que es el caso gaussiano unilateral cuando de nuevo tenemos un clúster. Mientras, como se ha visto antes, el modelo κ-μ se obtiene eliminando totalmente la aleatoriedad de las componentes dominantes, este no es el caso para el modelo η-μ.

El modelo de Nakagami- m se puede deducir también con un método similar, es decir, sin eliminar directamente la componente dominante.

Si $m = \mu$, se obtiene la distribución Nakagami-m a partir de (B.1) gracias a la propiedad

$$ {}_1\mathcal{F}_1\Big(a; a; z\Big) = e^z. \tag{B.6}$$

Obsérvese que al establecer $m = \mu$, se transforma las componentes dominantes aleatorias del modelo presentado en [52] en componentes difusas. En cierta manera, se está agregando dos variables aleatorias gaussianas juntas en cada clúster, lo que directamente conduce a una variable aleatoria gaussiana equivalente, de modo que los modelos gaussiano unilateral, Rayleigh o Nakagami- m se obtienen dependiendo del número de clusters μ considerado.

La tabla B.1 resume todos los modelos que se derivan del modelo κ-μ con ensombrecimiento, donde los parámetros de éste se subrayan por razones de claridad. Cuando los parámetros del modelo κ-μ con ensombrecimiento se fijan a algunos valores positivos reales específicos o tienden a ciertos límites específicos, podemos obtener todos los modelos centrales clásicos, es decir, los modelos Rayleigh, gaussiano unilateral, Nakagami- q y Nakagami- m, así como el modelo clásico no central de Rician, y sus generalizaciones más populares, los modelos Rician con ensombrecimiento, κ-μ y η-μ.

TABLE B.1: Modelos Clásicos y Generalizados Derivados a partir del Modelo κ-μ con Ensombrecimiento

Channels	κ-μ Shadowed Parameters
One-sided Gaussian	a) $\underline{\mu} = 0.5$, $\underline{\kappa} \to 0$
	b) $\underline{\mu} = 0.5$, $\underline{m} = 0.5$
Rayleigh	a) $\underline{\mu} = 1$, $\underline{\kappa} \to 0$
	b) $\underline{\mu} = 1$, $\underline{m} = 1$
Nakagami-m	a) $\underline{\mu} = m$, $\underline{\kappa} \to 0$
	b) $\underline{\mu} = m$, $\underline{m} = m$
Nakagami-q (Hoyt)	$\underline{\mu} = 1$, $\underline{\kappa} = (1-q^2)/2q^2$, $\underline{m}$ = 0.5
Rician with parameter K	$\underline{\mu} = 1$, $\underline{\kappa} = K$, $\underline{m} \to \infty$
κ-μ	$\underline{\mu} = \mu$, $\underline{\kappa} = \kappa$, $\underline{m} \to \infty$
η-μ	$\underline{\mu} = 2\mu$, $\underline{\kappa} = (1-\eta)/2\eta$, $\underline{m} = \mu$
Rician shadowed	$\underline{\mu} = 1$, $\underline{\kappa} = K$, $\underline{m} = m$

Es notable que hay dos maneras de derivar los modelos gaussiano unilateral, Rayleigh y Nakagami- m, dependiendo de si se usan los enfoques de las secciones B.3.2 o B.3.3.

B.3.4 Analisis de la Capacidad Ergódica

La caracterización de la capacidad ergódica de canales sujetos a desvanecimientos, definida como

$$\bar{C}[\text{bps/Hz}] \triangleq \int_0^{+\infty} \log_2(1+\gamma) f_\gamma(\gamma) d\gamma, \tag{B.7}$$

donde γ is relación señal-ruido instantánea en el transmisor, ha levantado gran interés a lo largo de varias décadas [74]–[77]. Mientras que para sistemas que sufren desvanecimientos de tipo Rayleigh es posible obtener expresiones relativamente sencillas y con forma cerrada para la capacidad

ergódica, la consideración de modelos más generales conlleva la obtención de expresiones muy complciadas que normalmente requieren el empleo de funciones especiales como la funciones Meijer G[25], [77], [78].

Con el fin de superar los problemas que se derivan de la caracterización exacta de la capacidad de un canal κ-μ con ensombrecimiento debido a su complicada forma cerrada [78], parece más conveniente analizar el régimen de alta relación señal-ruido. En esta situación, la capacidad ergódica puede ser aproximada por [53, ecuación (8)]

$$\bar{C}(\bar{\gamma})|_{\bar{\gamma}\Uparrow} = \log_2(\bar{\gamma}) - L, \tag{B.8}$$

que es asintoticamente exacta and donde L is a constante independiente of la relación señal-ruido media y puede ser dada por

$$L = -\log_2(e)\frac{d}{dt}\frac{\mathbb{E}[\gamma^t]}{\bar{\gamma}^t}\Big|_{t=0}. \tag{B.9}$$

El parámetro L puede interpretarse como la pérdida de capacidad con respecto al caso en el que el canal sólo introduce ruido aditivo blanco gaussiano (AWGN), ya que la presencia de desvanecimiento causa $L > 0$. Cuando no hay desvanecimiento, $L = 0$ y esto se reduce al bien conocido resultado de Shannon. Usando este enfoque, derivamos una simple expresión de forma cerrada para la capacidad asintótica de canales κ-μ con ensombrecimiento, y esto es un nuevo resultado en la literatura.

La capacidad ergódica de un enlace sin cables que sufre desvanecimientos con distribución κ-μ con ensombrecimiento puede ser acotada inferiormente con precisión en el régimen de alta relación señal-ruido por

$$\bar{C}_{\kappa\mu m}(\bar{\gamma})|_{\bar{\gamma}\Uparrow} = \log_2(\bar{\gamma}) - L_{\kappa\mu m}, \tag{B.10}$$

donde $\log_2(\cdot)$ es el logaritmo binario y $L_{\kappa\mu m}$ puede expresarse como

$$\begin{aligned} L_{\kappa\mu m} = &- \log_2(e)\psi(\mu) - \log_2\left(\frac{\mu\kappa + m}{\mu m(1+\kappa)}\right) \\ &+ \log_2(e)\frac{\kappa(\mu - m)}{\mu\kappa + m} \\ &\times_3 \mathcal{F}_2\Big(1, 1, \mu - m + 1; 2, \mu + 1; \frac{\mu\kappa}{\mu\kappa + m}\Big). \end{aligned} \tag{B.11}$$

Nótese que cuando $\mu = 1$, se obtiene la capacidad ergódica del canal Rician con ensombrecimiento propuesto en [65].

A diferencia del análisis exacto en [78], que requiere la evaluación de una función Meijer G bivariable, este resultado proporciona una expresión en forma cerrada muy simple para la capacidad en el régimen de alta relación señal-ruido. Además, puesto que los modelos κ-μ y η-μ son casos particulares de la distribución κ-μ con ensombrecimiento, obtener la capacidad en estos escenarios se puede realizar sin la necesidad de evaluar una suma infinita de funciones Meijer G como en trabajo presentado en [25]. Esto se declara formalmente de la forma siguiente.

En alta relación señal-ruido, la capacidad ergódica de un canal κ-μ puede ser acotada inferiormente con precisión por

$$\bar{C}_{\kappa\mu}(\bar{\gamma})|_{\bar{\gamma}\Uparrow} = \log_2(\bar{\gamma}) - L_{\kappa\mu}, \tag{B.12}$$

donde $L_{\kappa\mu}$ puede expresarse como

$$\begin{aligned} L_{\kappa\mu} = &- \log_2(e)\psi(\mu) + \log_2(\mu) + \log_2(1+\kappa) \\ &- \kappa\log_2(e)\,{}_2\mathcal{F}_2\Big(1, 1; 2, \mu + 1; -\mu\kappa\Big). \end{aligned} \tag{B.13}$$

(B.13) se deriva applicando el límite $m \to \infty$ en (B.11), de forma que la función ${}_3\mathcal{F}_2(\cdot)$ collapsa en una función hypergeométrica ${}_2\mathcal{F}_2(\cdot)$ puesto que

$$\lim_{c\to\infty}\ {}_3\mathcal{F}_2(a_1, a_2, c; b_1, b_2; \frac{z}{c}) = \ {}_2\mathcal{F}_2(a_1, a_2; b_1, b_2; z). \tag{B.14}$$

En alta relación señal-ruido, la capacidad ergódica de un canal η-μ puede ser acotada inferiormente con precisión por

$$\bar{C}_{\eta\mu}(\bar{\gamma})|_{\bar{\gamma}\Uparrow} = \log_2(\bar{\gamma}) - L_{\eta\mu}, \tag{B.15}$$

donde $L_{\eta\mu}$ puede expresarse como

$$\begin{aligned} L_{\eta\text{-}\mu} = &- \log_2(e)\psi(2\mu) + \log_2(\mu) + \log_2(1+\eta) \\ &+ \log_2(e)\frac{(1-\eta)}{2}\,{}_3\mathcal{F}_2\big(1,1,\mu+1;2,2\mu+1;1-\eta\big). \end{aligned} \tag{B.16}$$

Se ha obtenido la capacidad asintótica de un canal η-μ a partir de (B.11) fijando $\underline{m}= \mu$, $\underline{\mu}= 2\mu$ and $\underline{\kappa}= (1-\eta)/(2\eta)$ como indica la Tabla B.1.

Por lo tanto, las expresiones de las capacidades asintóticas para canales κ-μ y η-μ han sido deducidas conjuntamente del resultado en (B.10), que son también nuevos resultados. Además, derivar la capacidad asintótica del canal κ-μ con ensombrecimiento no ha sido más difícil que derivar las capacidades asíntóticas de los canales κ-μ o η-μ directamente, ya que los momentos de sus relaciones señal-ruido instantáneas se pueden expresar, como en el caso κ-μ con ensombrecimiento, en términos de una función hipergeométrica de tipo Gauss [29]. Así, se han matado dos (en realidad tres) pájaros con un mismo tiro.

Usando las equivalencias en la tabla B.1, se pueden obtener expresiones aún más simples para los modelos clásicos de desvanecimiento, que se reducen a los resultados existentes en la literatura, para Nakagami-m [53], Rician [72] y Hoyt [23]. Por razones de claridad, omitimos las derivaciones directas del resto de capacidades asintóticas. En su lugar, resumimos en la tabla B.2 las pérdidas de capacidad con respecto al canal AWGN en el régimen de alta relación señal-ruido, donde $\Gamma(a,b)$ es la función gamma incompleta y γ_e es la constante de Euler-Mascheroni, es decir, $\gamma_e \approx 0.5772$. También es notable que, por primera vez, se presenta la expresión de capacidad asintótica

TABLE B.2: Pérdida de Capacidad Ergódica en alta relación señal-ruido para Diferentes Canales

Channels	Ergodic capacity loss (L) [bps/Hz]
One-sided Gaussian	$1+\gamma_e \cdot \log_2(e) \approx 1.83$
Rayleigh	$\gamma_e \cdot \log_2(e) \approx 0.83$
Nakagami-m	$\log_2(m) - \log_2(e)\psi(m)$
Nakagami-q (Hoyt)	$1+\gamma_e \cdot \log_2(e) + \log_2\left(\frac{1+q^2}{(1+q)^2}\right)$
Rician with parameter K	$\log_2(1+1/K) - \log_2(e)\Gamma(0,K)$
κ-μ	$-\log_2(e)\psi(\mu) + \log_2(\mu) + \log_2(1+\kappa)$ $-\kappa\log_2(e)_2\mathcal{F}_2\Big(1,1;2,\mu+1;-\mu\kappa\Big)$
η-μ	$-\log_2(e)\psi(2\mu) + \log_2(\mu)$ $+\log_2(1+\eta) + \log_2(e)\frac{(1-\eta)}{2}$ $\times_3\mathcal{F}_2\big(1,1,\mu+1;2,2\mu+1;1-\eta\big)$
Rician shadowed	$\gamma_e \cdot \log_2(e)$ $-\log_2\left(\frac{K+m}{m(1+K)}\right) + \log_2(e)\frac{K(1-m)}{K+m}$ $\times_3\mathcal{F}_2\Big(1,1,2-m;2,2;\frac{K}{K+m}\Big)$

del Rician con ensombrecimiento propuesto en [65], que no es más que un caso particular del modelo κ-μ sombreado cuando $\mu = 1$.

B.3.5 Resultados Numéricos

Es importante estudiar la evolución de la pérdida de capacidad para los modelos de desvanecimiento κ-μ con ensombrecimiento, κ-μ y η- μ con respecto al caso AWGN. Subrayamos el hecho de que los diferentes valores paramétricos aquí presentados no provienen de canales prácticos reales, sino que permiten verificar las expresiones teóricas.

Dependiendo de las condiciones de propagación, los parámetros κ y μ pueden tomar valores muy diferentes [52], [67], [79]–[81]. Por ejemplo, en

algunos escenarios de comunicación acústica subacuática [79], los parámetros del canal $\kappa \in [0.03 - 9.56]$, $\mu \in [0.90 - 1.27]$ y $m \in [1.32 - 18.01]$, mientras que en algunos escenarios de comunicación *body-centric* [67], [80], [81], se tiene $\kappa \in [1.08 - 481]$, $\mu \in [0.01 - 3.22]$ y $m \in [0.04 - 2876]$.

En las Fig. 4.1 y Fig. 4.2, se representan las expresiones analíticas exactas de la capacidad ergódica de modelos de desvanecimiento clásicos y generalizados, respectivamente, que están disponibles en la literatura [25], [78], y los comparamos con la expresión analítica asintótica obtenida en (B.10).

Obsérvese que todos los modelos convergen con precisión a sus valores asintóticos, permaneciendo por debajo del límite de Shannon, es decir, la capacidad del canal AWGN. Por lo tanto, la expresión de la capacidad ergódica asintótica derivada anteriormente para el modelo κ-μ con ensombrecimiento se valida aquí con las expresiones correspondientes de los modelos gaussiano unilateral, Rayleigh, Nakagami- m, Nakagami- q, Rician, Rician con ensombrecimiento, κ-μ y η-μ.

En las figuras 4.3-4.6, se muestra la evolución de la pérdida de capacidad asintótica L, definida en (B.9), del canal κ-μ con ensombrecimiento cuando m crece. Téngase en cuenta que esta métrica no depende de la relación señal-ruido promedio recibida $\bar{\gamma}$. Cuando el ensombrecimiento no es despreciable, es decir, en las figuras 4.3-4.5, tener más potencia en las componentes dominantes no siempre mejora la capacidad ergódica, sino que a veces eleva considerablemente la pérdida de capacidad, especialmente para un gran número de clusters. Cuando $m \geq 20$, es decir, en la Fig. 4.6, el efecto del ensombrecimiento se puede despreciar y el modelo en realidad tiende al modelo κ-μ, donde un aumento en la potencia de los componentes dominantes es obviamente favorable para la capacidad del canal. Por lo tanto, recibir más potencia a través de los componentes dominantes no siempre aumenta la capacidad en presencia de ensombrecimiento. Se observan dos comportamientos diferentes en la evolución de pérdida de capacidad con respecto al parámetro

κ. Cuando $m < \mu$, el aumento del parámetro κ es perjudicial para la capacidad. Por el contrario, cuando $m > \mu$ la capacidad se mejora a medida que κ se incrementa, es decir, en presencia de una componente dominante más fuerte. En el caso límite de $m = \mu$, se comprueba que la pérdida de capacidad es independiente de κ. Ésto se puede explicar de la forma siguiente. Supóngase que las componentes difusas y dominantes con ensombrecimiento en cada clúster son variables aleatorias gaussianas complejas, que es el caso más simple posible a considerar cuando $m = \mu$. Se obtendrá una variable aleatoria gaussiana equivalente cuya potencia no se ve afectada por el parámetro κ. Para $m > \mu$, el modelo κ-μ con ensombrecimiento puede ser aproximado por el modelo κ-μ para un parámetro m suficientemente alto, como muestra la Tabla B.1. En este caso, es fácil comprender que un aumento del parámetro κ implica la disminución de las pérdidas de capacidad asintótica, ya que una mayor potencia de las componentes dominantes implica mejorar la capacidad del canal κ-μ. Por el contrario, cuando $m < \mu$, la observación anterior puede parecer contraintuitiva a primera vista. Considérese el caso particular donde $m = \mu/2$, que coincide con el caso de desvanecimiento de tipo η-μ. En ese caso, incrementar el parámetro κ implica aumentar la asimetría de las variables aleatorias subyacentes gaussianas no-circularmente simétricas del modelo, lo que degrada la capacidad. Para el resto de casos donde $m < \mu$, se puede hacer una justificación similar.

También se observa que la pérdida de capacidad disminuye a medida que μ crece, ya que tener un mayor número de clusters reduce la severidad de desvanecimiento de los efectos de propagación a pequeña escala.

Por último, las Fig. 4.7 y Fig. 4.8 representan la pérdida de capacidad ergódica asintótica para los modelos de desvanecimiento κ-μ y η-μ, respectivamente. Se observa que la Fig. 4.7 es bastante similar a la Fig. 4.6 porque, como se mencionó anteriormente, el modelo κ-μ con ensombrecimiento con $m \geq 20$ puede ser aproximado por el modelo κ-μ. En la Fig. 4.8, se observa

que, independientemente del número de clusters 2μ, hay un mínimo en la pérdida de capacidad de canal en $\eta = 1$ que divide en dos partes simétricas, como se esperaba, el comportamiento del desvanecimiento. También se puede observar que en la Fig. 4.8 se ha especificado los casos límite para $\eta \to 0$ y $\eta \to \infty$. Cuando $\mu = 0.5$, el modelo η-μ colapsa en el modelo gaussiano unilateral para $\eta = 0$ o $\eta \to \infty$, mientras que para $\eta = 1$ colapsa en el modelo Rayleigh. Cuando $\mu = 1$, el modelo η-μ se reduce al caso Rayleigh para $\eta = 0$ o $\eta \to \infty$. Esto se muestra en la figura incluyendo también los valores de pérdida de capacidad de los canales Rayleigh y gaussiano unilateral con líneas punteadas y discontinuas horizontales, respectivamente.

B.3.6 Conclusiones

Se ha demostrado que el modelo κ-μ con ensombrecimiento unifica las distribuciones κ-μ y η-μ. Con una interpretación de variables subyacentes gaussianas novedosa del efecto de ensombrecimiento en las componentes dominantes, se ha demostrado que el modelo κ-μ con ensombrecimiento también puede ser empleado en escenarios en los que las componentes difusas son modeladas con variables aleatorias gaussianas complejas no-circularmente simétricas, lo que da a la distribución κ-μ con ensombrecimiento una mayor flexibilidad para modelar diferentes condiciones de propagación que las alternativas existentes cuando se opera en entornos inalámbricos. Por lo tanto, el modelo κ-μ con ensombrecimiento unifica todos los modelos clásicos de desvanecimiento, es decir, los canales gaussiano unilateral, Rayleigh, Nakagami- m, Nakagami- q y Rician, y sus generalizaciones, los modelos κ-μ, η-μ y Rician con ensombrecimiento. Se han deducido nuevas expresiones sencillas en forma cerrada para evaluar la capacidad ergódica en el régimen de alta relación señal-ruido para el modelo κ-μ con ensombrecimiento, y por lo tanto, usando la conexión aquí desvelada, para los modelos κ-μ, η- μ y

Rician con ensombrecimiento, dándose una visión clara de cómo afectan los parámetros de desvanecimiento en la mejora o degradación de la capacidad.

Como comentario final, se puede pensar si el nombre de la distribución κ-μ con ensombrecimiento sigue siendo apropiado para este modelo, ya que su flexibilidad trasciende las características originales presentadas en [52].

B.4 Máximo Autovalor de Matrices de tipo Wishart no-Circularmente Simétricas

La distribución del máximo autovalor de las llamadas matrices aleatorias de tipo Wishart juega un papel importante en una amplia gama de aplicaciones, incluyendo la detección de señales [95], el modelado de desvanecimiento [45] y el análisis de componentes principales [4]. A pesar de la rica caracterización de las conocidas matrices Wishart complejas y reales, los resultados para modelos de tipo Wishart generados a partir de matrices Gaussianas complejas no-circularmente simétricas son mucho más escasos. En particular, se distinguen las matrices hermitianas de la forma:

$$\mathbf{W} = \begin{cases} \mathbf{X}\mathbf{X}^{\dagger}, & p \leq n \\ \mathbf{X}^{\dagger}\mathbf{X}, & p > n \end{cases} \tag{B.17}$$

donde $\mathbf{X} \in \mathbb{C}^{p \times n}$ tiene entradas gaussianas complejas independientes e idénticamente distribuidas (i.i.d.) con $\mathrm{Re}(\{\mathbf{X}\}_{i,j}) \sim \mathcal{N}(0, \sigma^2_{\mathrm{Re}})$ y $\mathrm{Im}(\{\mathbf{X}\}_{i,j}) \sim \mathcal{N}(0, \sigma^2_{\mathrm{Im}})$, es decir, con variances arbitrarias en sus partes real e imaginaria, y donde $\mathrm{Re}(\{\mathbf{X}\}_{i,j})$ y $\mathrm{Im}(\{\mathbf{X}\}_{i,j})$ son mútuamente independientes.

El modelo en (B.17) se ha referido como el conjunto cruzado entre los *ensembles* unitarios (LUE) y ortogonales (LOE) de Laguerre [26]. Cuando ambas varianzas son iguales, es decir, $\sigma^2_{\mathrm{Re}} = \sigma^2_{\mathrm{Im}}$, $\mathbf{W}$ es una matriz de Wishart

compleja central (LUE); Cuando una de las varianzas es cero, $\mathbf{W}$ es una matriz Wishart real central (LOE). Conjuntos intermedios similares han sido un tema de interés en el contexto de *ensembles* gaussianos (no de tipo Wishart), es decir, GUE y GOE, con aplicaciones al estudio de los espaciamientos de niveles de energía en física nuclear [8].

Con aplicaciones al modelado de desvanecimiento, las obras de [28] y [26] hicieron un progreso inicial para caracterizar el conjunto intermedio de tipo Wishart de (B.17). En [28], el análisis se limita a una matriz $\mathbf{X}$ 2×2 y la función densidad de probabilidad conjunta (jpdf) de los valores propios de $\mathbf{W}$ se da en una forma muy complicada que implica seis integrales. En [26], la jpdf de los autovalores se deriva para dimensiones arbitrarias usando propiedades de movimiento brownianas con una variable ficticia de tiempo que está relacionada con la relación entre las varianzas σ^2_{Re} y σ^2_{Im}. Sin embargo, esta expresión sigue siendo complicada y no permite ningún análisis más profundo. La complejidad y escasez de resultados para el modelo en (B.17) se deben principalmente al desafío que plantea un perfil de varianza asimétrico, que hace que las propiedades clásicas de matriz aleatoria ya no sean aplicables. En particular, a pesar de su interés interdisciplinario, los resultados para el máximo autovalor no están disponibles hasta ahora, ni siquiera para una matriz $\mathbf{X}$ de dimensiones 2×2, y las implicaciones de este perfil de varianza asimétricos permanecen en gran medida desconocidas.

En esta sección, se propone un nuevo enfoque para caracterizar el máximo autovalor de $\mathbf{W}$ para dimensiones arbitrarios de p, n. Al aprovechar una nueva conexión estadística entre $\mathbf{W}$ y la bien conocida matriz de Wishart compleja no central, se deriva una expresión exacta y una expansión asintótica (en la cola) para la distribución del máximo autovalor, que proporciona nuevas conclusiones sobre los efectos del perfil asimétrico de varianza de $\mathbf{X}$. Después, se utilizarán estas expresiones para estudiar el rendimiento de los sistemas de comunicación MIMO sujetos al desvanecimiento de tipo

Nakagami- q (Hoyt), en un contexto similar al de los trabajos en [26], [28]. En particular, los resultados analíticos que aquí se muestran explicarán el impacto del parámetro de desvanecimiento q sobre la probabilidad y la capacidad de *outage* de los sistemas MIMO con *maximal ratio combining* (MIMO-MRC).

Se debe señalar que parte del trabajo presentado en este capítulo se ha realizado en colaboración con Matthew R. McKay, durante mi estancia en HKUST.

B.4.1 Distribución del Máximo Autovalor de W

En el modelo (B.17), resulta conveniente reescribir $\mathbf{X}$ como

$$\mathbf{X} = \mathbf{X}_C + \mathbf{X}_R \tag{B.18}$$

donde las matrices $\mathbf{X}_C \in \mathbb{C}^{p\times n}$ y $\mathbf{X}_R \in \mathbb{R}^{p\times n}$ son mútuamente independientes con media cero y entradas i.i.d.. Las entradas $\{\mathbf{X}_C\}_{i,j}$ son $\mathcal{CN}(0,\sigma_C^2)$ circularmente simétricas, mientras que $\{\mathbf{X}_R\}_{ij} \sim \mathcal{N}(0,\sigma_R^2)$, con las correspondencias:

$$\sigma_C^2 = 2\sigma_{\mathrm{Im}}^2 \,, \qquad \sigma_R^2 = \sigma_{\mathrm{Re}}^2 - \sigma_{\mathrm{Im}}^2 \,. \tag{B.19}$$

Esta redefinición (B.17) facilitará el subsecuente análisis. Hay que destacar que, aunque (B.18) impone $\sigma_{\mathrm{Re}} \geq \sigma_{\mathrm{Im}}$, esto no implica ninguna pérdida de generalidad, puesto que remplazar σ_{Re} por σ_{Im} y viceversa no affecta los estadísticos de los autovalores de $\mathbf{W}$.

Sean $s = \min(p,n)$, $t = \max(p,n)$ y $\mathbf{W}$ definida en (B.17). Cuando $\sigma_C^2 = 0$ ó $\sigma_R^2 = 0$, $\mathbf{W}$ collapsa una matrix Wishart (real or compleja) central, cuyas propiedades se conocen ampliamente. No obstante, cuando ambas $\sigma_C, \sigma_R > 0$, la matriz se desvía de estos modelos clásicos, y la caracterización estadística se vuelve un reto más difícil.

La clave para abordar el problema es utilizar un método de "condicionar y promediar" que permite conectar las propiedades estadísticas de la matrix $\mathbf{W}$ con aquellas de la matrices Wishart no centrales, haciendo uso de los resultados de estas últimas. Específicamente, defínase $\mathbf{W}_R = \mathbf{X}_R\mathbf{X}_R^\dagger$ si $p \leq n$ o $\mathbf{W}_R = \mathbf{X}_R^\dagger\mathbf{X}_R$ en cualquier otro caso. Cuando se condiciona a la matriz $\mathbf{W}_R \in \mathbb{R}^{s\times s}$, $\mathbf{W}$ sigue una distribución de Wishart compleja no central con t grados de libertad y matriz de descentralidad $\mathbf{W}_R$, i.e., $\mathbf{W}|\mathbf{W}_R \sim \mathcal{CW}(t, \sigma_C^2\mathbf{I}_s, \mathbf{W}_R)$. La distribución del máximo autovalor de $\mathbf{W}$ puede ser obtenida promediando la de $\mathbf{W}|\mathbf{W}_R$ por la de $\mathbf{W}_R$, que pertenece al espacio de matrices reales definidas positivas.

La ventaja principal de este enfoque es que evita la necesidad de integrar directamente la jpdf de autovalores de $\mathbf{W}$. Dicha densidad conjunta se conoce para s, t arbitrarios [26], sin embargo la expresión es complicada, involucrando pfaffianos de matrices cuyas entradas contienen series infinitas dobles con términos que implican productos de polinomios de Laguerre generalizados. Como tal, parece difícil calcular la distribución del máximo autovalor marginalizando la jpdf de autovalares presentada en [26]. A continuación, explotando la conexión con la matrix Wishart no central, se proporcionan resultados, por primera vez, exactos y asintóticos para la distribución del máximo autovalor de $\mathbf{W}$.

Considere $\mathbf{W}$ definida en (B.17), con $\sigma_C, \sigma_R > 0$. La función distribución del máximo autovalor de $\mathbf{W}$ admite

$$F_{\phi_{\max}}(x) = \frac{\text{Pf}(\mathbf{\Xi}_1(x))}{\text{Pf}(\mathbf{\Xi}_2)} \tag{B.20}$$

donde $\text{Pf}(\cdot)$ denota la operación matricial pfaffiana, $\mathbf{\Xi}_1(x)$ es de dimensiones $s \times s$ y con entradas

$$\{\mathbf{\Xi}_1(x)\}_{i,j} = \int_0^\infty \int_0^\infty f_i(x,u) f_j(x,z) \text{sgn}(z-u) du dz \tag{B.21}$$

donde sgn$(\cdot)$ es la función signo, y

$$f_k(x,y) = \sqrt{\frac{e^{-y/\sigma_R^2}}{(\sigma_C^2/2)^{2k}y}}\left[Q_{s+t-2k+1,t-s}\left(\sqrt{2y/\sigma_C^2},0\right) - Q_{s+t-2k+1,t-s}\left(\sqrt{2y/\sigma_C^2},\sqrt{2x/\sigma_C^2}\right)\right] \tag{B.22}$$

donde $Q_{\cdot,\cdot}(\cdot,\cdot)$ es la función Nuttall Q [40]. La matriz $\boldsymbol{\Xi}_2$ es de dimensiones $s \times s$ con entradas

$$\{\boldsymbol{\Xi}_2\}_{i,j} = \int_0^{+\infty}\int_0^{+\infty} g_i(u)g_j(z)\text{sgn}(z-u)dudz \tag{B.23}$$

donde

$$g_k(y) = \sqrt{\frac{e^{-y/\sigma_R^2}}{(\sigma_C^2/2)^{2k}y}}Q_{s+t-2k+1,t-s}\left(\sqrt{2y/\sigma_C^2},0\right). \tag{B.24}$$

El cálculo específico de los pfaffianos en (B.20) depende de si la dimensión s de la matriz es par o impar. En cualquier caso, sin embargo, pueden ser evaluados como la raíz cuadrada de un determinante [43].

Aunque esta expresión es exacta, no da una idea de cómo se comporta la distribución del máximo autovalor cuando cambia el desequilibrio de varianza entre las partes real e imaginaria de $\mathbf{X}$. Con esto en mente, se establece una expansión simplificada de la cola de la distribución en la subsección siguiente.

B.4.2 Expansión Asintótica en la Cola

Cuando $x \to 0$,

$$F_{\phi_{\max}}(x) = h_{s,t}\, a_{s,t}^{\text{CW}} x^{st} + o(x^{st}) \tag{B.25}$$

donde

$$a_{s,t}^{\text{CW}} = \prod_{i=1}^{s}\frac{(s-i)!}{(s+t-i)!} \tag{B.26}$$

y

$$h_{s,t} = \frac{1}{\left(\sigma_C\sqrt{2\sigma_R^2 + \sigma_C^2}\right)^{st}} \ . \tag{B.27}$$

En la expresión anterior, $a_{s,t}^{\text{CW}}$ corresponde con el coeficiente de expansión para el autovalor máximo de una matriz Wishart compleja central [57], [93]. Por lo tanto, en la cola izquierda, el efecto del desbalanceo de potencia de las componentes real e imaginaria de $\mathbf{X}$ se revela claramente, y se desacopla en la función $h_{s,t}$ en (B.27). La simplicidad de la ecuación es bastante notable, particularmente cuando se considera la complejidad de la distribución exacta del máximo autovalor en (B.20), así como la de la distribución conjunta de los autovalores presentada en [26].

Para interpretar mejor el resultado en (B.25), se expresa la función $h_{s,t}$ en términos de las varianzas originales σ_{Re}^2 y σ_{Im}^2, mientras que se fija la varianza total como $\sigma_{\text{Re}}^2 + \sigma_{\text{Im}}^2 = 1$. Entonces,

$$h_{s,t} = \frac{1}{(4\sigma_{\text{Re}}^2(1-\sigma_{\text{Re}}^2))^{st/2}} \ . \tag{B.28}$$

A partir de (B.28), el factor $h_{s,t}$ se minimiza claramente en el caso "equilibrado", $\sigma_{\text{Re}}^2 = 1/2$, para el cual $h_{s,t} = 1$, como debería ser. Se observa una desviación significativa, sin embargo, a medida que las componentes real e imaginaria se vuelven más desequilibradas en potencia. Es decir, cuanto mayor es el desequilibrio, más lenta es el decaimiento de la cola izquierda de $F_{\phi_{\text{max}}}(x)$.

B.4.3 Probabilidad y capacidad de *outage* de sistemas MIMO-MRC en entornos Nakagami-q (Hoyt)

Aquí se ofrece un ejemplo de aplicación para los resultados previamente derivados. Considere un enlace de comunicación entre un transmisor,

equipado con N_t antenas, y un receptor con N_r antenas. El enlace multi-antena está sujeto a un desvanecimiento de tipo Nakagami- q (Hoyt), típicamente asumido en comunicaciones por satélite [5] o, en general, cuando las condiciones de desvanecimiento son más severas que las de un entorno Rayleigh. El canal está modelado por $\mathbf{H} \in \mathbb{C}^{N_r \times N_t}$ con media cero y entradas i.i.d. de la forma $\{\mathbf{H}\}_{i,j}$, que representan la ganancia compleja entre las antenas de recepción j-ésima e i-ésima, donde $\mathrm{Re}(\{\mathbf{H}\}_{i,j}) \sim \mathcal{N}(0, \sigma^2_{\mathrm{Re}})$ y $\mathrm{Im}(\{\mathbf{H}\}_{i,j}) \sim \mathcal{N}(0, \sigma^2_{\mathrm{Im}})$ son mútuamente independentes, $\sigma^2_{\mathrm{Re}} = 1/(1+q^2)$, $\sigma^2_{\mathrm{Im}} = q^2/(1+q^2)$, y $q \in (0,1)$ denota el parámetro de desvanecimiento Hoyt, que define el desbalanceo de potencia entre parte real e imaginaria de las componentes del canal. Utilizando la redefinición en (B.18),

$$\mathbf{H} = \sqrt{\frac{2q^2}{1+q^2}}\mathbf{H}_C + \sqrt{\frac{1-q^2}{1+q^2}}\mathbf{H}_R \tag{B.29}$$

donde las entradas $\mathbf{H}_C$ son circularmente simétricas $\mathcal{CN}(0,1)$, donde las matrices $\mathbf{H}_R$ son $\mathcal{N}(0,1)$. Defínase $\mathbf{W}_{\mathrm{H}} = \mathbf{H}\mathbf{H}^\dagger$, si $N_r \leq N_t$, o $\mathbf{W}_{\mathrm{H}} = \mathbf{H}^\dagger\mathbf{H}$ en otro caso.

Supóngase además que el receptor tiene un conocimiento perfecto de la matriz del canal $\mathbf{H}$ mientras que el transmisor, con sólo un conocimiento parcial, utiliza el conocido principio de *beamforming* (BF) [15] para enviar datos con una potencia total fija P. El ruido en cada antena de recepción se supone independiente $calCN(0,1)$ y definimos la relación señal-ruido de transmisión como $\bar{\gamma} \triangleq P$. El vector de señal recibido $\mathbf{r} \in \mathbb{C}^{N_r}$ puede entonces expresarse como

$$\mathbf{r} = \sqrt{\bar{\gamma}}\mathbf{H}\mathbf{w}x + \mathbf{n} \tag{B.30}$$

donde x is el símbolo transmitido con $\mathbb{E}[|x|^2] = 1$, $\mathbf{n}$ es el vector de ruido, y $\mathbf{w}$ es el vector de BF con $||\mathbf{w}|| = 1$. La detección de x es óptima cuando $\mathbf{w}$ iguala el autovector correspondiente al máximo autovalor de $\mathbf{W}_{\mathrm{H}}$ y cuando

el principio de MRC es aplicado a la señal recibida $\mathbf{r}$, que lleva a una relación señal-ruido post-procesada de [15]

$$\gamma = \bar{\gamma}\lambda_{\max} \tag{B.31}$$

donde $\lambda_{\max}$ denota el máximo autovalor de $\mathbf{W}_{\mathrm{H}}$.

Definiendo γ_{th} como la mínima relación señal-ruido requerida para una comunicación fiable (es decir, con el símbolo x detectado con fiabilidad), la probabilidad de *outage* se puede obtener excatamente como

$$P_{\text{out}} = \Pr(\gamma \leq \gamma_{\text{th}}) = F_{\phi_{\max}}\left(\frac{\gamma_{\text{th}}}{\bar{\gamma}}\right) \tag{B.32}$$

donde $\sigma_C^2 = 2q^2/(1+q^2)$, $\sigma_R^2 = (1-q^2)/(1+q^2)$, $s = \min(N_t, N_r)$ y $t = \max(N_t, N_r)$.

Para profundizar en el análisis, se aproxima P_{out} utilizando la caracterización asintótica de la subsección anterior. En la práctica, es interesante considerar pequeñas probabilidades de *outage*, esto es pequeños valores de $\gamma_{\text{th}}/\bar{\gamma}$. Gracias a (B.25), cuando $\gamma_{\text{th}}/\bar{\gamma} \to 0$,

$$P_{\text{out}} \approx \hat{P}_{\text{out}} = a_{s,t}^{\text{CW}}\left(\frac{\gamma_{\text{th}}}{\theta(q)\bar{\gamma}}\right)^{st} \tag{B.33}$$

donde $\theta(q) = 2q/(1+q^2)$ y $q > 0$. Esto revela explícitamente que la ganancia de potencia que se obtiene dirigiendo la señal hacia el mayor autocanal disminuye a medida que las componentes del canal real e imaginaria sufren mayor desequilibrio. Específicamente, el efecto de tal desequilibrio puede ser visto como una reducción en la relación señal-ruido media — con respecto al caso perfectamente equilibrado (desvanecimiento Rayleigh, $q = 1$) — por un factor de $\theta(q) < 1$. La probabilidad de *outage* se degradada (aumenta) a razón del factor $\theta(q)^{-st}$, que puede ser aproximado por $(2q)^{-st}$ para q pequeños. Obsérvese que esta degradación se acentúa exponencialmente a medida que

aumenta el número de antenas.

La Fig. 5.1 representa la probabilidad de interrupción de sistemas MIMO 2×2 y 2×3 en función de la relación señal-ruido media $\bar{\gamma}$, operando en tres condiciones diferentes de desvanecimiento ($q = 1$, $q = 0,5$ y $q = 0,3$). Por cada q, se traza: (i) la probabilidad empírica — obtenida a través de simulaciones de tipo Monte-Carlo (10^6 realizaciones), (ii) la exacta P_{out} en (B.32) — donde se calcula $F_{\phi_{\max}}(x)$ a partir de (B.20) numéricamente [3], y (iii) la probabilidad de *outage* asintótica $\hat{P}_{\text{out}}$ en (B.33). Se observa un buen acuerdo entre los resultados analíticos (exactos) y simulados en todos los casos y, como se esperaba, el resultado asintótico coincide con el exacto cuando P_{out} se hace más pequeño. Como se anticipó, P_{out} se degrada significativamente a medida que q disminuye, y tal degradación es más pronunciada en el escenario 2×3. Incluso para un sistema de doble antena (2×2), esta degradación en $\bar{\gamma} = 10$ dB es aproximadamente un orden de magnitud para el caso $q = 0,3$ (90% de la ganancia del canal en la parte real y 10% en la parte imaginaria, o viceversa) con respecto al caso $q = 1$ (Rayleigh). Esto es consistente con la predicción analítica anterior, donde la degradación P_{out} fue dada por el factor $\theta(q)^{-st}$ cuando $\gamma_{\text{th}}/\bar{\gamma} \to 0$. Para $q = 0.3$ y $st = 4$, este factor es ~ 10.9.

También es interesante estudiar la capacidad de *outage*, definida como la máxima tasa de transmisión (en bits/s/Hz) que se puede garantizar de forma fiable al menos $(1 - \epsilon) \times 100\%$ del tiempo, es decir

$$R_{\text{out}}(\epsilon) = \sup_{R \geq 0}(R : P_{\text{out}}(R) < \epsilon) \tag{B.34}$$

[3] Para calcular (B.21) y (B.23), se usa el método de Gauss-Laguerre, donde las funciones Nuttall Q son evaluadas a partir de una suma finita de funciones Marcum Q, ya que la suma de sus órdenes es impar [41].

donde ϵ es the máximo nivel de *outage* y $P_{\text{out}}(R)$ es la proabilidad de *outage* para una tasa de datos R dada, esto es

$$\begin{aligned} P_{\text{out}}(R) \triangleq &\Pr\left(\log_2(1+\gamma) \leq R\right) \\ =&F_{\phi_{\text{max}}}((2^R-1)/\bar{\gamma}). \end{aligned} \tag{B.35}$$

Entonces,

$$R_{\text{out}}(\epsilon) = \log_2(1+\bar{\gamma}F^{-1}_{\phi_{\text{max}}}(\epsilon)) \tag{B.36}$$

donde $F^{-1}_{\phi_{\text{max}}}(\cdot)$ denota la inversa de la functión $F_{\phi_{\text{max}}}(\cdot)$. De nuevo, (B.25) permite aproximar $R_{\text{out}}(\epsilon)$ para valores pequeños de ϵ con una expresión compacta e intuitiva; cuando $\epsilon \to 0$,

$$R_{\text{out}}(\epsilon) \approx \hat{R}_{\text{out}}(\epsilon, q) = \log_2\left(1+\theta(q)\bar{\gamma}\left(\frac{\epsilon}{a^{\text{CW}}_{s,t}}\right)^{1/st}\right) \tag{B.37}$$

donde, una vez más, se ve claramente el efecto del desvanecimiento a través del factor aislado $\theta(q)$ que, for $q < 1$, causa una reducción en la relación señal-ruido "efectiva". Para ilustrar mejor la degradación de la tasa de *outage* con respecto al caso Rayleigh ($q = 1$), se define una aproximación de la pérdida de tasa de outage fraccional como

$$\hat{RL}(\%) \approx \frac{\hat{R}_{\text{out}}(\epsilon,1) - \hat{R}_{\text{out}}(\epsilon,q)}{\hat{R}_{\text{out}}(\epsilon,1)} \times 100. \tag{B.38}$$

La Tabla B.3 la $\hat{RL}$ aproximada junto con la RL exacta, evaluadas a partir de (B.36) con la inversión numérica de $F_{\phi_{\text{max}}}(\cdot)$, para un escenario 2×2 con máximo nivel de *outage* de $\epsilon = 10^{-3}$ y $\bar{\gamma} = 10$ dB. Los números revelan una degradación substancial de dicha tasa conforme el valor de q se vuelve más pequeño, hasta un $\sim 37\%$ de pérdida ($q = 0.2$).

TABLE B.3: Pérdida de tasa de datos para un sistema MIMO 2×2 para $\bar{\gamma} = 10\,\mathrm{dB}$, $\epsilon = 10^{-3}$

q	0.5	0.4	0.3	0.2
RL	9%	17%	26%	37%
$\hat{RL}$	9%	18%	27%	43%

B.4.4 Conclusiones

Se ha simplificado el estudio de matrices de tipo Wishart no-circularmente simétricas, que ha permitido dar, por primera vez, resultados sobre la distribución del máximo autovalor, conectando los estadísticos de estas matrices y la de las conocidas matrices Wishart complejas no centrales. Aunque la distribución exacta del máximo autovalor no permite realizar un análisis profundo del efecto de un perfil asimétrico de potencia entre las partes real e imaginaria del modelo, la expansión asintótica en la cola traduce claramente este efecto en un simple factor aislado.

Estos resultados se han aplicado a sistemas MIMO 2×2 y 2×3 bajo diferentes condiciones de desvanacimiento de tipo Nakagami- q (Hoyt). Se ha visto que la presencia de un desequilibrio entre las componentes real e imaginaria de canal degrada significativamente la probabilidad y la capacidad de *outage*. Este efecto se acentúa exponencialmente para un gran número de antenas en ambos lados del transmisor y del receptor. También se ha observado que los resultados asintóticos, a pesar de ser muy simples, son notablemente ajustados a los exactos, incluso para casos extremos de desvanacimiento (q pequeños).

Bibliography

[1] D. Marcuse, "Derivation of analytical expressions for the bit-error probability in lightwave systems with optical amplifiers", *J. Lightw. Technol.*, vol. 8, no. 12, pp. 1816–1823, 1990.

[2] F. J. Dyson, "Statistical theory of the energy levels of complex systems. i", *J. Math. Phys.*, vol. 3, no. 1, pp. 140–156, 1962.

[3] S. M. Kay, *Fundamentals of Statistical Signal Processing, Volume I: Estimation Theory*. Prentice-Hall, 1993.

[4] I. M. Johnstone, "On the distribution of the largest eigenvalue in principal components analysis", *Ann. Stat.*, vol. 29, no. 2, pp. 295–327, Apr. 2001.

[5] M. K. Simon and M.-S. Alouini, *Digital Communication over Fading Channels*. John Wiley & Sons, 2005.

[6] J. W. Goodman, "Dependence of image speckle contrast on surface roughness", *Opt. Commun.*, vol. 14, no. 3, pp. 324–327, 1975.

[7] J. Ohtsubo and T. Asakura, "Statistical properties of laser speckle produced in the diffraction field", *Appl. Opt*, vol. 16, no. 6, pp. 1742–1753, 1977.

[8] A Pandey and M. Mehta, "Gaussian ensembles of random Hermitian matrices intermediate between orthogonal and unitary ones", *Commun. Math. Phys.*, vol. 87, no. 4, pp. 449–468, 1983.

[9] L. Anttila, M. Valkama, and M. Renfors, "Circularity-based I/Q imbalance compensation in wideband direct-conversion receivers", *IEEE Trans. Veh. Technol.*, vol. 57, no. 4, pp. 2099–2113, Jul. 2008.

[10] B. Chytil, "The distribution of amplitude scintillation and the conversion of scintillation indices", *J. Atmos. Terr. Phys*, vol. 29, no. 9, pp. 1175 –1177, 1967.

[11] N. Youssef, C.-X. Wang, and M. Patzold, "A study on the second order statistics of Nakagami-Hoyt mobile fading channels", *IEEE Trans. Veh. Technol.*, vol. 54, no. 4, pp. 1259–1265, Jul. 2005.

[12] J. G. Proakis, "Digital communications", *McGraw-Hill, New York*, 1995.

[13] M. Nakagami, "The m-distribution-A general formula of intensity distribution of rapid fading", in *Statistical Method of Radio Propagation*, Pergamon Press, 1960, pp. 3–36.

[14] R. S. Hoyt, "Probability functions for the modulus and angle of the normal complex variate", *Bell Syst. Tech. J.*, vol. 26, no. 2, pp. 318–359, 1947.

[15] A. Goldsmith, *Wireless Communications*. Cambridge University Press, 2005.

[16] M. K. Simon and M.-S. Alouini, "A unified approach to the performance analysis of digital communication over generalized fading channels", *Proc. IEEE*, vol. 86, no. 9, pp. 1860–1877, Sep. 1998.

[17] A. Annamalai, C. Tellambura, and V. Bhargava, "Simple and accurate methods for outage analysis in cellular mobile radio systems-a unified approach", *IEEE Trans. Commun.*, vol. 49, no. 2, pp. 303–316, Feb. 2001.

[18] N. Youssef, W. Elbahri, M. Patzold, and S. Elasmi, "On the crossing statistics of phase processes and random FM noise in Nakagami-q

mobile fading channels", *IEEE Trans. Wireless Commun.*, vol. 4, no. 1, pp. 24–29, Jan. 2005.

[19] J. Paris, "Nakagami-q (Hoyt) distribution function with applications", *IEEE Electron. Lett.*, vol. 45, no. 4, pp. 210–211, Feb. 2009.

[20] E. J. Leonardo and M. D. Yacoub, "Exact formulations for the throughput of IEEE 802.11 DCF in Hoyt, Rice, and Nakagami-m fading channels", *IEEE Trans. Wireless Commun.*, vol. 12, no. 5, pp. 2261–2271, May 2013.

[21] V. Bhaskar and N. Peram, "Performance modeling of finite state Markov chains for Nakagami-q and α-μ distributions over adaptive modulation and coding schemes", *AEU - Int. J. Electron. Commun.*, vol. 67, no. 1, pp. 64 –71, Jan. 2013.

[22] P. C. Sofotasios, M. K. Fikadu, K. Ho-Van, M. Valkama, and G. K. Karagiannidis, "The area under a receiver operating characteristic curve over enriched multipath fading conditions", in *2014 IEEE Global Communications Conference*, Dec. 2014, pp. 3490–3495.

[23] J. M. Romero-Jerez and F. J. Lopez-Martinez, "A new framework for the performance analysis of wireless communications under Hoyt (Nakagami- q) fading", *IEEE Trans. Inf. Theory*, vol. 63, no. 3, pp. 1693–1702, Mar. 2017.

[24] D. Morales-Jimenez and J. F. Paris, "Outage probability analysis for η-μ fading channels", *IEEE Communications Letters*, vol. 14, no. 6, pp. 521–523, Jun. 2010.

[25] D. B. Da Costa and M. D. Yacoub, "Average channel capacity for generalized fading scenarios", *IEEE Commun. Lett.*, vol. 11, no. 12, Dec. 2007.

[26] S. Kumar and A. Pandey, "Random matrix model for Nakagami-Hoyt fading", *IEEE Trans. Inf. Theory*, vol. 56, no. 5, pp. 2360–2372, May 2010.

[27] M. L. Mehta, *Random Matrices*, 3rd. Academic press, 2004.

[28] G. Fraidenraich, O. Lévêque, and J. Cioffi, "On the MIMO channel capacity for the dual and asymptotic cases over Hoyt channels", *IEEE Commun. Lett.*, vol. 11, no. 1, Jan. 2007.

[29] M. Yacoub, "The κ-μ distribution and the η-μ distribution", *IEEE Antennas Propag. Mag.*, vol. 49, no. 1, pp. 68–81, Aug. 2007.

[30] L. Moreno-Pozas, F. J. Lopez-Martinez, S. L. Cotton, J. F. Paris, and E. Martos-Naya, "Comments on "Human body shadowing in cellular device-to-device communications: channel modeling using the shadowed κ-μ fading model"", *IEEE J. Sel. Areas Commun.*, vol. 35, no. 02, pp. 517–520, Feb. 2017.

[31] L. Moreno-Pozas, F. J. Lopez-Martinez, J. F. Paris, and E. Martos-Naya, "The κ-μ shadowed fading model: unifying the κ-μ and η-μ distributions", *IEEE Trans. Veh. Technol.*, no. 12, pp. 9630–9641, Dec. 2016.

[32] J. Lopez-Fernandez, L. Moreno-Pozas, F. J. Lopez-Martinez, and E. Martos-Naya, "Joint parameter estimation for the two-wave with diffuse power fading model", *Sensors*, vol. 16, no. 7, Jun. 2016.

[33] F. J. Lopez-Martinez, L. Moreno-Pozas, and E. Martos-Naya, "Novel results for the κ-μ extreme fading distribution: generation of white samples and capacity analysis", *IEEE Commun. Lett.*, vol. 19, no. 9, pp. 1580–1583, Sep. 2015.

[34] J. Lopez-Fernandez, L. Moreno-Pozas, F. J. Lopez-Martinez, and E. Martos-Naya, "Moment-based parameter estimation for the two-wave with diffuse power fading model", in *2016 IEEE 83rd Vehicular Technology Conference (VTC Spring)*, Sep. 2016.

[35] L. Moreno-Pozas and E. Martos-Naya, "On some unifications arising from the MIMO Rician shadowed model", in *2016 IEEE 83rd Vehicular Technology Conference (VTC Spring)*, May 2016, pp. 1–5.

[36] L. Moreno-Pozas, F. J. Lopez-Martinez, J. F. Paris, and E. Martos-Naya, "The Nakagami-q fading distribution: a particular case of the Rician shadowed model", in *XXXI Simposium Nacional de la Unión Científica Internacional de Radio, URSI*, Sep. 2016.

[37] M. Abramowitz and I. A. Stegun, *Handbook of Mathematical Functions*. Dover New York, 1972.

[38] I. S. Gradshteyn and I. Ryzhik, "Table of integrals, Series, and Products", *USA: Academic*, 2007.

[39] J. Marcum, "A statistical theory of target detection by pulsed radar", *IRE Trans. Inf. Theory*, vol. 6, no. 2, pp. 59–267, 1960.

[40] A. H. Nuttall, "Some integrals involving the Q-function", DTIC Document, Tech. Rep., 1972.

[41] M. K. Simon, "The Nuttall Q function-its relation to the Marcum Q function and its application in digital communication performance evaluation", *IEEE Trans. Commun.*, vol. 50, no. 11, pp. 1712–1715, Nov. 2002.

[42] C Andreief, "Note sur une relation entre les integrales definies des produits des fonctions", *Mem. de la Soc. Sci. Bordeaux*, 2, 1883.

[43] N. De Bruijn, "On some multiple integrals involving determinants", *J. Indian Math. Soc.*, vol. 19, pp. 133–151, 1955.

[44] C. Khatri, "Non-central distributions of ith largest characteristic roots of three matrices concerning complex multivariate normal populations", *Ann. Inst. Stat. Math.*, vol. 21, no. 1, pp. 23–32, 1969.

[45] M. Kang and M.-S. Alouini, "Largest eigenvalue of complex Wishart matrices and performance analysis of MIMO MRC systems", *IEEE J. Sel. Areas Commun.*, vol. 21, no. 3, pp. 418–426, Apr. 2003.

[46] A. Lozano, A. M. Tulino, and S. Verdú, "High-SNR power offset in multiantenna communication", *IEEE Trans. Inf. Theory*, vol. 51, no. 12, pp. 4134–4151, 2005.

[47] M. Chiani, "Distribution of the largest eigenvalue for real Wishart and Gaussian random matrices and a simple approximation for the Tracy–Widom distribution", *J. Multivar. Anal.*, vol. 129, pp. 69–81, Aug. 2014.

[48] A. G. Constantine, "Some non-central distribution problems in multivariate analysis", *Ann. Math. Statist.*, vol. 34, no. 4, pp. 1270–1285, 1963.

[49] H. Weyl, *The Classical Groups: Their Invariants and Representations*. Princeton University Press, 2016.

[50] I. G. Macdonald, *Symmetric functions and Hall polynomials*. Oxford University Press, 1995.

[51] A. T. James, "Distributions of matrix variates and latent roots derived from normal samples", *Ann. Math. Statist.*, vol. 35, no. 2, pp. 475–501, Jun. 1964.

[52] J. Paris, "Statistical characterization of κ - μ shadowed fading", *IEEE Trans. Veh. Technol.*, vol. 63, no. 2, pp. 518–526, Feb. 2014.

[53] F. Yilmaz and M.-S. Alouini, "Novel asymptotic results on the high-order statistics of the channel capacity over generalized fading channels", in *Signal Processing Advances in Wireless Communications (SPAWC), 2012 IEEE 13th International Workshop on*, IEEE, 2012, pp. 389–393.

[54] A. Erdelyi, W Magnus, F Oberhettinger, and F. Tricomi, *Tables of Integral Transforms*. New York, NY, USA: McGraw-Hill, 1954.

[55] L. U. Ancarani and G Gasaneo, "Derivatives of any order of the hypergeometric function 2 F 1 (a , b, ; c ; z) with respect to the parameters a, b and c", *J. Phys. A: Math. Theor.*, vol. 42, no. 39, p. 085 210, Sep. 2009.

[56] R. J. Muirhead, *Aspects of multivariate statistical theory*. John Wiley & Sons, 2009, vol. 197.

[57] S. Jin, M. McKay, X. Gao, and I. Collings, "MIMO multichannel beamforming: SER and outage using new eigenvalue distributions of complex noncentral Wishart matrices", *IEEE Trans. Commun.*, vol. 56, no. 3, pp. 424–434, Mar. 2008.

[58] G. L. Stüber, *Principles of Mobile Communication*. Springer Science & Business Media, 2011.

[59] S. Basu, E. MacKenzie, S. Basu, E. Costa, P. Fougere, H. Carlson, and H. Whitney, "250 MHz/GHz scintillation parameters in the equatorial, polar, and auroral environments", *IEEE J. Sel. Areas Commun.*, vol. 5, no. 2, pp. 102–115, Feb. 1987.

[60] N. C. Beaulieu and A. M. Rabiei, "Linear diversity combining on Nakagami-0.5 fading channels", *IEEE Trans. Commun.*, vol. 59, no. 10, pp. 2742–2752, Oct. 2011.

[61] A. Behnad, N. C. Beaulieu, and B. Maham, "Multi-hop amplify-and-forward relaying on Nakagami-0.5 fading channels", *IEEE Wireless Commun. Lett.*, vol. 1, no. 3, pp. 173–176, Jun. 2012.

[62] S. O. Rice, "Statistical properties of a sine wave plus random noise", *Bell Syst. Tech. J.*, vol. 27, no. 1, pp. 109–157, 1948.

[63] C. Loo, "A statistical model for a land mobile satellite link", *IEEE Trans. Veh. Technol.*, vol. 34, no. 3, pp. 122–127, Aug. 1985.

[64] C. Loo, "Measurements and models of a land mobile satellite channel and their applications to MSK signals", *IEEE Trans. Veh. Technol.*, vol. 36, no. 3, pp. 114–121, Aug. 1987.

[65] A. Abdi, W. Lau, M.-S. Alouini, and M. Kaveh, "A new simple model for land mobile satellite channels: first- and second-order statistics", *IEEE Trans. Wireless Commun.*, vol. 2, no. 3, pp. 519–528, May 2003.

[66] N. C. Beaulieu and X. Jiandong, "A novel fading model for channels with multiple dominant specular components", *IEEE Wireless Commun. Lett.*, vol. 4, no. 1, pp. 54–57, Feb. 2015.

[67] S. L. Cotton, "Human body shadowing in cellular device-to-device communications: channel modeling using the shadowed κ-μ fading model", *IEEE J. Sel. Areas Commun.*, vol. 33, no. 1, pp. 111–119, 2015.

[68] I. Porto, M. Yacoub, J. Santos Filho, S. Cotton, and W. Scanlon, "Nakagami-m phase model: further results and validation", *IEEE Wireless Commun. Lett.*, vol. 2, no. 5, pp. 523–526, Oct. 2013.

[69] M. Yacoub, "Nakagami-m phase-envelope joint distribution: a new model", *IEEE Trans. Veh. Technol.*, no. 3, pp. 1552–1557, Mar. 2010.

[70] N. Beaulieu and S. Saberali, "A generalized diffuse scatter plus line-of-sight fading channel model", in *IEEE International Conference on Communications (ICC)*, Jun. 2014, pp. 5849–5853.

[71] G. D. Durgin, T. S. Rappaport, and D. A. De Wolf, "New analytical models and probability density functions for fading in wireless communications", *IEEE Trans. Commun.*, vol. 50, no. 6, pp. 1005–1015, Jun. 2002.

[72] M. Rao, F. Lopez-Martinez, M.-S. Alouini, and A. Goldsmith, "Mgf approach to the analysis of generalized two-ray fading models", *IEEE Wireless Commun.*, vol. 14, no. 5, pp. 2548–2561, May 2015.

[73] J. M. Romero-Jerez, F. J. Lopez-Martinez, J. F. Paris, and A. J. Goldsmith, "The fluctuating two-ray fading model: statistical characterization and performance analysis", *To appear in IEEE Transactions on Wireless Communications*, 2017.

[74] W. C. Lee, "Estimate of channel capacity in Rayleigh fading environment", *IEEE Trans. Veh. Technol.*, vol. 39, no. 3, pp. 187–189, Aug. 1990.

[75] C. G. Gunther, "Comment on "estimate of channel capacity in Rayleigh fading environment", *IEEE Trans. Veh. Technol.*, vol. 45, no. 2, pp. 401–403, May 1996.

[76] M. S. Alouini and A. J. Goldsmith, "Capacity of Rayleigh fading channels under different adaptive transmission and diversity-combining techniques", *IEEE Trans. Veh. Technol.*, vol. 48, no. 4, pp. 1165–1181, Jul. 1999.

[77] N. Sagias and G. Karagiannidis, "Gaussian class multivariate Weibull distributions: theory and applications in fading channels", *IEEE Trans. Inf. Theory*, vol. 51, no. 10, pp. 3608–3619, Oct. 2005.

[78] C. Garcıa-Corrales, F. J. Canete, and J. F. Paris, "Capacity of κ-μ shadowed fading channels", *International Journal of Antennas and Propagation*, vol. 2014,

[79] A Sánchez, E Robles, F. Rodrigo, F Ruiz-Vega, U Fernández-Plazaola, and J. Paris, "Measurement and Modelling of Fading in Ultrasonic Underwater Channels", in *Proc. Underwater Acoustic Conf.*, 2014.

[80] S. L. Cotton, "Shadowed fading in body-to-body communications channels in an outdoor environment at 2.45 GHz", in *2014 IEEE-APS Topical Conf. Antennas Propag. Wireless Commun. (APWC)*, 2014.

[81] S. L. Cotton, S. K. Yoo, and W. G. Scanlon, "A measurements based comparison of new and classical models used to characterize fading

in body area networks", in *IEEE MTT-S International Microwave Workshop Series on RF and Wireless Technologies for Biomedical and Healthcare Applications (IMWS-Bio) 2014*, IEEE, 2014, pp. 1–4.

[82] J. Winters, "Optimum Combining in Digital Mobile Radio with Cochannel Interference", *IEEE J. Sel. Areas Commun.*, vol. 2, no. 4, pp. 528–539, Jul. 1984.

[83] ——, "On the Capacity of Radio Communication Systems with Diversity in a Rayleigh Fading Environment", *IEEE J. Sel. Areas Commun.*, vol. 5, no. 5, pp. 871–878, Jun. 1987.

[84] I. E. Telatar *et al.*, "Capacity of multi-antenna Gaussian channels", *European transactions on telecommunications*, vol. 10, no. 6, pp. 585–595, 1999.

[85] M. Chiani, M. Win, and A. Zanella, "On the capacity of spatially correlated MIMO Rayleigh-fading channels", *IEEE Trans. Inf. Theory*, vol. 49, no. 10, pp. 2363–2371, Oct. 2003.

[86] M.-A. Khalighi, J. Brossier, G. Jourdain, and K. Raoof, "On capacity of Rician MIMO channels", in *12th IEEE International Symposium on Personal, Indoor and Mobile Radio Communications*, vol. 1, Sep. 2001, pp. 150–154.

[87] M. McKay and I. Collings, "General capacity bounds for spatially correlated Rician MIMO channels", *IEEE Trans. Inf. Theory*, vol. 51, no. 9, pp. 3121–3145, Sep. 2005.

[88] M. Kang and M.-S. Alouini, "Capacity of MIMO Rician channels", *IEEE Trans. Wireless Commun.*, vol. 5, no. 1, pp. 112–122, Jan. 2006.

[89] C. Khatri, "Distribution of the largest or the smallest characteristic root under null hypothesis concerning complex multivariate normal populations", *Ann. Math. Statist.*, vol. 35, pp. 1807–1810, Dec. 1964.

[90] G. Alfano, A. De Maio, and A. M. Tulino, "A theoretical framework for LMS MIMO communication systems performance analysis", *IEE Trans. Inf. Theory*, vol. 56, no. 11, pp. 5614–5630, 2010.

[91] P. Dharmawansa and M. R. McKay, "Extreme eigenvalue distributions of some complex correlated non-central Wishart and gamma-Wishart random matrices", *J. Multivar. Anal*, vol. 102, no. 4, pp. 847–868, 2011.

[92] R. W. Heath and D. J. Love, "Multimode antenna selection for spatial multiplexing systems with linear receivers", *IEEE Trans. Signal Process.*, vol. 53, no. 8, pp. 3042–3056, Aug. 2005.

[93] L. Garcia-Ordonez, D. P. Palomar, A. Pages-Zamora, and J. R. Fonollosa, "Analytical BER performance in spatial multiplexing MIMO systems", in *Proc. IEEE Workshop on Signal Processing Advances in Wireless Communications (SPAWC)*, Jun. 2005, pp. 460–464.

[94] P. C. Sofotasios, K. Ho-Van, T. D. Anh, and H. D. Quoc, "Analytic results for efficient computation of the Nuttall-Q and incomplete Toronto functions", in *2013 International Conference on Advanced Technologies for Communications (ATC 2013)*, IEEE, 2013, pp. 420–425.

[95] J. Mitola and G. Q. Maguire, "Cognitive radio: making software radios more personal", *IEEE Pers. Commun.*, vol. 6, no. 4, pp. 13–18, Aug. 1999.